

EUROPEAN ORGANISATION FOR NUCLEAR RESEARCH (CERN)



Phys. Rev. D94 (2016) 052002
DOI: [10.1103/PhysRevD.94.052002](https://doi.org/10.1103/PhysRevD.94.052002)



CERN-EP-2016-142
6th September 2016

Search for pair production of Higgs bosons in the $b\bar{b}b\bar{b}$ final state using proton–proton collisions at $\sqrt{s} = 13$ TeV with the ATLAS detector

The ATLAS Collaboration

Abstract

A search for Higgs-boson pair production in the $b\bar{b}b\bar{b}$ final state is carried out with 3.2 fb^{-1} of proton–proton collision data collected at $\sqrt{s} = 13$ TeV with the ATLAS detector. The data are consistent with the estimated background and are used to set upper limits on the production cross section of Higgs-boson pairs times branching ratio to $b\bar{b}b\bar{b}$ for both non-resonant and resonant production. In the case of resonant production of Kaluza–Klein gravitons within the Randall–Sundrum model, upper limits in the 24 to 91 fb range are obtained for masses between 600 and 3000 GeV, at the 95% confidence level. The production cross section times branching ratio for nonresonant Higgs-boson pairs is also constrained to be less than 1.22 pb, at the 95% confidence level.

1 Introduction

The discovery of a Higgs boson (h) [1, 2] at the Large Hadron Collider (LHC) provides an opportunity to search for physics beyond the Standard Model (SM) in channels involving couplings with the Higgs boson. In particular, the production cross section for Higgs-boson pairs in the SM is significantly smaller than predicted by a host of models, making this channel promising for a search for new phenomena. Examples of such models are the bulk Randall–Sundrum (RS) model [3, 4] with a warped extra dimension and the two-Higgs-doublet model (2HDM) [5]. In the RS model, spin-2 Kaluza–Klein (KK) excitations of the graviton G_{KK}^* are produced via gluon fusion with subsequent decay to the hh final state. Similarly, a heavy spin-0 scalar, H , in the 2HDM also gives rise to a resonant hh signature. Enhanced nonresonant hh production is expected in models with light colored scalars [6] or direct $t\bar{t}hh$ vertices [7, 8].

Previous searches for hh production have been performed by the ATLAS and CMS collaborations with pp collisions at $\sqrt{s} = 8$ TeV. The final states include $b\bar{b}b\bar{b}$ [9, 10], $b\bar{b}\tau^+\tau^-$ [11, 12], $b\bar{b}\gamma\gamma$ [13, 14], and $\gamma\gamma WW^*$ [11]. A combination of these different channels has been performed by ATLAS [11], which shows that for resonance masses above 500 GeV the sensitivity is highest in the $b\bar{b}b\bar{b}$ channel.

The dominant $h \rightarrow b\bar{b}$ decay mode is exploited in this paper to search for both resonant and nonresonant production of Higgs-boson pairs in pp collisions at $\sqrt{s} = 13$ TeV. Two analyses are presented. The “resolved” analysis is optimized for hh systems that have sufficiently low mass to be resolved into four distinct b -jet signatures in the ATLAS detector. The “boosted” analysis focuses on higher-mass hh systems that are characterized by higher-momentum Higgs bosons for which the two b -jets cannot be resolved due to the high boost. In this situation, large-radius jets are utilized to capture the by-products of each Higgs-boson decay and small-radius track jets are used to identify the presence of b -hadrons. The final results are obtained using the resolved analysis up to resonance masses of 1100 GeV, where its expected sensitivity is higher than that of the boosted analysis, whereas the boosted analysis is used for masses above 1100 GeV.

The two analyses generally follow the same approach as that adopted for the 8 TeV data (see Ref. [9]). The analysis of the 13 TeV data reported in this paper benefits from an enhanced sensitivity to high-mass resonances due to the significant increase in the production cross section in that kinematic region. Furthermore, the boosted analysis includes a channel with only three b -tagged track jets, in addition to the channel with four b -tagged track jets already included in the previous analysis. This new channel improves sensitivity for resonances with mass above 2000 GeV because the b -jet identification efficiency decreases sharply at high transverse momenta. The boosted analysis also operates with smaller track-jet radii to account for the larger boost at 13 TeV.

2 The ATLAS detector

The ATLAS experiment [15] at the LHC is a multipurpose particle detector with a forward-backward symmetric cylindrical geometry and a near 4π coverage in solid angle.¹ It consists of an inner tracking

¹ ATLAS uses a right-handed coordinate system with its origin at the nominal interaction point (IP) in the center of the detector and the z -axis along the beam pipe. The x -axis points from the IP to the center of the LHC ring, and the y -axis points upwards. Cylindrical coordinates (r, ϕ) are used in the transverse plane, ϕ being the azimuthal angle around the z -axis. The pseudorapidity is defined in terms of the polar angle θ as $\eta = -\ln \tan(\theta/2)$. Angular distance is measured in units of $\Delta R \equiv \sqrt{(\Delta\eta)^2 + (\Delta\phi)^2}$.

detector surrounded by a thin superconducting solenoid providing a 2 T axial magnetic field, electromagnetic and hadronic calorimeters, and a muon spectrometer. The inner tracking detector (ID) covers the pseudorapidity range $|\eta| < 2.5$. It consists of silicon pixel, silicon microstrip, and transition radiation tracking (TRT) detectors. A new innermost pixel layer [16] inserted at a mean radius of 3.3 cm is used for the first time in the 2015 data taking. Lead/liquid-argon (LAr) sampling calorimeters provide electromagnetic (EM) energy measurements. A steel/scintillator-tile hadronic calorimeter covers the central pseudorapidity range ($|\eta| < 1.7$). The endcap and forward regions are instrumented with LAr calorimeters for both the EM and hadronic energy measurements up to $|\eta| = 4.9$. The muon spectrometer (MS) surrounds the calorimeters and includes three large superconducting air-core toroids. The field integral of the toroids ranges between 2.0 and 6.0 T m for most of the detector. The MS includes a system of fast detectors for triggering and precision tracking chambers. A dedicated trigger system is used to select events. The first-level trigger is implemented in hardware and uses the calorimeter and muon detectors to reduce the accepted rate to 100 kHz. This is followed by a software-based high-level trigger (HLT) that reduces the accepted event rate to 1 kHz on average.

3 Data and simulation samples

The data sample used in this analysis was collected during the 2015 LHC run with pp collisions at $\sqrt{s} = 13$ TeV. After requiring that the data be collected during stable beam conditions and that relevant detector systems be functional, the total integrated luminosity is estimated to be 3.2 fb^{-1} with an uncertainty of 5.0% derived following the methodology detailed in Ref. [17]. In the resolved analysis, events are selected by a combination of three triggers requiring either one or two jets selected by a dedicated HLT b -tagging algorithm [18]. These triggers require either one b -tagged jet with transverse momentum $p_T > 225$ GeV, two b -tagged jets with $p_T > 55$ GeV and an additional jet with $p_T > 100$ GeV, or four jets with $p_T > 35$ GeV, two of which are b -tagged. A trigger requiring a single jet of radius 1.0 and $p_T > 360$ GeV is used to select events in the boosted analysis. The p_T thresholds for these single- or multiple-jet triggers are lower at the first level of the trigger system. The combination of all the above triggers has an efficiency rising from 95% to 99% for selecting $b\bar{b}b\bar{b}$ signal events passing the full analysis selection as the resonance mass increases.

Simulated Monte Carlo (MC) event samples are used to model signal production and the background from $t\bar{t}$ and Z +jets events. A method based on data is used to model the dominant multijet background. Signal G_{KK}^* events are generated at leading order (LO) with MG5_AMC@NLO v2.2.2 [19] using the NNPDF2.3 LO parton distribution function (PDF) set [20], and PYTHIA 8.186 [21] to model the parton shower and hadronization process using the A14 set of tuned underlying-event parameters [22]. The Higgs-boson mass is set to 125.0 GeV. Values of the signal cross section times branching ratio for $G_{\text{KK}}^* \rightarrow hh \rightarrow b\bar{b}b\bar{b}$ with the coupling constant $k/\bar{M}_{\text{Pl}} = 1$ are 11.2 fb and 0.185 fb for G_{KK}^* masses of 1000 GeV and 2000 GeV, respectively. The parameter k corresponds to the curvature of the warped extra dimension and the effective four-dimensional Planck scale $\bar{M}_{\text{Pl}} = 2.4 \times 10^{18}$ GeV. Signal samples are also generated with $k/\bar{M}_{\text{Pl}} = 2$ to study broader resonances. Both the cross section and natural width depend on $(k/\bar{M}_{\text{Pl}})^2$. Generation of the heavy H scalar in a simplified model with a fixed narrow width $\Gamma_H = 1$ GeV is performed with MG5_AMC@NLO and the CT10 PDF set [23]. With this Γ_H choice, the width of the reconstructed hh resonance is dominated by the experimental resolution. For this model, parton showering and hadronization are handled by HERWIG++ [24] with the CTEQ6L1 PDF set [25] and the UEEE5 underlying-event tune [26]. The scalar interpretation for this search only makes use of the acceptance times efficiency from this model and no interpretation in terms of 2HDM parameters is

presented. Nonresonant SM $pp \rightarrow hh \rightarrow b\bar{b}b\bar{b}$ events are generated via the gluon-fusion process with MG5_AMC@NLO using form factors for the top-quark loop from HPAIR [27, 28]. The cross section times branching ratio to the $b\bar{b}b\bar{b}$ final state, evaluated at next-to-next-to-leading order with the summation of logarithms at next-to-next-leading-logarithm accuracy, is $11.3_{-1.0}^{+0.9}$ fb [29]. The uncertainty includes the effects due to renormalization and factorization scales, PDF set, α_S , effects of finite top-quark mass in loops, and the $h \rightarrow b\bar{b}$ branching ratio.

Generation of $t\bar{t}$ events is performed with POWHEG-BOX v1 using the CT10 PDF set. The parton shower, hadronization, and the underlying event are simulated using PYTHIA 6.428 [30] with the CTEQ6L1 PDF set and the corresponding Perugia 2012 tune [31]. The top-quark mass is set to 172.5 GeV. Higher-order corrections to $t\bar{t}$ cross sections are computed with Top++ 2.0 [32]. These incorporate NNLO corrections in QCD, including resummation of next-to-next-to-leading logarithmic soft gluon terms. The overall $t\bar{t}$ normalization is extracted from the data while the shape of kinematic distributions is taken from MC simulation. The Z +jets sample is generated using PYTHIA 8.186 with the NNPDF2.3 LO PDF set.

For all MC samples, charm-hadron and bottom-hadron decays are handled by EVTGEN 1.2.0 [33]. To simulate the impact of multiple pp interactions that occur within the same or nearby bunch crossings (pileup), minimum-bias events generated with PYTHIA 8 are overlaid on top of the hard scatter event. The detector response is simulated with GEANT 4 [34, 35] and the events are processed with the same reconstruction software as that used for the data.

4 Event reconstruction

The resolved and boosted analyses rely on the reconstruction of jets with the anti- k_t clustering algorithm [36] but with different values of the radius parameter R . Calorimeter jets with $R = 0.4$ (1.0) are used to determine the kinematic properties of Higgs-boson candidates in the resolved (boosted) analysis. Those jets are reconstructed from topological clusters of energy deposits in calorimeter cells. The $R = 0.4$ jet energies are determined from reconstructed cluster energies at the electromagnetic scale with correction factors derived from simulation to account for the response of the calorimeter to hadrons [37]. Jets from pileup are suppressed with the use of tracking information as detailed in Ref. [38]. The $R = 1.0$ jets are built from locally calibrated clusters [37] and are trimmed [39] to minimize the impact of pileup. This trimming proceeds by reclustering the jet with the k_t algorithm [40] into smaller $R = 0.2$ subjets and removing those subjets with $p_T^{\text{subjet}}/p_T^{\text{jet}} < 0.05$, where p_T^{subjet} is the transverse momentum of the subjet and p_T^{jet} that of the original jet. In addition to the above large- R trimmed jets, the boosted analysis uses track jets with $R = 0.2$ to identify b -hadrons from Higgs-boson decays [41]. Such jets are reconstructed from charged-particle tracks with $p_T > 0.4$ GeV and $|\eta| < 2.5$ that satisfy a set of hit and impact parameter criteria to make sure that the tracks originate from the primary vertex, thereby minimizing the impact of pileup. Track jets are associated to large- R jets using ghost association [42]. In this method, the large- R jet algorithm is rerun with both the four-momenta of track jets modified to have infinitesimally small momentum (the ‘‘ghosts’’) and all topological energy clusters in the event as potential constituents of jets. As a result, the presence of track jets does not alter the large- R jets already found and their association to specific large- R jets is determined by the jet algorithm. Collision vertices are reconstructed requiring a minimum of two tracks with $p_T > 0.4$ GeV in each vertex. The primary vertex is chosen to be the vertex with the largest $\sum p_T^2$, where the sum extends over all tracks associated with the vertex.

The identification of jets containing b -hadrons is based on the $R = 0.4$ calorimeter ($R = 0.2$ track) jets in the resolved (boosted) analysis and a multivariate tagging algorithm [43]. This algorithm is applied to a set of tracks with loose impact parameter constraints in a region of interest around each jet axis to enable the reconstruction of the b -hadron decay vertex. The b -tagging requirements result in an efficiency of 70% (77%) for jets containing b -hadrons in the resolved (boosted) analysis, as determined in a sample of simulated $t\bar{t}$ events. The corresponding efficiencies for c -hadron jets and light-quark or gluon jets are 12% (29%) and 0.2% (1.4%), respectively. Different b -tagging operating points are chosen in the two analyses to maximize their respective sensitivities.

Muons are reconstructed by combining tracks in the ID and MS, and are required to satisfy tight muon identification criteria [44]. The four-momentum of muons with $p_T > 4$ GeV and $|\eta| < 2.5$, that are within ΔR of 0.4 (0.2) of jets used for b -tagging in the resolved (boosted) analysis, is added to the calorimeter jet four-momentum to partially account for the energy lost in semileptonic b -hadron decays.

5 Event selection

The event selection for the resolved and boosted analyses is described below. These analyses are optimized independently for the reconstruction and selection of $hh \rightarrow b\bar{b}b\bar{b}$ final states, with the resolved analysis aiming at event topologies containing four distinct b -jets, whereas the boosted analysis focuses on topologies with higher-momentum Higgs bosons resulting in merged jets.

Different selection and background estimation strategies are adopted for the two analyses. To facilitate the comparison between these different choices, Table 1 summarizes each of the requirements and approaches described in this section.

5.1 Resolved analysis

5.1.1 Selection

Events selected for the resolved analysis must contain at least four b -tagged jets with $|\eta| < 2.5$ and $p_T > 40$ GeV. The four highest- p_T b -tagged jets are used to form two dijet systems, requiring an angular distance ΔR between the jets within the dijet system smaller than 1.5. The transverse momentum of the leading (subleading) dijet system is required to be greater than 200 (150) GeV. These requirements are made to ensure a high trigger efficiency and to avoid ambiguities in forming dijets. In the rare case that a jet is assigned to more than one dijet system, only the combination containing the jets with the highest probability of being b -jets according to the multivariate b -tagging algorithm is considered.

The resolved analysis considers resonance masses in the range 400–1500 GeV. Event selection that varies as a function of the reconstructed resonance mass (m_{4j}) is used to increase the analysis sensitivity across the mass range searched. Mass-dependent selection requirements are made on the leading dijet p_T , the subleading dijet p_T and the pseudorapidity difference between the dijets as follows [9]:

$$p_T^{\text{lead}} > \begin{cases} 400 \text{ GeV} & \text{if } m_{4j} > 910 \text{ GeV,} \\ 200 \text{ GeV} & \text{if } m_{4j} < 600 \text{ GeV,} \\ 0.65 m_{4j} - 190 \text{ GeV} & \text{otherwise,} \end{cases}$$

	Resolved	Boosted
Event preselection	≥ 4 jets with $p_T > 40$ GeV, $ \eta < 2.5$ ≥ 2 dijets with $p_T > 200$ (150) GeV, $\Delta R < 1.5$, $p_T > f(m_{4j})$, $ \Delta\eta < f'(m_{4j})$	≥ 2 large- R jets with 350 (250) $< p_T < 1500$ GeV, $ \eta < 2.0$, $m_J > 50$ GeV ≥ 2 track jets associated to each large- R jet with $p_T > 10$ GeV, $ \eta < 2.5$, $ \Delta\eta < 1.7$
$t\bar{t}$ veto	$X_{t\bar{t}} < 3.2$	–
Tagging	4 b -tagged jets	3 or 4 b -tagged jets
Signal region (SR)	$X_{hh} < 1.6$	
Sideband region (SB)	Resolved: $\sqrt{(m_{2j}^{\text{lead}} - 124 \text{ GeV})^2 + (m_{2j}^{\text{subl}} - 115 \text{ GeV})^2} > 58 \text{ GeV}$ Boosted: $\sqrt{(m_J^{\text{lead}} - 124 \text{ GeV})^2 + (m_J^{\text{subl}} - 115 \text{ GeV})^2} > 36 \text{ GeV}$	
Control region (CR)	complementary to SR and SB	
Multijet normalization	scaled yields from 2-tag SR, scaling derived from 4-tag to 2-tag ratio in SB	scaled yields from 2-tag SR, scaling derived from 3(4)-tag to 2-tag fit to leading jet mass in SB
Multijet shape	derived from 2-tag SR	
$t\bar{t}$ normalization	scaled yields from $t\bar{t}$ CR, scaling derived from semileptonic $t\bar{t}$ events	scaled yields from MC simulation, scaling derived from 3(4)-tag to 2-tag fit to leading jet mass in SB
$t\bar{t}$ shape	derived from MC simulation	

Table 1: Event selection requirements and definition of the different regions used in the resolved and boosted analyses. The methodologies used to estimate the background normalization and shape are also outlined. The variables are defined in the text. Dijet and large- R jet minimum p_T values are indicated for leading (subleading) such objects. The functions $f(m_{4j})$ and $f'(m_{4j})$ represent the mass dependence of the minimum p_T and maximum $|\Delta\eta|$ requirements placed on the dijet candidates in the resolved analysis.

$$p_T^{\text{subl}} > \begin{cases} 260 \text{ GeV} & \text{if } m_{4j} > 990 \text{ GeV}, \\ 150 \text{ GeV} & \text{if } m_{4j} < 520 \text{ GeV}, \\ 0.23 m_{4j} + 30 \text{ GeV} & \text{otherwise,} \end{cases}$$

$$|\Delta\eta_{\text{dijets}}| < \begin{cases} 1.0 & \text{if } m_{4j} < 820 \text{ GeV}, \\ 1.6 \times 10^{-3} m_{4j} - 0.28 & \text{otherwise.} \end{cases}$$

These selection requirements were optimized simultaneously by performing a three-dimensional scan of threshold values, using the expected exclusion limit on the G_{KK}^* resonance with $k/\bar{M}_{\text{Pl}} = 1$ as a metric.

After selecting two dijets that satisfy the mass-dependent criteria, 15% of the total background consists of $t\bar{t}$ events. This $t\bar{t}$ background mainly comprises events where both top quarks decay hadronically. These

hadronic decays often lead to three jets for each top quark – one b -jet directly from the top-quark decay and two from the decay of the W boson. Reduction of the $t\bar{t}$ background is important as relatively large systematic uncertainties are associated with modeling $t\bar{t}$ in the signal region. In order to reduce the $t\bar{t}$ background, jets not already used in the formation of the two dijets (“extra jets”) in the event are used to reconstruct W -boson and top-quark candidates by combining them with one or both of the jets in a given dijet. These extra jets are required to have $p_T > 30$ GeV, $|\eta| < 2.5$, and $\Delta R < 1.5$ relative to the dijet. The W -boson candidate is reconstructed by adding the four-momentum of the extra jet to the four-momentum of the jet in the dijet system with the lowest probability of being a b -jet according to the multivariate b -tagging algorithm. The top-quark candidate is reconstructed by summing the dijet and the extra jet. The compatibility with the top-quark decay hypothesis is then determined using the variable:

$$X_{tt} = \sqrt{\left(\frac{m_W - 80.4 \text{ GeV}}{0.1 m_W}\right)^2 + \left(\frac{m_t - 172.5 \text{ GeV}}{0.1 m_t}\right)^2}, \quad (1)$$

where m_W and m_t are the invariant masses of the W -boson and top-quark candidates. The values in the denominator approximate the dijet and three-jet system mass resolutions. If either dijet in an event has $X_{tt} < 3.2$ for any possible combination with an extra jet, the event is rejected. This requirement, referred to as the “ $t\bar{t}$ veto”, reduces the $t\bar{t}$ background by $\sim 60\%$, while retaining $\sim 90\%$ of signal events. The event selection criteria described above are collectively referred to as the “4-tag” selection requirements.

Following the 4-tag selection, a requirement on the combination of the leading and subleading dijet masses (m_{2j}^{lead} and m_{2j}^{subl} , respectively) is used to define the signal region. The signal region is defined using the variable:

$$X_{hh} = \sqrt{\left(\frac{m_{2j}^{\text{lead}} - 124 \text{ GeV}}{0.1 m_{2j}^{\text{lead}}}\right)^2 + \left(\frac{m_{2j}^{\text{subl}} - 115 \text{ GeV}}{0.1 m_{2j}^{\text{subl}}}\right)^2}, \quad (2)$$

where the $0.1 m_{2j}$ terms approximate the widths of the mass distributions. The center of the signal region was optimized using G_{KK}^* samples with $k/\bar{M}_{\text{Pl}} = 1$. On average, the subleading Higgs-boson candidate is reconstructed at lower masses as a result of energy lost from semileptonic b -hadron decays and final-state radiation. The signal region is defined as $X_{hh} < 1.6$. This corresponds to the kinematic requirements illustrated by the inner region in Figure 1. The data shown in this figure are derived from a sample of events that satisfy all selection criteria except for having only two jets that pass the b -tagging requirements, referred to as the “2-tag” sample.

The acceptance times efficiency for each stage of the resolved-analysis event selection is shown in Figure 2 for spin-2 and spin-0 resonances. The acceptance times efficiency, $A \times \varepsilon$, of the full selection for the G_{KK}^* with $k/\bar{M}_{\text{Pl}} = 1$ ranges from 0.1% for a G_{KK}^* of mass 400 GeV to 5.3% for a G_{KK}^* with a mass of 1000 GeV. The spin of the resonance affects the angular distribution of the decay products, resulting in a lower acceptance in the case of a spin-0 H boson than for the spin-2 G_{KK}^* . As a result, the spin-0 resonance search is performed starting at a mass of 500 GeV. Nonresonant di-Higgs production occurs primarily at the low end of the m_{4j} spectrum, leading to $A \times \varepsilon = 0.64\%$ for the full selection.

The final step in the resonant analysis is to search for an excess in the m_{4j} distribution for events in the signal region. The sensitivity of the search is increased by improving the m_{4j} resolution in this region. This is achieved by scaling the four-momentum of each of the Higgs-boson candidates such that their mass is

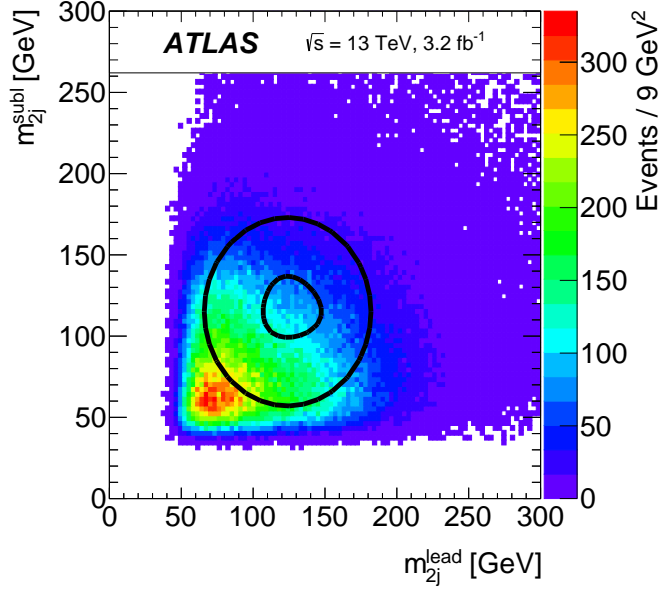


Figure 1: The m_{2j}^{subl} vs. m_{2j}^{lead} distribution for the 2-tag data sample used to model the multijet background in the resolved analysis. The signal region is the area surrounded by the inner black contour line, centered on $m_{2j}^{\text{lead}} = 124$ GeV, $m_{2j}^{\text{subl}} = 115$ GeV. The control region is the area inside the outer black contour line, excluding the signal region. The sideband region is the area outside the outer contour line.

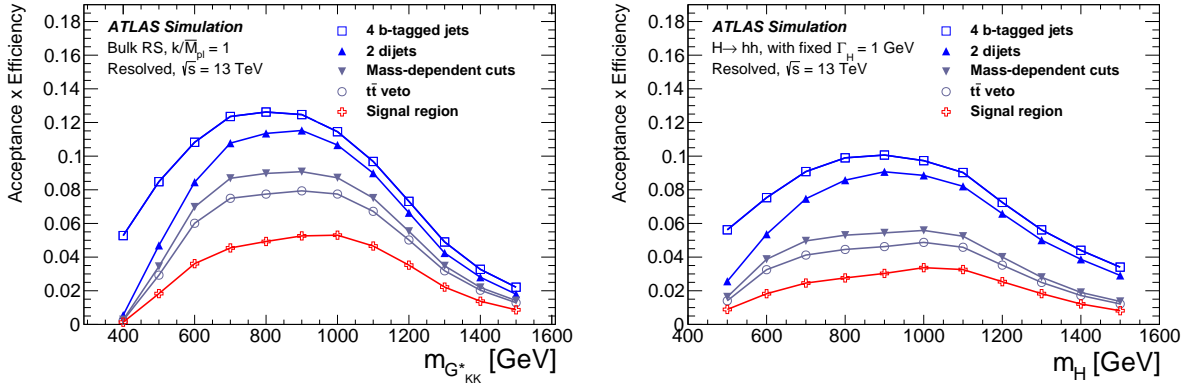


Figure 2: The selection efficiency as a function of resonance mass at each stage of the event selection for (left) $G_{\text{KK}}^* \rightarrow hh \rightarrow b\bar{b}b\bar{b}$ and (right) $H \rightarrow hh \rightarrow b\bar{b}b\bar{b}$ decays in the resolved analysis.

equal to the Higgs-boson mass. This leads to an improvement of $\sim 30\%$ in the signal m_{4j} resolution with little impact on the background.

5.1.2 Background estimation

After the 4-tag selection described above, $\sim 90\%$ of the remaining background in the signal region originates from multijet events, which are modeled using data. The remaining $\sim 10\%$ of the background is expected from $t\bar{t}$ events. The $t\bar{t}$ yield is determined from data, while the m_{4j} shape is taken from MC simulation. The Z +jets contribution is less than 1% of the total background and is estimated from MC simulation. The background from all other sources – including processes featuring Higgs bosons – is negligible.

Multijet background

The multijet background is modeled using an independent data sample selected using the same trigger and selection requirements as described above, except for the b -tagging requirement: only one of the two selected dijets is formed from b -tagged jets, while the other dijet is formed from jets that both fail the b -tagging requirements. This “2-tag” selection yields a data sample that consists of 98% multijet events and 2% $t\bar{t}$ events. The predicted signal contamination is negligible.

The 2-tag sample is normalized to the 4-tag sample and its kinematics corrected for differences introduced by the additional b -tagging requirement on the 4-tag sample. These kinematic differences arise because the b -tagging efficiency varies as a function of jet p_T and η , the various multijet processes contribute in different fractions, and the fraction of events passed by each trigger path changes. The normalization and kinematic corrections are determined using a signal-free sideband region of the $m_{2j}^{\text{lead}}-m_{2j}^{\text{subl}}$ plane. The resulting background model is verified and the associated uncertainties are estimated using a control region. The sideband and control regions are shown in Figure 1. The sideband region is defined as $\sqrt{(m_{2j}^{\text{lead}} - 124 \text{ GeV})^2 + (m_{2j}^{\text{subl}} - 115 \text{ GeV})^2} > 58 \text{ GeV}$, while the control region is defined as the region in the $m_{2j}^{\text{lead}}-m_{2j}^{\text{subl}}$ plane between the signal and sideband regions. These definitions are chosen to be orthogonal to the signal region and to give approximately equal event yields in both the sideband and control regions.

The normalization of the multijet background prediction is set by scaling the number of events in each region of the 2-tag sample by the following factor μ_{Multijet} calculated in the sideband region:

$$\mu_{\text{Multijet}} = \frac{N_{\text{Multijet}}^{4\text{-tag}}}{N_{\text{Multijet}}^{2\text{-tag}}} = \frac{N_{\text{data}}^{4\text{-tag}} - N_{t\bar{t}}^{4\text{-tag}} - N_{Z+\text{jets}}^{4\text{-tag}}}{N_{\text{data}}^{2\text{-tag}} - N_{t\bar{t}}^{2\text{-tag}} - N_{Z+\text{jets}}^{2\text{-tag}}}, \quad (3)$$

where $N_{\text{data}}^{2-/4\text{-tag}}$ is the number of events observed in the sideband region in the 2- or 4-tag data sample, respectively. The yields $N_{t\bar{t}}^{2-/4\text{-tag}}$ are the estimated number of $t\bar{t}$ events in the 2-/4-tag selected sideband region estimated from MC simulation. To predict the distributions of the multijet background in each region, the predicted $t\bar{t}$ 2-tag distributions are first subtracted from the 2-tag data sample before the distribution is scaled by μ_{Multijet} .

The correction for the kinematic differences between 2-tag and 4-tag samples is performed by reweighting events in the 2-tag sample. The weights are derived in the sideband region, from linear fits to the ratio of the total background model to data for three kinematic distributions that are found to have the largest disagreement between 2-tag and 4-tag: the leading dijet p_T , the angular separation between the jets in the

Sample	Sideband Region	Control Region
Multijet	485.1 ± 2.1	401.5 ± 2.0
$t\bar{t}$	9.6 ± 0.9	14.0 ± 1.2
Z+jets	3.1 ± 0.7	4.9 ± 1.0
Total	497.8 ± 2.4	420.3 ± 2.5
Data	496	396

Table 2: The number of events in data and predicted background events after applying the $t\bar{t}$ veto in the sideband and control regions for the resolved analysis. The uncertainties are purely statistical. The $t\bar{t}$ yield in this table, in contrast to the final result, is estimated using MC simulation.

subleading dijet, and the angular separation between the two dijets. The reweighting is performed using one-dimensional distributions but is iterated so that correlations between the three variables are taken into account. After the correction process, there is agreement between the background model and sideband region data.

The multijet background model is validated in the control region. Table 2 compares the observed data yield in the control region with the corresponding background estimate. The modeling of the m_{4j} distribution in the control region is shown in Figure 3. The 4-tag events in the control region are well-described by the background model in both normalization and m_{4j} shape.

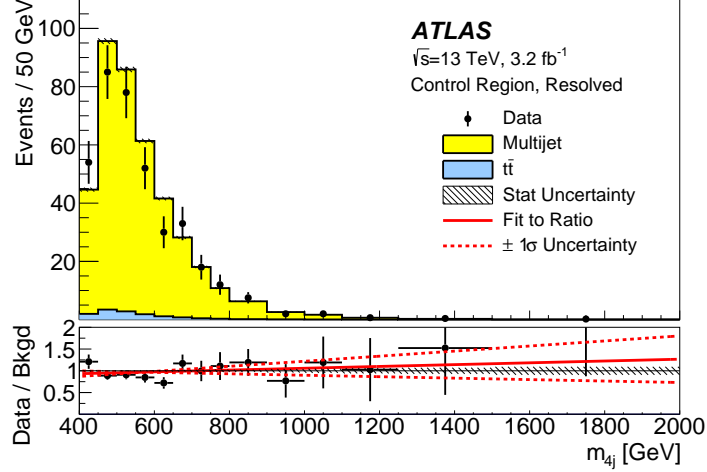


Figure 3: The m_{4j} distribution in the control region of the resolved analysis for the data and the predicted background (top panel). The small hatched bands drawn on the histogram and on the horizontal line in the data to background ratio (bottom panel) represent the statistical uncertainty in the total background estimate. The bottom panel also includes a first-order polynomial fit to the data-to-background ratio. The dashed lines show the $\pm 1\sigma$ uncertainties in the two fitted parameters.

$t\bar{t}$ background

The normalization of the $t\bar{t}$ background is derived from data in a $t\bar{t}$ control region. Due to the limited yield in this control region, the shape of the $t\bar{t}$ background is taken from MC simulation. To further decrease statistical uncertainties, the $t\bar{t}$ shape is derived from MC simulation using the “2-tag” selection, with a systematic uncertainty assigned to cover the differences between the 2-tag and 4-tag m_{4j} distributions.

The $t\bar{t}$ control region is formed from events which pass the 4-tag selection, except for the $t\bar{t}$ veto, which is reversed: if either of the dijets fails the $X_{t\bar{t}}$ requirement, the event enters the $t\bar{t}$ control region. This selection leads to a sample of 21 events, of which 13.3 are estimated to be multijet events using the 2-tag sample described previously. After subtracting the multijet background, the $t\bar{t}$ control region yield is extrapolated to predict the $t\bar{t}$ yield in the signal region, $N_{t\bar{t}}$, using the following equation:

$$N_{t\bar{t}} = \frac{\epsilon_t^2}{1 - \epsilon_t^2} \times N_{t\bar{t}}^{\text{CR}}, \quad (4)$$

where $N_{t\bar{t}}^{\text{CR}}$ is the number of events in the $t\bar{t}$ control region, after subtraction of multijet background, and ϵ_t is the efficiency for a selected dijet in a $t\bar{t}$ event to pass the $t\bar{t}$ veto. This equation relies on the assumption that the ϵ_t of each dijet in the event is uncorrelated, an assumption validated in $t\bar{t}$ MC simulation. The ϵ_t is measured using an independent, high-purity “semileptonic $t\bar{t}$ ” data sample. Events in this sample are selected by requiring one dijet candidate passing the nominal selection with $p_T > 150$ GeV and one “leptonic top-quark” candidate. The leptonic top-quark candidate is defined using a reconstructed muon and one b -tagged jet. This b -tagged jet is required to be distinct from jets in the dijet candidate, and the muon is required to have $p_T > 25$ GeV, be isolated, and fall a distance $\Delta R < 1.5$ of the b -tagged jet. The leptonic top-quark candidate is required to have $p_T > 150$ GeV, where the leptonic top \vec{p}_T is defined as the vector sum of the b -jet \vec{p}_T and the muon \vec{p}_T . The $t\bar{t}$ veto efficiency is then measured as the fraction of the reconstructed dijet candidates which passed the $t\bar{t}$ veto, yielding $\epsilon_{t\bar{t}} = 0.60 \pm 0.04$ (stat.) ± 0.06 (syst.). A 10% systematic uncertainty is assigned to cover potential differences between ϵ_t as measured in the semileptonic $t\bar{t}$ sample and ϵ_t in the full 4-tag selection, where the method is applied in $t\bar{t}$ MC simulation to evaluate such differences. The measured ϵ_t agrees well with the corresponding semileptonic $t\bar{t}$ MC prediction of 0.58.

Equation (4) gives a data-driven $t\bar{t}$ background prediction of 4.2 ± 3.8 events. The uncertainty is dominated by the statistical uncertainty in the yield in the $t\bar{t}$ control region, with a smaller contribution from the uncertainty in the measured $t\bar{t}$ veto efficiency.

5.1.3 Systematic uncertainties

Two classes of systematic uncertainties are evaluated: those affecting the modeling of the signal and those affecting the background prediction.

The signal modeling uncertainties comprise: theoretical uncertainties in the acceptance, uncertainties in the jet energy scale (JES) and resolution (JER), and uncertainties in the b -tagging efficiency.

The following sources of theoretical uncertainty in the acceptance are evaluated: missing higher-order terms in the matrix elements and PDF set, as well as modeling of the underlying event, hadronic showers, initial- and final-state radiation. The total theoretical uncertainty is dominated by the uncertainties associated with the modeling of the initial- and final-state radiation.

The jet energy uncertainties are derived based on in situ measurements performed during Run 1 and from MC simulation extrapolations from Run-1 to Run-2 conditions [45]. The JES systematic uncertainty is evaluated using three separate and orthogonal uncertainty components [46]. The JER uncertainty is evaluated by smearing jet energies according to the systematic uncertainties of the resolution measurement [46]. The uncertainty in the b -tagging efficiency is evaluated by propagating the systematic uncertainty in the measured tagging efficiency for b -jets [47]. The efficiencies are measured as a function of b -jet p_T and η . For b -jets with $p_T > 300$ GeV, systematic uncertainties in the tagging efficiencies are extrapolated with MC simulation and are consequently larger [18].

Systematic uncertainties in the normalization and shape of the multijet background model are assessed in the control region. The background prediction in the control region agrees with the observed data to within $\pm 5\%$, which is taken as the uncertainty in the predicted multijet yield. To further test the robustness of the background estimation, the background model is re-evaluated using different sideband and control region definitions and different b -tagging requirements on the “2-tag” sample. These changes affect the kinematic and flavor compositions of the various regions used in the background prediction. The control region agreement and signal region predictions of all variations considered are all consistent to within the assigned $\pm 5\%$ uncertainty in the multijet background prediction.

The uncertainty in the description of the multijet m_{4j} distribution is determined by comparing the background prediction to the data in the control region as shown in Figure 3. To evaluate the level of agreement, a linear fit is performed on the ratio of the distributions. This fit, along with its uncertainties, shown in the bottom panel of Figure 3, gives a slope consistent with zero. The uncertainty in the multijet background shape is defined using the uncertainty in the fitted slope.

The uncertainty in the $t\bar{t}$ normalization is described above. The uncertainty in the MC-derived $t\bar{t}$ m_{4j} distribution is dominated by the uncertainty associated with using the 2-tag selection to model the 4-tag selection. This uncertainty is assessed by comparing the 2-tag and 4-tag $t\bar{t}$ MC predictions in the signal region.

Table 3 summarizes the relative impact of the uncertainties in the event yields.

Source	Background	SM hh	G_{KK}^* (500 GeV) $\frac{k}{\bar{M}_{\text{Pl}}} = 1$	G_{KK}^* (800 GeV) $\frac{k}{\bar{M}_{\text{Pl}}} = 1$	G_{KK}^* (800 GeV) $\frac{k}{\bar{M}_{\text{Pl}}} = 2$	H (800 GeV)
Luminosity	–	5	5	5	5	5
JER	–	2	3	3	3	4
JES	–	12	14	5	4	6
b -tagging	–	18	15	26	27	26
Theoretical	–	9	2	3	3	3
Multijet	5	–	–	–	–	–
$t\bar{t}$	6	–	–	–	–	–
Total	8	24	21	28	28	28

Table 3: Summary of systematic uncertainties (expressed in percentage yield) in the total background and signal event yields in the signal region of the resolved analysis. Uncertainties are provided for nonresonant SM Higgs pair production, for a G_{KK}^* resonance with $k/\bar{M}_{\text{Pl}} = 1$ and $m = 500$ GeV, and for three resonances with $m = 800$ GeV: a G_{KK}^* resonance with $k/\bar{M}_{\text{Pl}} = 1$, a G_{KK}^* resonance with $k/\bar{M}_{\text{Pl}} = 2$, and a spin-0 narrow-width H boson.

5.1.4 Event yields

The predicted number of background events in the signal region, the number of events observed in the data, and the predicted yield for two potential signals are presented in Table 4. The numbers of predicted background events and observed events are in agreement.

Sample	Signal Region Yield
Multijet	43.3 ± 2.3
$t\bar{t}$	4.3 ± 3.0
Z+jets	–
Total	47.6 ± 3.8
Data	46
SM hh	0.22 ± 0.05
G_{KK}^* (800 GeV), $k/\bar{M}_{\text{Pl}} = 1$	5.7 ± 1.5

Table 4: The number of predicted background events in the hh signal region for the resolved analysis, compared to the data. The yield for two potential signals, SM nonresonant Higgs pair production and an 800 GeV G_{KK}^* resonance with $k/\bar{M}_{\text{Pl}} = 1$ are shown. The quoted errors include both the statistical and systematic uncertainties.

Figure 4 shows a comparison of the predicted m_{4j} background distribution to that observed in the data. The predicted background and observed distributions are in agreement, with no significant local excesses.

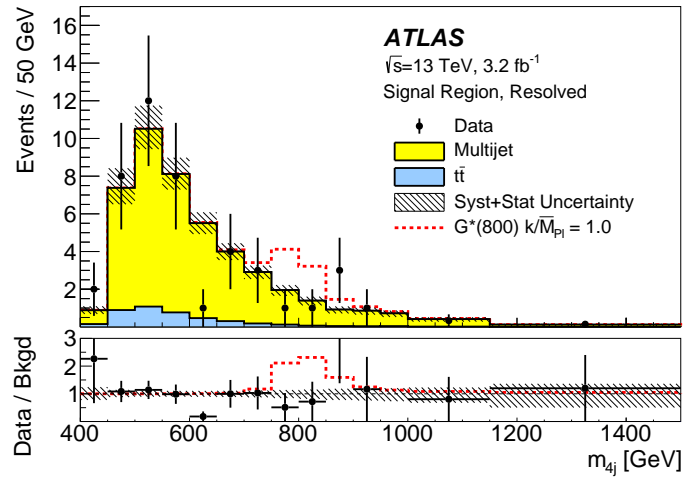


Figure 4: Distribution of m_{4j} in the signal region of the resolved analysis for data compared to the predicted background. The hatched bands represent the combined statistical and systematic uncertainty in the total background estimate. The expected signal distribution for a G_{KK}^* resonance with mass of 800 GeV is also shown.

5.2 Boosted analysis

5.2.1 Selection

The boosted analysis selects events with at least two large- R jets with $250 < p_T < 1500$ GeV, $|\eta| < 2.0$, and mass $m_J > 50$ GeV. The upper bound on the transverse momentum and the mass requirement correspond to the kinematic region where jet calibration uncertainties are available from Refs. [41] and [48]. Only the two large- R jets with highest p_T are retained for further selection. In order to reduce the contamination from $t\bar{t}$ events, the leading jet is additionally required to have $p_T > 350$ GeV, thus ensuring that all top-quark decay products are contained in a single large- R jet with mass close to that of the top quark.

At least two track jets must be found by the ghost method [42] to be associated with each large- R jet. They are required to be consistent with the primary vertex of the event as well as to satisfy $p_T > 10$ GeV and $|\eta| < 2.5$.

Since high-mass resonances tend to produce jets that are more central than multijet background processes, the two large- R jets are required to have a separation $|\Delta\eta| < 1.7$.

Signal event candidates are selected if each of the large- R jets has a mass consistent with that of the Higgs boson. This is defined as for the resolved analysis in Eq. (2), where the small- R dijet mass is replaced by the large- R jet mass, requiring $X_{hh} < 1.6$. This requirement defines the signal region in the leading–subleading large- R jet mass plane.

Two samples of events are selected based on the number of b -tagged leading and subleading track jets associated with each large- R jet. They are referred to as the “3-tag” and the “4-tag” samples, and require exactly three or at least four track jets passing the b -tagging selection, respectively. In the 3-tag sample, the fourth jet is explicitly required to fail the b -tagging requirements to define orthogonal samples.

The signal region corresponds to the kinematic requirements illustrated by the inner region in Figure 5. The data shown in this figure are derived from a sample of events that satisfy all selection criteria except for having only two track jets that pass the b -tagging requirements, referred to as the “2-tag” sample. This sample is used to estimate the background contribution as described below.

The acceptance times efficiency for each stage of the boosted-analysis event selection is shown in Figure 6 for the G_{KK}^* and heavy scalar models. The requirement that at least two individual track jets be associated to the large- R jets becomes less efficient at high mass due to merging. The full selection for a G_{KK}^* resonance with a mass of 1000 GeV (2000 GeV) and $k/\bar{M}_{P1} = 1$ has an acceptance times efficiency of 9% (11%) in the 3-tag sample and 8% (5%) in the 4-tag sample.

5.2.2 Background estimation

As in the resolved analysis, the dominant source of background stems from multijet (80–90%) events and the rest is primarily due to $t\bar{t}$ production. The background estimation method generally follows the same approach as that described in Section 5.1.2. Differences are highlighted below.

The shape of the multijet background in both the 3-tag and 4-tag samples is derived from the 2-tag sample. Due to the large statistical uncertainty in the background prediction for dijet masses (m_{2J}) above 1500 GeV, an exponential fit to the data in the range between 900 and 2000 GeV is used to model the

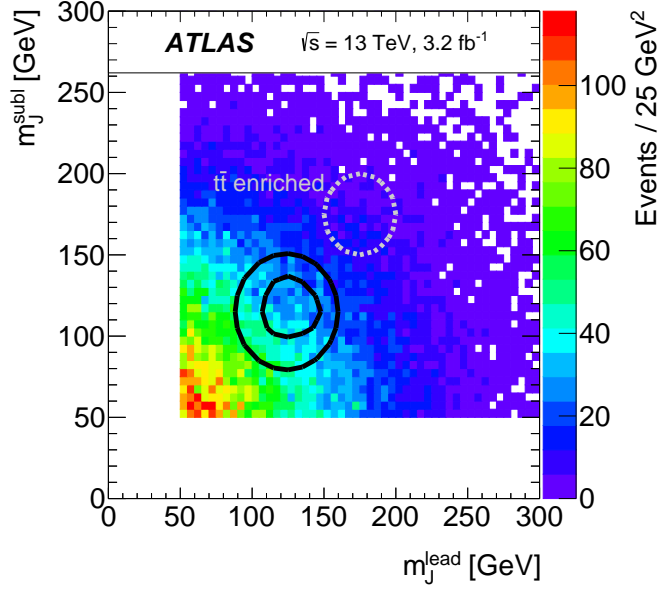


Figure 5: The m_j^{subl} vs. m_j^{lead} distribution for the 2-tag data sample used to model the multijet background in the boosted analysis. The signal region is the area surrounded by the inner black contour line, centered on $m_j^{\text{lead}} = 124$ GeV, $m_j^{\text{subl}} = 115$ GeV. The control region is the area inside the outer black contour line, excluding the signal region. The sideband region is the area outside the outer contour line. The kinematic region enriched in $t\bar{t}$ events is indicated by the dashed white contour line.

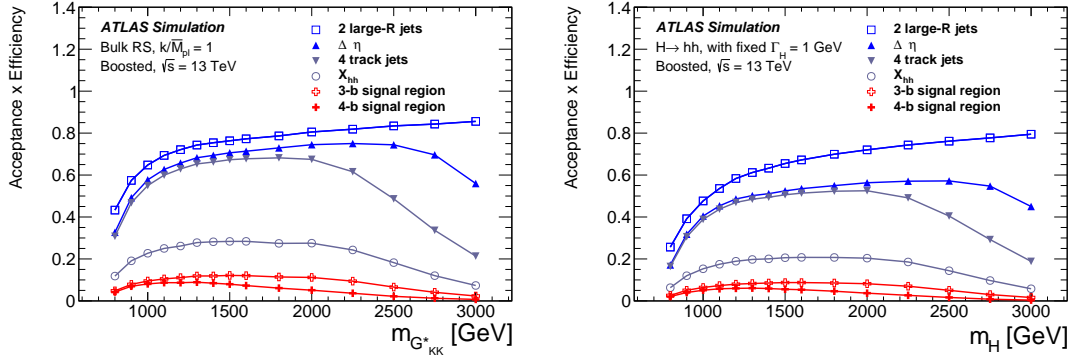


Figure 6: The selection efficiency as a function of resonance mass at each stage of the event selection for (left) $G_{\text{KK}}^* \rightarrow hh \rightarrow b\bar{b}b\bar{b}$ and (right) $H \rightarrow hh \rightarrow b\bar{b}b\bar{b}$ decays in the boosted analysis. The “2 large-R Jets” curve includes the requirements that the leading jet has $p_T > 350$ GeV and that the large-R jets have a mass greater than 50 GeV.

high-mass tail of the dijet distribution in the signal region. The estimated background yield in each signal region, $N_{\text{bkg}}^{3(4)\text{-tag}}$, is computed according to

$$N_{\text{bkg}}^{3(4)\text{-tag}} = \mu_{\text{Multijet}}^{3(4)\text{-tag}} N_{\text{Multijet}}^{2\text{-tag}} + \alpha_{t\bar{t}}^{3(4)\text{-tag}} N_{t\bar{t}}^{3(4)\text{-tag}} + N_{Z+\text{jets}}^{3(4)\text{-tag}}, \quad (5)$$

where $N_{\text{Multijet}}^{2\text{-tag}}$ is the number of multijet events in the 2-tag sample, $N_{t\bar{t}}^{3(4)\text{-tag}}$ and $N_Z^{3(4)\text{-tag}}$ are the numbers

of events predicted by the 3(4)-tag $t\bar{t}$ and Z+jets MC samples. The parameter $\mu_{\text{Multijet}}^{3(4)\text{-tag}}$ corresponds to the ratio of multijet event yields in the 3(4)-tag and 2-tag samples, as defined in Eq. (3), except for considering 3- or 4-tag events in the numerator. Finally, the parameter $\alpha_{t\bar{t}}^{3(4)\text{-tag}}$ is a scale factor designed to correct the $t\bar{t}$ event yield estimated from the MC simulation.

A sideband region defined by $\sqrt{(m_J^{\text{lead}} - 124 \text{ GeV})^2 + (m_J^{\text{subl}} - 115 \text{ GeV})^2} > 36 \text{ GeV}$ is used to measure $\mu_{\text{Multijet}}^{3(4)\text{-tag}}$ and $\alpha_{t\bar{t}}^{3(4)\text{-tag}}$ from the data. The background estimate is validated in a control region defined to be complementary to the sideband and signal regions.

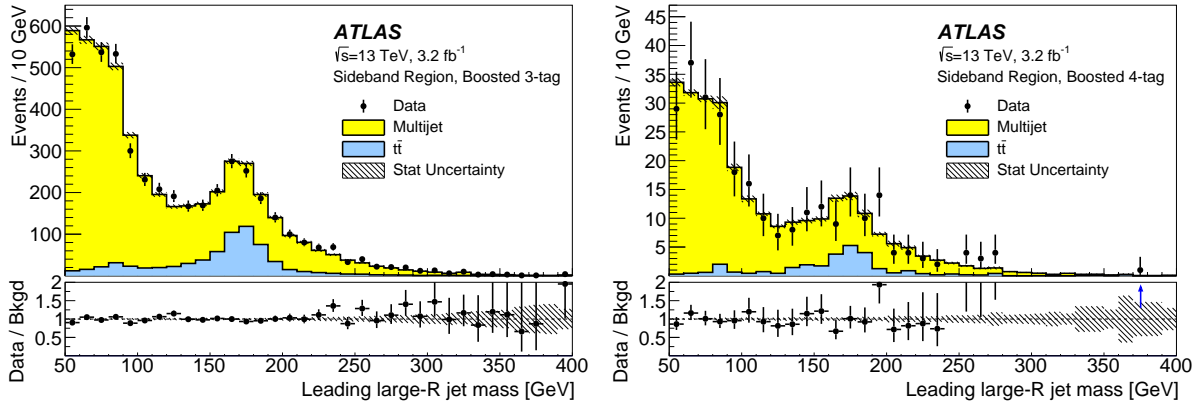


Figure 7: The leading large- R jet mass distribution in the hh sideband region for data (points) and background estimate (histograms) in the boosted analysis for events in the (left) 3-tag and (right) 4-tag categories. The shape of the multijet distributions is taken from the 2-tag region and is fitted to the data. The hatched bands represent the statistical uncertainty in the total background estimate.

Both $\mu_{\text{Multijet}}^{3(4)\text{-tag}}$ and $\alpha_{t\bar{t}}^{3(4)\text{-tag}}$ are extracted from a binned likelihood fit to the leading large- R jet mass distribution obtained in the sideband region of the 3(4)-tag sample, as shown in Figure 7. In this fit, the multijet distribution is extracted from the 2-tag sample, after subtraction of the $t\bar{t}$ and Z+jets contributions predicted by the MC simulation. The $t\bar{t}$ and Z+jets distributions in the sideband region of the 3(4)-tag sample are taken from the MC simulation. The resulting fit values and their statistical uncertainties for the 3-tag sample are $\mu_{\text{Multijet}}^{3\text{-tag}} = 0.160 \pm 0.003$ and $\alpha_{t\bar{t}}^{3\text{-tag}} = 1.02 \pm 0.09$, with a correlation coefficient of -0.60 between these two parameters. The corresponding values measured in the 4-tag sample are $\mu_{\text{Multijet}}^{4\text{-tag}} = 0.0091 \pm 0.0007$ and $\alpha_{t\bar{t}}^{4\text{-tag}} = 0.82 \pm 0.39$, with a correlation coefficient of -0.58 . A large anti-correlation is observed since the multijet and $t\bar{t}$ background contributions are constrained to add up to the total number of events in the sideband region of the 3-tag and 4-tag data samples.

The modeling of the background yield and kinematics is validated in the control region of the 3-tag and 4-tag samples. Good agreement is observed between the data and the predicted background in both the sideband and control regions of the 3-tag and 4-tag samples as shown in Table 5. The shapes of the $t\bar{t}$ kinematic distributions in the 4-tag signal region are extracted from the MC simulation in the 3-tag signal region due to the limited size of the 4-tag MC sample.

Sample (3-tag)	Sideband Region	Control Region
Multijet	4328 ± 27	607 ± 10
$t\bar{t}$	683.5 ± 8.1	99.6 ± 3.1
Z+jets	31.8 ± 3.7	7.7 ± 1.8
Total	5043 ± 28	715 ± 11
Data	5043	724
Sample (4-tag)	Sideband Region	Control Region
Multijet	247.4 ± 1.5	34.7 ± 0.6
$t\bar{t}$	28.4 ± 1.5	5.1 ± 0.7
Z+jets	3.4 ± 1.2	0.6 ± 0.5
Total	279.2 ± 2.5	40.3 ± 1.0
Data	279	45

Table 5: The number of events in data and predicted background events in the hh sideband and control regions of the 3-tag and 4-tag samples for the boosted analysis. The number of multijet and $t\bar{t}$ background events in the sideband regions are constrained by the number of observed events, as explained in the text. The uncertainties are purely statistical.

5.2.3 Systematic uncertainties

Evaluation of systematic uncertainties in the boosted analysis generally follows the same approach as that described in Section 5.1.3. Differences are highlighted here.

The large- R jet energy resolution and scale uncertainties as well as the jet mass resolution (JMR) and scale (JMS) uncertainties are derived in situ from 8 TeV pp collisions, taking into account MC simulation extrapolations for the different detector and beam conditions present in 8 and 13 TeV data-taking periods [49]. The uncertainty in the b -tagging efficiency for track jets is evaluated with the same method used for $R = 0.4$ calorimeter jets.

Systematic uncertainties in the normalization and shape of the background model are assessed in the control region. The background predictions in both the 3-tag and 4-tag control regions agree with the observed data to within statistical uncertainties. The statistical uncertainties in the control region yields are assigned as systematic uncertainties in the multijet background normalization. The uncertainty in the shape of the multijet background is assessed in the control region via a linear fit to the ratio of the distributions shown in Figure 8.

An additional uncertainty in the shape of the tail of the background prediction is assigned by fitting the 2-tag dijet mass distribution with a variety of empirical functions designed to model power-law behavior, as described in Ref. [50]. The largest difference between the exponential function predictions and those from alternative fit functions, considering the variation of the fitted parameters within their statistical uncertainties, is taken as a systematic uncertainty.

Relative systematic uncertainties in both the background and signal event yields are summarized in Table 6 for the 3-tag and 4-tag selections. For the background, the entry labeled ‘‘Statistical’’ corresponds to the statistical uncertainty from the fit to the leading large- R jet mass (see Section 5.2.2) used to

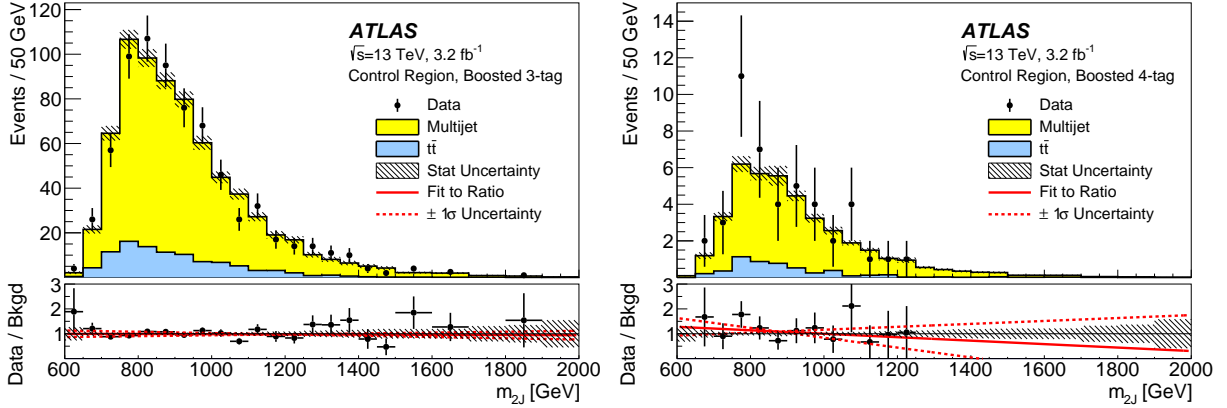


Figure 8: Dijet mass distribution in the control region for data (points) and background estimate (histograms) in the boosted analysis for events in the (left) 3-tag and (right) 4-tag categories. The hatched bands represent the statistical uncertainty in the total background estimate.

extract the multijet and $t\bar{t}$ background yields, taking the correlation between these yields into account. It also includes the $t\bar{t}$ modeling uncertainties and the statistical uncertainty associated with the data yield in the 2-tag sample. Uncertainties in the m_{2J} shape of the multijet and $t\bar{t}$ backgrounds are not listed in Table 6, as they do not affect the event yields, but are accounted for in the statistical analysis.

5.2.4 Event yields

The predicted number of background events in the 3-tag and 4-tag signal regions, the number of events observed in the data, and the predicted yield for a potential signal are reported in Table 7. One event in the 4-tag signal region, with a mass of 852 GeV, is in common with the resolved analysis. The dijet mass distribution in the signal region is shown in Figure 9. An excess of data is observed in the 3-tag signal region for $m_{2J} \sim 900$ GeV and in the range between 1600 and 2000 GeV. The significance of these excesses is evaluated below.

6 Results

The results from the resolved and boosted analyses are interpreted separately using the statistical procedure described in Ref. [1] and references therein. A test statistic based on the profile likelihood ratio [51] is used to test hypothesized values of μ , the global signal strength factor, separately for each model tested. The statistical analysis described below is performed using the data observed in the signal regions. The systematic uncertainties are treated as independent within each signal region using Gaussian or log-normal constraint terms in the definition of the likelihood function. In the boosted analysis, the data from the 3-tag and 4-tag signal regions are fitted simultaneously treating data-derived systematic uncertainties related to the multijet background estimate as uncorrelated and all other systematic uncertainties as fully correlated. In the case of the search for nonresonant hh production, only the number of events passing the final selection is used whereas the m_{4j} or m_{2J} distributions are used in the case of the search for hh resonances.

Source	Background	G_{KK}^* (1500 GeV)		H (1500 GeV)
		$k/\bar{M}_{\text{Pl}} = 1$	$k/\bar{M}_{\text{Pl}} = 2$	
Luminosity	–	5.0	5.0	5.0
3-tag				
JER	< 1	< 1	< 1	< 1
JES	2	< 1	< 1	< 1
JMR	1	12	12	11
JMS	5	14	13	17
b -tagging	1	23	22	23
Theoretical	–	3	3	3
Multijet	3	–	–	–
Statistical	2	1	1	1
Total	7	31	30	33
4-tag				
JER	< 1	< 1	< 1	< 1
JES	< 1	< 1	< 1	< 1
JMR	4	12	13	13
JMS	5	13	13	14
b -tagging	2	36	36	36
Theoretical	–	3	3	3
Multijet	14	–	–	–
Statistical	3	1	1	1
Total	15	42	42	43

Table 6: Summary of systematic uncertainties (expressed in percentage yield) in the total background and signal event yields in the 3-tag and 4-tag signal regions in the boosted analysis. Uncertainties are provided for a G_{KK}^* resonance mass of 1500 GeV with $k/\bar{M}_{\text{Pl}} = 1$ or 2, as well as for a spin-0 narrow-width H boson.

Sample	Signal Region (3-tag)	Signal Region (4-tag)
Multijet	235 ± 14	13.5 ± 2.4
$t\bar{t}$	48 ± 22	1.2 ± 1.0
Z +jets	2.0 ± 2.2	–
Total	285 ± 19	14.6 ± 2.4
Data	316	20
G_{KK}^* (1000 GeV), $k/\bar{M}_{\text{Pl}} = 1$	3.4 ± 0.9	2.9 ± 1.1

Table 7: The number of predicted background events in the hh 3-tag and 4-tag signal regions, compared to the data for the boosted analysis. Errors correspond to the total uncertainties in the predicted event yields. The yields for a 1000 GeV G_{KK}^* in the bulk RS model with $k/\bar{M}_{\text{Pl}} = 1$ is also given.

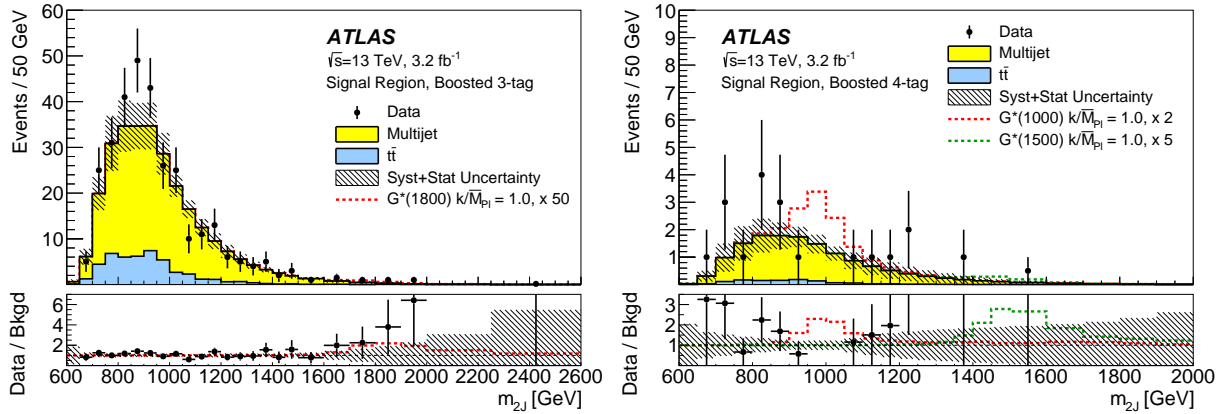


Figure 9: Dijet mass distribution in the hh signal region for data (points) and background estimate (histograms) in the boosted analysis for events in the (left) 3-tag and (right) 4-tag categories. The expected signal distributions for G_{KK}^* masses of 1000, 1500 and 1800 GeV are also shown. The uncertainty band includes both the statistical and systematic uncertainties in the background estimate.

6.1 Background-only hypothesis tests

In order to determine if there are any statistically significant local excesses in the data, a test of the background-only hypothesis ($\mu = 0$) is performed. The significance of an excess is quantified using the local p_0 , the probability that the background could produce a fluctuation greater than or equal to the excess observed in data. A global p_0 is also calculated for the most significant discrepancy, using background-only pseudoexperiments to derive a correction for the look-elsewhere effect across the mass range tested [52].

In the case of the resolved analysis, the largest deviation from the background-only hypothesis occurs around 900 GeV and is found to have a local significance less than 2σ .

In the case of the boosted analysis, the largest local deviation corresponds to a broad data excess in the 3-tag signal region starting at $m_{2J} \sim 1700$ GeV. The local significance of this excess is 2.0σ assuming a G_{KK}^* resonance with $k/\bar{M}_{Pl} = 1$.

6.2 Exclusion limits

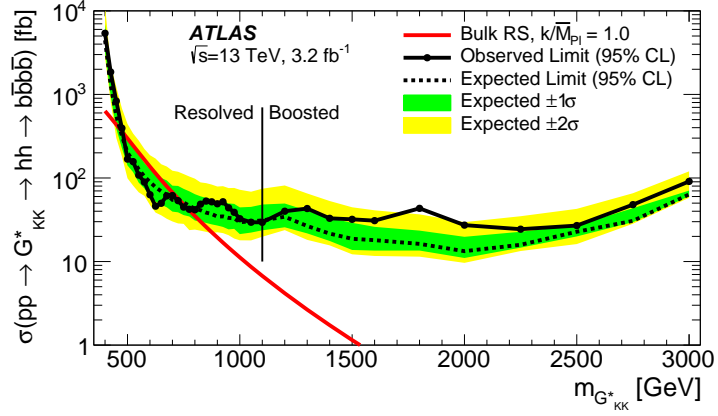
The data are used to set upper limits on the cross sections for the different benchmark signal processes. Exclusion limits are based on the value of the statistic CL_s [53], with a value of μ regarded as excluded at the 95% confidence level (CL) when CL_s is less than 5%.

The nonresonant search is performed using the resolved analysis, since it has better sensitivity than the boosted analysis. Using the SM hh nonresonant production as the signal model, the observed 95% CL upper limit is $\sigma(pp \rightarrow hh \rightarrow b\bar{b}b\bar{b}) < 1.22$ pb, a value to be compared with the inclusive SM prediction (as defined in Section 3) of $\sigma(pp \rightarrow hh \rightarrow b\bar{b}b\bar{b}) = 11.3_{-1.0}^{+0.9}$ fb.

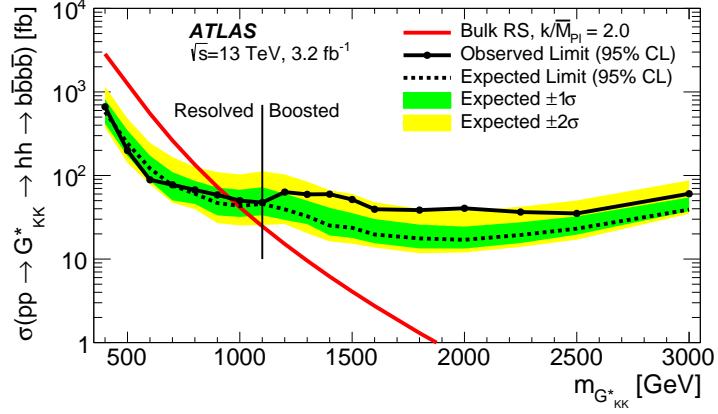
For the resonant Higgs-boson pair production search, the resolved and boosted analyses offer their best sensitivity in complementary resonance mass regions. The resolved analysis gives a more stringent expected exclusion limit for resonance masses up to (and including) 1100 GeV, while the boosted analysis offers better sensitivity beyond that mass. A simple combination of the separate exclusion limits from the resolved and boosted analyses is used. This is achieved by taking the limit from the analysis with the more stringent expected exclusion at each mass point for each of the signal models.

Figure 10 shows the combined 95% CL upper limits for three different resonances: a spin-2 G_{KK}^* in the bulk RS model with $k/\bar{M}_{\text{Pl}} = 1$ and 2, and a spin-0 narrow-width H boson. For the spin-2 G_{KK}^* with $k/\bar{M}_{\text{Pl}} = 1$, limits on $\sigma(pp \rightarrow G_{\text{KK}}^* \rightarrow hh \rightarrow b\bar{b}b\bar{b})$ are set in the range between 21 and 73 fb for masses between 600 and 3000 GeV. The corresponding range of limits for the G_{KK}^* resonance with $k/\bar{M}_{\text{Pl}} = 2$ is 34 to 86 fb. Although no events are observed at masses near 3000 GeV, the observed limit remains about 1σ weaker than the expected limit due to a substantial low-mass tail in the shape of high-mass resonance signals and the slight data excess observed at high mass. The cross-section limits for resonance masses below 600 GeV weaken substantially due to the lower acceptance times efficiency (see Figure 2) and the increased level of background. These cross-section upper limits translate into observed (expected) excluded mass ranges of 480–770 (470–735) GeV for $k/\bar{M}_{\text{Pl}} = 1$ and < 965 (< 995) GeV for $k/\bar{M}_{\text{Pl}} = 2$. The cross-section upper limits for the spin-0 narrow-width H boson are similar, with 95% CL exclusion limits ranging from 30 to 300 fb in the mass range between 500 and 3000 GeV.

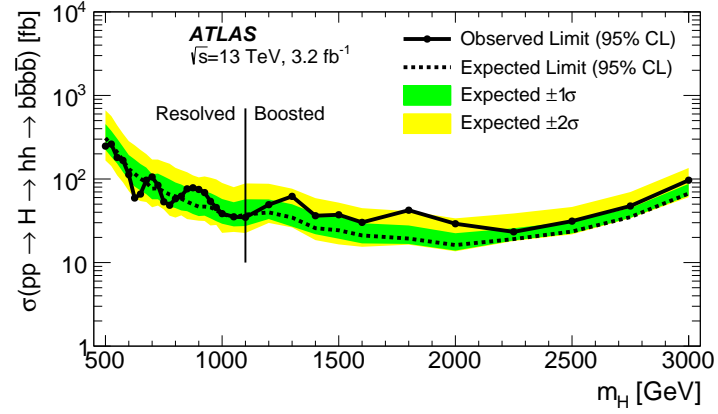
The search sensitivity of this analysis is similar to that achieved at $\sqrt{s} = 8$ TeV with 19.5 fb^{-1} for resonance masses below 1350 GeV but exceeds it above that mass by factors of 1.4 at 1500 GeV and 12 at 2000 GeV. The search has also been extended to resonance masses beyond 2000 GeV, up to 3000 GeV.



(a) Bulk RS, $k/\bar{M}_{\text{Pl}} = 1$



(b) Bulk RS, $k/\bar{M}_{\text{Pl}} = 2$



(c) Spin-0 narrow-width H boson

Figure 10: The expected and observed upper limit for $pp \rightarrow G_{\text{KK}}^* \rightarrow hh \rightarrow b\bar{b}b\bar{b}$ in the bulk RS model with (a) $k/\bar{M}_{\text{Pl}} = 1$ and (b) $k/\bar{M}_{\text{Pl}} = 2$, as well as (c) $pp \rightarrow H \rightarrow hh \rightarrow b\bar{b}b\bar{b}$ with fixed $\Gamma_H = 1$ GeV, at the 95% confidence level. The results of the resolved analysis are used up to a mass of 1100 GeV and those of the boosted analysis are used at higher mass where its expected sensitivity is higher. The red curves show the predicted cross sections as a function of resonance mass for the models considered.

7 Conclusions

A search for both resonant and nonresonant production of pairs of Standard Model Higgs bosons has been carried out in the dominant $b\bar{b}b\bar{b}$ channel with 3.2 fb^{-1} of pp collision data collected by ATLAS during the 2015 run of the LHC at $\sqrt{s} = 13 \text{ TeV}$. Results are reported for the resolved analysis with each $h \rightarrow b\bar{b}$ decay reconstructed as two separate b -tagged jets and for the boosted analysis with each $h \rightarrow b\bar{b}$ decay reconstructed as a single large-radius jet associated with two small-radius track jets and a minimum of three b -tags for the hh system. No significant data excess is observed above the estimated background consisting mainly of multijet and $t\bar{t}$ events. Upper limits on the production cross section times branching ratio to the $b\bar{b}b\bar{b}$ final state are set for spin-0 and spin-2 resonances with values ranging between 24 and 113 fb (at 95% CL) for resonance masses in the range between 600 and 3000 GeV. For nonresonant production, the upper limit is 1.22 pb (at 95% CL). The search sensitivity of this analysis exceeds that achieved at $\sqrt{s} = 8 \text{ TeV}$ with 19.5 fb^{-1} for resonance masses above 1350 GeV. Furthermore, the search has been extended to cover the mass range between 2000 and 3000 GeV.

Acknowledgements

We thank CERN for the very successful operation of the LHC, as well as the support staff from our institutions without whom ATLAS could not be operated efficiently.

We acknowledge the support of ANPCyT, Argentina; YerPhI, Armenia; ARC, Australia; BMWFW and FWF, Austria; ANAS, Azerbaijan; SSTC, Belarus; CNPq and FAPESP, Brazil; NSERC, NRC and CFI, Canada; CERN; CONICYT, Chile; CAS, MOST and NSFC, China; COLCIENCIAS, Colombia; MSMT CR, MPO CR and VSC CR, Czech Republic; DNRF and DNSRC, Denmark; IN2P3-CNRS, CEA-DSM/IRFU, France; GNSF, Georgia; BMBF, HGF, and MPG, Germany; GSRT, Greece; RGC, Hong Kong SAR, China; ISF, I-CORE and Benoziyo Center, Israel; INFN, Italy; MEXT and JSPS, Japan; CNRST, Morocco; FOM and NWO, Netherlands; RCN, Norway; MNiSW and NCN, Poland; FCT, Portugal; MNE/IFA, Romania; MES of Russia and NRC KI, Russian Federation; JINR; MESTD, Serbia; MSSR, Slovakia; ARRS and MIZŠ, Slovenia; DST/NRF, South Africa; MINECO, Spain; SRC and Wallenberg Foundation, Sweden; SERI, SNSF and Cantons of Bern and Geneva, Switzerland; MOST, Taiwan; TAEK, Turkey; STFC, United Kingdom; DOE and NSF, United States of America. In addition, individual groups and members have received support from BCKDF, the Canada Council, CANARIE, CRC, Compute Canada, FQRNT, and the Ontario Innovation Trust, Canada; EPLANET, ERC, FP7, Horizon 2020 and Marie Skłodowska-Curie Actions, European Union; Investissements d’Avenir Labex and Idex, ANR, Région Auvergne and Fondation Partager le Savoir, France; DFG and AvH Foundation, Germany; Herakleitos, Thales and Aristeia programmes co-financed by EU-ESF and the Greek NSRF; BSF, GIF and Minerva, Israel; BRF, Norway; Generalitat de Catalunya, Generalitat Valenciana, Spain; the Royal Society and Leverhulme Trust, United Kingdom.

The crucial computing support from all WLCG partners is acknowledged gratefully, in particular from CERN, the ATLAS Tier-1 facilities at TRIUMF (Canada), NDGF (Denmark, Norway, Sweden), CC-IN2P3 (France), KIT/GridKA (Germany), INFN-CNAF (Italy), NL-T1 (Netherlands), PIC (Spain), ASGC (Taiwan), RAL (UK) and BNL (USA), the Tier-2 facilities worldwide and large non-WLCG resource providers. Major contributors of computing resources are listed in Ref. [54].

References

- [1] ATLAS Collaboration, *Observation of a new particle in the search for the Standard Model Higgs boson with the ATLAS detector at the LHC*, *Phys. Lett. B* **716** (2012) 1, arXiv:1207.7214 [hep-ex].
- [2] CMS Collaboration, *Observation of a new boson at a mass of 125 GeV with the CMS experiment at the LHC*, *Phys. Lett. B* **716** (2012) 30, arXiv:1207.7235 [hep-ex].
- [3] K. Agashe et al., *Warped Gravitons at the LHC and Beyond*, *Phys. Rev. D* **76** (2007) 036006, arXiv:hep-ph/0701186.
- [4] L. Fitzpatrick et al., *Searching for the Kaluza-Klein graviton in bulk RS models*, *JHEP* **09** (2007) 013, arXiv:hep-ph/0701150.
- [5] G. Branco et al., *Theory and phenomenology of two-Higgs-doublet models*, *Phys. Rept.* **516** (2012) 1, arXiv:1106.0034 [hep-ph].
- [6] G. D. Kribs and A. Martin, *Enhanced di-Higgs production through light colored scalars*, *Phys. Rev. D* **86** (2012) 095023, arXiv:1207.4496 [hep-ph].
- [7] R. Gröber and M. Mühlleitner, *Composite Higgs Boson Pair Production at the LHC*, *JHEP* **06** (2011) 020, arXiv:1012.1562 [hep-ph].
- [8] R. Contino et al., *Anomalous Couplings in Double Higgs Production*, *JHEP* **08** (2012) 154, arXiv:1205.5444 [hep-ph].
- [9] ATLAS Collaboration, *Search for Higgs boson pair production in the $b\bar{b}b\bar{b}$ final state from pp collisions at $\sqrt{s} = 8$ TeV with the ATLAS detector*, *Eur. Phys. J. C* **75** (2015) 412, arXiv:1506.00285 [hep-ex].
- [10] CMS Collaboration, *Search for resonant pair production of Higgs bosons decaying to two bottom quark–antiquark pairs in proton–proton collisions at 8 TeV*, *Phys. Lett. B* **749** (2015) 560–582, arXiv:1503.04114 [hep-ex].
- [11] ATLAS Collaboration, *Searches for Higgs boson pair production in the $hh \rightarrow b\bar{b}\tau\tau, \gamma\gamma WW^*, \gamma\gamma b\bar{b}, b\bar{b}b\bar{b}$ channels with the ATLAS detector*, *Phys. Rev. D* **92** (2015) 092004, arXiv:1509.04670 [hep-ex].
- [12] CMS Collaboration, *Searches for a heavy scalar boson H decaying to a pair of 125 GeV Higgs bosons hh or for a heavy pseudoscalar boson A decaying to Zh , in the final states with h to tautau*, *Phys. Lett. B* **755** (2016) 217–244, arXiv:1510.01181 [hep-ex].
- [13] ATLAS Collaboration, *Search For Higgs Boson Pair Production in the $\gamma\gamma b\bar{b}$ Final State using pp Collision Data at $\sqrt{s} = 8$ TeV from the ATLAS Detector*, *Phys. Rev. Lett.* **114** (2015) 081802, arXiv:1406.5053 [hep-ex].
- [14] CMS Collaboration, *Search for two Higgs bosons in final states containing two photons and two bottom quarks* (2016), arXiv:1603.06896 [hep-ex].
- [15] ATLAS Collaboration, *The ATLAS Experiment at the CERN Large Hadron Collider*, *JINST* **3** (2008) S08003.
- [16] ATLAS Collaboration, *ATLAS Insertable B-Layer Technical Design Report*, ATLAS-TDR-19 (2010), URL: <http://cds.cern.ch/record/1291633>, ATLAS Insertable B-Layer Technical Design Report Addendum, ATLAS-TDR-19-ADD-1 (2012), URL: <http://cds.cern.ch/record/1451888>.

- [17] ATLAS Collaboration, *Improved luminosity determination in pp collisions at $\sqrt{s} = 7$ TeV using the ATLAS detector at the LHC*, *Eur. Phys. J. C* **73** (2013) 2518, arXiv:1302.4393 [hep-ex].
- [18] ATLAS Collaboration, *Performance of b-Jet Identification in the ATLAS Experiment*, *JINST* **11** (2016) P04008, arXiv:1512.01094 [hep-ex].
- [19] J. Alwall et al., *The automated computation of tree-level and next-to-leading order differential cross sections, and their matching to parton shower simulations*, *JHEP* **07** (2014) 079, arXiv:1405.0301 [hep-ph].
- [20] R. D. Ball et al., *Parton distributions with LHC data*, *Nucl. Phys. B* **867** (2013) 244, arXiv:1207.1303 [hep-ph].
- [21] T. Sjöstrand, S. Mrenna and P. Z. Skands, *A Brief Introduction to PYTHIA 8.1*, *Comput. Phys. Commun.* **178** (2008) 852, arXiv:0710.3820 [hep-ph].
- [22] ATLAS Collaboration, *ATLAS Run 1 Pythia8 tunes*, ATL-PHYS-PUB-2014-021 (2014), URL: <http://cds.cern.ch/record/1966419>.
- [23] H.-L. Lai et al., *New parton distributions for collider physics*, *Phys. Rev. D* **82** (2010) 074024, arXiv:1007.2241 [hep-ph].
- [24] M. Bahr et al., *Herwig++ Physics and Manual*, *Eur. Phys. J. C* **58** (2008) 639–707, arXiv:0803.0883 [hep-ph].
- [25] P. M. Nadolsky et al., *Implications of CTEQ global analysis for collider observables*, *Phys. Rev. D* **78** (2008) 013004, arXiv:0802.0007 [hep-ph].
- [26] S. Gieseke, C. Rohr and A. Siodmok, *Colour reconnections in Herwig++*, *Eur. Phys. J. C* **72** (2012) 2225, arXiv:1206.0041 [hep-ph].
- [27] S. Dawson, S. Dittmaier and M. Spira, *Neutral Higgs boson pair production at hadron colliders: QCD corrections*, *Phys. Rev. D* **58** (1998) 115012, arXiv:hep-ph/9805244.
- [28] T. Plehn, M. Spira and P. Zerwas, *Pair production of neutral Higgs particles in gluon-gluon collisions*, *Nucl. Phys. B* **479** (1996) 46, [Erratum: *Nucl. Phys. B* **531** (1998) 655], arXiv:hep-ph/9603205.
- [29] LHC Higgs Cross Section Working Group, *Current recommendations for di-Higgs cross-sections* (2016), URL: <http://twiki.cern.ch/twiki/bin/view/LHCPhysics/LHCHXSWG>.
- [30] T. Sjöstrand, S. Mrenna and P. Z. Skands, *PYTHIA 6.4 Physics and Manual*, *JHEP* **05** (2006) 026, arXiv:hep-ph/0603175.
- [31] P. Z. Skands, *Tuning Monte Carlo Generators: The Perugia Tunes*, *Phys. Rev. D* **82** (2010) 074018, arXiv:1005.3457 [hep-ph].
- [32] M. Czakon and A. Mitov, *Top++: A Program for the Calculation of the Top-Pair Cross-Section at Hadron Colliders* (2011), arXiv:1112.5675 [hep-ph].
- [33] D. J. Lange, *The EvtGen particle decay simulation package*, *Nucl. Instrum. Meth. A* **462** (2001) 152.
- [34] S. Agostinelli et al., *GEANT4: A Simulation toolkit*, *Nucl. Instrum. Meth. A* **506** (2003) 250–303.
- [35] ATLAS Collaboration, *The ATLAS Simulation Infrastructure*, *Eur. Phys. J. C* **70** (2010) 823–874, arXiv:1005.4568 [physics.ins-det].
- [36] M. Cacciari, G. P. Salam and G. Soyez, *The anti- k_t jet clustering algorithm*, *JHEP* **04** (2008) 063, arXiv:0802.1189 [hep-ph].

- [37] ATLAS Collaboration, *Jet energy measurement with the ATLAS detector in proton-proton collisions at $\sqrt{s} = 7$ TeV*, *Eur. Phys. J. C* **73** (2013) 2304, arXiv:1112.6426 [hep-ex].
- [38] ATLAS Collaboration, *Tagging and suppression of pileup jets with the ATLAS detector*, ATLAS-CONF-2014-018 (2014), URL: <http://cds.cern.ch/record/1700870>.
- [39] D. Krohn, J. Thaler and L.-T. Wang, *Jet Trimming*, *JHEP* **02** (2010) 084, arXiv:0912.1342 [hep-ph].
- [40] S. D. Ellis and D. E. Soper, *Successive combination jet algorithm for hadron collisions*, *Phys. Rev. D* **48** (1993) 3160, arXiv:hep-ph/9305266.
- [41] ATLAS Collaboration, *Expected Performance of Boosted Higgs ($\rightarrow b\bar{b}$) Boson Identification with the ATLAS Detector at $\sqrt{s} = 13$ TeV*, ATL-PHYS-PUB-2015-035 (2015), URL: <http://cds.cern.ch/record/2042155>.
- [42] M. Cacciari and G. P. Salam, *Pileup subtraction using jet areas*, *Phys. Lett. B* **659** (2008) 119, arXiv:0707.1378 [hep-ph].
- [43] ATLAS Collaboration, *Expected performance of the ATLAS b-tagging algorithms in Run-2*, ATL-PHYS-PUB-2015-022 (2015), URL: <http://cds.cern.ch/record/2037697>.
- [44] ATLAS Collaboration, *Muon reconstruction performance of the ATLAS detector in proton-proton collision data at $\sqrt{s}=13$ TeV* (2016), arXiv:1603.05598 [hep-ex].
- [45] ATLAS Collaboration, *Jet Calibration and Systematic Uncertainties for Jets Reconstructed in the ATLAS Detector at $\sqrt{s} = 13$ TeV*, ATL-PHYS-PUB-2015-015 (2015), URL: <http://cds.cern.ch/record/2037613>.
- [46] ATLAS Collaboration, *Jet energy measurement and its systematic uncertainty in proton-proton collisions at $\sqrt{s} = 7$ TeV with the ATLAS detector*, *Eur. Phys. J. C* **75** (2015) 17, arXiv:1406.0076 [hep-ex].
- [47] ATLAS Collaboration, *Calibration of b-tagging using dileptonic top pair events in a combinatorial likelihood approach with the ATLAS experiment*, ATLAS-CONF-2014-004, 2014, URL: <http://cdsweb.cern.ch/record/1664335>.
- [48] ATLAS Collaboration, *Identification of Boosted, Hadronically Decaying W Bosons and Comparisons with ATLAS Data Taken at $\sqrt{s} = 8$ TeV*, *Eur. Phys. J. C* **76** (2016) 154, arXiv:1510.05821 [hep-ex].
- [49] ATLAS Collaboration, *Identification of boosted, hadronically-decaying W and Z bosons in $\sqrt{s} = 13$ TeV Monte Carlo Simulations for ATLAS*, ATL-PHYS-PUB-2015-033 (2015), URL: <http://cds.cern.ch/record/2041461>.
- [50] ATLAS Collaboration, *Search for strong gravity in multijet final states produced in pp collisions at $\sqrt{s} = 13$ TeV using the ATLAS detector at the LHC*, *JHEP* **03** (2016) 026, arXiv:1512.02586 [hep-ex].
- [51] G. Cowan et al., *Asymptotic formulae for likelihood-based tests of new physics*, *Eur. Phys. J. C* **71** (2011) 1554, arXiv:1007.1727 [physics.data-an], Erratum: *Eur. Phys. J. C* **73** (2013) 2501.
- [52] E. Gross and O. Vitells, *Trial factors or the look elsewhere effect in high energy physics*, *Eur. Phys. J. C* **70** (2010) 525–530, arXiv:1005.1891 [physics.data-an].
- [53] A. L. Read, *Presentation of search results: The $CL(s)$ technique*, *J. Phys. G* **28** (2002) 2693.
- [54] ATLAS Collaboration, *ATLAS Computing Acknowledgements 2016-2017* (2016), URL: <http://cds.cern.ch/record/2202407>.

The ATLAS Collaboration

M. Aaboud^{136d}, G. Aad⁸⁷, B. Abbott¹¹⁴, J. Abdallah⁶⁵, O. Abdinov¹², B. Abeloos¹¹⁸, R. Aben¹⁰⁸, O.S. AbouZeid¹³⁸, N.L. Abraham¹⁵⁰, H. Abramowicz¹⁵⁴, H. Abreu¹⁵³, R. Abreu¹¹⁷, Y. Abulaiti^{147a,147b}, B.S. Acharya^{164a,164b,a}, L. Adamczyk^{40a}, D.L. Adams²⁷, J. Adelman¹⁰⁹, S. Adomeit¹⁰¹, T. Adye¹³², A.A. Affolder⁷⁶, T. Agatonovic-Jovin¹⁴, J. Agricola⁵⁶, J.A. Aguilar-Saavedra^{127a,127f}, S.P. Ahlen²⁴, F. Ahmadov^{67,b}, G. Aielli^{134a,134b}, H. Akerstedt^{147a,147b}, T.P.A. Åkesson⁸³, A.V. Akimov⁹⁷, G.L. Alberghi^{22a,22b}, J. Albert¹⁶⁹, S. Albrand⁵⁷, M.J. Alconada Verzini⁷³, M. Aleksa³², I.N. Aleksandrov⁶⁷, C. Alexa^{28b}, G. Alexander¹⁵⁴, T. Alexopoulos¹⁰, M. Alhroob¹¹⁴, M. Aliev^{75a,75b}, G. Alimonti^{93a}, J. Alison³³, S.P. Alkire³⁷, B.M.M. Allbrooke¹⁵⁰, B.W. Allen¹¹⁷, P.P. Allport¹⁹, A. Aloisio^{105a,105b}, A. Alonso³⁸, F. Alonso⁷³, C. Alpigiani¹³⁹, M. Alstаты⁸⁷, B. Alvarez Gonzalez³², D. Álvarez Piqueras¹⁶⁷, M.G. Alvigi^{105a,105b}, B.T. Amadio¹⁶, K. Amako⁶⁸, Y. Amaral Coutinho^{26a}, C. Amelung²⁵, D. Amidei⁹¹, S.P. Amor Dos Santos^{127a,127c}, A. Amorim^{127a,127b}, S. Amoroso³², G. Amundsen²⁵, C. Anastopoulos¹⁴⁰, L.S. Ancu⁵¹, N. Andari¹⁰⁹, T. Andeen¹¹, C.F. Anders^{60b}, G. Anders³², J.K. Anders⁷⁶, K.J. Anderson³³, A. Andreazza^{93a,93b}, V. Andrei^{60a}, S. Angelidakis⁹, I. Angelozzi¹⁰⁸, P. Anger⁴⁶, A. Angerami³⁷, F. Anghinolfi³², A.V. Anisenkov^{110,c}, N. Anjos¹³, A. Annovi^{125a,125b}, M. Antonelli⁴⁹, A. Antonov^{99,*}, F. Anulli^{133a}, M. Aoki⁶⁸, L. Aperio Bella¹⁹, G. Arabidze⁹², Y. Arai⁶⁸, J.P. Araque^{127a}, A.T.H. Arce⁴⁷, F.A. Arduh⁷³, J-F. Arguin⁹⁶, S. Argyropoulos⁶⁵, M. Arik^{20a}, A.J. Armbruster¹⁴⁴, L.J. Armitage⁷⁸, O. Arnaez³², H. Arnold⁵⁰, M. Arratia³⁰, O. Arslan²³, A. Artamonov⁹⁸, G. Artoni¹²¹, S. Artz⁸⁵, S. Asai¹⁵⁶, N. Asbah⁴⁴, A. Ashkenazi¹⁵⁴, B. Åsman^{147a,147b}, L. Asquith¹⁵⁰, K. Assamagan²⁷, R. Astalos^{145a}, M. Atkinson¹⁶⁶, N.B. Atlay¹⁴², K. Augsten¹²⁹, G. Avolio³², B. Axen¹⁶, M.K. Ayoub¹¹⁸, G. Azuelos^{96,d}, M.A. Baak³², A.E. Baas^{60a}, M.J. Baca¹⁹, H. Bachacou¹³⁷, K. Bachas^{75a,75b}, M. Backes³², M. Backhaus³², P. Bagiacchi^{133a,133b}, P. Bagnaia^{133a,133b}, Y. Bai^{35a}, J.T. Baines¹³², O.K. Baker¹⁷⁶, E.M. Baldin^{110,c}, P. Balek¹³⁰, T. Balestri¹⁴⁹, F. Balli¹³⁷, W.K. Balunas¹²³, E. Banas⁴¹, Sw. Banerjee^{173,e}, A.A.E. Bannoura¹⁷⁵, L. Barak³², E.L. Barberio⁹⁰, D. Barberis^{52a,52b}, M. Barbero⁸⁷, T. Barillari¹⁰², T. Barklow¹⁴⁴, N. Barlow³⁰, S.L. Barnes⁸⁶, B.M. Barnett¹³², R.M. Barnett¹⁶, Z. Barnovska⁵, A. Baroncelli^{135a}, G. Barone²⁵, A.J. Barr¹²¹, L. Barranco Navarro¹⁶⁷, F. Barreiro⁸⁴, J. Barreiro Guimarães da Costa^{35a}, R. Bartoldus¹⁴⁴, A.E. Barton⁷⁴, P. Bartos^{145a}, A. Basalae¹²⁴, A. Bassalat¹¹⁸, R.L. Bates⁵⁵, S.J. Batista¹⁵⁹, J.R. Batley³⁰, M. Battaglia¹³⁸, M. Baucé^{133a,133b}, F. Bauer¹³⁷, H.S. Bawa^{144,f}, J.B. Beacham¹¹², M.D. Beattie⁷⁴, T. Beau⁸², P.H. Beauchemin¹⁶², P. Bechtel²³, H.P. Beck^{18,g}, K. Becker¹²¹, M. Becker⁸⁵, M. Beckingham¹⁷⁰, C. Becot¹¹¹, A.J. Beddall^{20e}, A. Beddall^{20b}, V.A. Bednyakov⁶⁷, M. Bedognetti¹⁰⁸, C.P. Bee¹⁴⁹, L.J. Beemster¹⁰⁸, T.A. Beermann³², M. Begel²⁷, J.K. Behr⁴⁴, C. Belanger-Champagne⁸⁹, A.S. Bell⁸⁰, G. Bella¹⁵⁴, L. Bellagamba^{22a}, A. Bellerive³¹, M. Bellomo⁸⁸, K. Belotskiy⁹⁹, O. Beltramello³², N.L. Belyaev⁹⁹, O. Benary¹⁵⁴, D. Benchekroun^{136a}, M. Bender¹⁰¹, K. Bendtz^{147a,147b}, N. Benekos¹⁰, Y. Benhammou¹⁵⁴, E. Benhar Nocchioli¹⁷⁶, J. Benitez⁶⁵, D.P. Benjamin⁴⁷, J.R. Bensinger²⁵, S. Bentvelsen¹⁰⁸, L. Beresford¹²¹, M. Beretta⁴⁹, D. Berge¹⁰⁸, E. Bergeaas Kuutmann¹⁶⁵, N. Berger⁵, J. Beringer¹⁶, S. Berlendis⁵⁷, N.R. Bernard⁸⁸, C. Bernius¹¹¹, F.U. Bernlochner²³, T. Berry⁷⁹, P. Berta¹³⁰, C. Bertella⁸⁵, G. Bertoli^{147a,147b}, F. Bertolucci^{125a,125b}, I.A. Bertram⁷⁴, C. Bertsche⁴⁴, D. Bertsche¹¹⁴, G.J. Besjes³⁸, O. Bessidskaia Bylund^{147a,147b}, M. Bessner⁴⁴, N. Besson¹³⁷, C. Betancourt⁵⁰, S. Bethke¹⁰², A.J. Bevan⁷⁸, W. Bhimji¹⁶, R.M. Bianchi¹²⁶, L. Bianchini²⁵, M. Bianco³², O. Biebel¹⁰¹, D. Biedermann¹⁷, R. Bielski⁸⁶, N.V. Biesuz^{125a,125b}, M. Biglietti^{135a}, J. Bilbao De Mendizabal⁵¹, H. Bilokon⁴⁹, M. Bindi⁵⁶, S. Binet¹¹⁸, A. Bingul^{20b}, C. Bini^{133a,133b}, S. Biondi^{22a,22b}, D.M. Bjergaard⁴⁷, C.W. Black¹⁵¹, J.E. Black¹⁴⁴, K.M. Black²⁴, D. Blackburn¹³⁹, R.E. Blair⁶, J.-B. Blanchard¹³⁷, J.E. Blanco⁷⁹, T. Blazek^{145a}, I. Bloch⁴⁴, C. Blocker²⁵, W. Blum^{85,*}, U. Blumenschein⁵⁶, S. Blunier^{34a},

G.J. Bobbink¹⁰⁸, V.S. Bobrovnikov^{110,c}, S.S. Bocchetta⁸³, A. Bocci⁴⁷, C. Bock¹⁰¹, M. Boehler⁵⁰, D. Boerner¹⁷⁵, J.A. Bogaerts³², D. Bogavac¹⁴, A.G. Bogdanchikov¹¹⁰, C. Bohm^{147a}, V. Boisvert⁷⁹, P. Bokan¹⁴, T. Bold^{40a}, A.S. Boldyrev^{164a,164c}, M. Bomben⁸², M. Bona⁷⁸, M. Boonekamp¹³⁷, A. Borisov¹³¹, G. Borissov⁷⁴, J. Bortfeldt¹⁰¹, D. Bortoletto¹²¹, V. Bortolotto^{62a,62b,62c}, K. Bos¹⁰⁸, D. Boscherini^{22a}, M. Bosman¹³, J.D. Bossio Sola²⁹, J. Boudreau¹²⁶, J. Bouffard², E.V. Bouhova-Thacker⁷⁴, D. Boumediene³⁶, C. Bourdarios¹¹⁸, S.K. Boutle⁵⁵, A. Boveia³², J. Boyd³², I.R. Boyko⁶⁷, J. Bracinik¹⁹, A. Brandt⁸, G. Brandt⁵⁶, O. Brandt^{60a}, U. Bratzler¹⁵⁷, B. Brau⁸⁸, J.E. Brau¹¹⁷, H.M. Braun^{175,*}, W.D. Breaden Madden⁵⁵, K. Brendlinger¹²³, A.J. Brennan⁹⁰, L. Brenner¹⁰⁸, R. Brenner¹⁶⁵, S. Bressler¹⁷², T.M. Bristow⁴⁸, D. Britton⁵⁵, D. Britzger⁴⁴, F.M. Brochu³⁰, I. Brock²³, R. Brock⁹², G. Brooijmans³⁷, T. Brooks⁷⁹, W.K. Brooks^{34b}, J. Brosamer¹⁶, E. Brost¹¹⁷, J.H. Broughton¹⁹, P.A. Bruckman de Renstrom⁴¹, D. Bruncko^{145b}, R. Bruneliere⁵⁰, A. Bruni^{22a}, G. Bruni^{22a}, L.S. Bruni¹⁰⁸, B.H. Brunt³⁰, M. Bruschi^{22a}, N. Brusino²³, P. Bryant³³, L. Bryngemark⁸³, T. Buanes¹⁵, Q. Buat¹⁴³, P. Buchholz¹⁴², A.G. Buckley⁵⁵, I.A. Budagov⁶⁷, F. Buehrer⁵⁰, M.K. Bugge¹²⁰, O. Bulekov⁹⁹, D. Bullock⁸, H. Burckhart³², S. Burdin⁷⁶, C.D. Burgard⁵⁰, B. Burghgrave¹⁰⁹, K. Burka⁴¹, S. Burke¹³², I. Burmeister⁴⁵, E. Busato³⁶, D. Büscher⁵⁰, V. Büscher⁸⁵, P. Bussey⁵⁵, J.M. Butler²⁴, C.M. Buttar⁵⁵, J.M. Butterworth⁸⁰, P. Butti¹⁰⁸, W. Buttinger²⁷, A. Buzatu⁵⁵, A.R. Buzykaev^{110,c}, S. Cabrera Urbán¹⁶⁷, D. Caforio¹²⁹, V.M. Cairo^{39a,39b}, O. Cakir^{4a}, N. Calace⁵¹, P. Calafiura¹⁶, A. Calandri⁸⁷, G. Calderini⁸², P. Calfayan¹⁰¹, L.P. Caloba^{26a}, D. Calvet³⁶, S. Calvet³⁶, T.P. Calvet⁸⁷, R. Camacho Toro³³, S. Camarda³², P. Camarri^{134a,134b}, D. Cameron¹²⁰, R. Caminal Armadans¹⁶⁶, C. Camincher⁵⁷, S. Campana³², M. Campanelli⁸⁰, A. Camplani^{93a,93b}, A. Campoverde¹⁴², V. Canale^{105a,105b}, A. Canepa^{160a}, M. Cano Bret^{35e}, J. Cantero¹¹⁵, R. Cantrill^{127a}, T. Cao⁴², M.D.M. Capeans Garrido³², I. Caprini^{28b}, M. Caprini^{28b}, M. Capua^{39a,39b}, R. Caputo⁸⁵, R.M. Carbone³⁷, R. Cardarelli^{134a}, F. Cardillo⁵⁰, I. Carli¹³⁰, T. Carli³², G. Carlino^{105a}, L. Carminati^{93a,93b}, S. Caron¹⁰⁷, E. Carquin^{34b}, G.D. Carrillo-Montoya³², J.R. Carter³⁰, J. Carvalho^{127a,127c}, D. Casadei¹⁹, M.P. Casado^{13,h}, M. Casolino¹³, D.W. Casper¹⁶³, E. Castaneda-Miranda^{146a}, R. Castelijm¹⁰⁸, A. Castelli¹⁰⁸, V. Castillo Gimenez¹⁶⁷, N.F. Castro^{127a,i}, A. Catinaccio³², J.R. Catmore¹²⁰, A. Cattai³², J. Caudron⁸⁵, V. Cavaliere¹⁶⁶, E. Cavallaro¹³, D. Cavalli^{93a}, M. Cavalli-Sforza¹³, V. Cavasinni^{125a,125b}, F. Ceradini^{135a,135b}, L. Cerda Alberich¹⁶⁷, B.C. Cerio⁴⁷, A.S. Cerqueira^{26b}, A. Cerri¹⁵⁰, L. Cerrito⁷⁸, F. Cerutti¹⁶, M. Cerv³², A. Cervelli¹⁸, S.A. Cetin^{20d}, A. Chafaq^{136a}, D. Chakraborty¹⁰⁹, S.K. Chan⁵⁹, Y.L. Chan^{62a}, P. Chang¹⁶⁶, J.D. Chapman³⁰, D.G. Charlton¹⁹, A. Chatterjee⁵¹, C.C. Chau¹⁵⁹, C.A. Chavez Barajas¹⁵⁰, S. Che¹¹², S. Cheatham⁷⁴, A. Chegwiddden⁹², S. Chekanov⁶, S.V. Chekulaev^{160a}, G.A. Chelkov^{67,j}, M.A. Chelstowska⁹¹, C. Chen⁶⁶, H. Chen²⁷, K. Chen¹⁴⁹, S. Chen^{35c}, S. Chen¹⁵⁶, X. Chen^{35f}, Y. Chen⁶⁹, H.C. Cheng⁹¹, H.J. Cheng^{35a}, Y. Cheng³³, A. Cheplakov⁶⁷, E. Cheremushkina¹³¹, R. Cherkaoui El Moursli^{136e}, V. Chernyatin^{27,*}, E. Cheu⁷, L. Chevalier¹³⁷, V. Chiarella⁴⁹, G. Chiarelli^{125a,125b}, G. Chiodini^{75a}, A.S. Chisholm¹⁹, A. Chitan^{28b}, M.V. Chizhov⁶⁷, K. Choi⁶³, A.R. Chomont³⁶, S. Chouridou⁹, B.K.B. Chow¹⁰¹, V. Christodoulou⁸⁰, D. Chromek-Burckhart³², J. Chudoba¹²⁸, A.J. Chuinard⁸⁹, J.J. Chwastowski⁴¹, L. Chytka¹¹⁶, G. Ciapetti^{133a,133b}, A.K. Ciftci^{4a}, D. Cinca⁵⁵, V. Cindro⁷⁷, I.A. Cioara²³, A. Ciocio¹⁶, F. Ciroto^{105a,105b}, Z.H. Citron¹⁷², M. Citterio^{93a}, M. Ciubancan^{28b}, A. Clark⁵¹, B.L. Clark⁵⁹, M.R. Clark³⁷, P.J. Clark⁴⁸, R.N. Clarke¹⁶, C. Clement^{147a,147b}, Y. Coadou⁸⁷, M. Cobal^{164a,164c}, A. Coccaro⁵¹, J. Cochran⁶⁶, L. Coffey²⁵, L. Colasurdo¹⁰⁷, B. Cole³⁷, A.P. Colijn¹⁰⁸, J. Collot⁵⁷, T. Colombo³², G. Compostella¹⁰², P. Conde Muiño^{127a,127b}, E. Coniavitis⁵⁰, S.H. Connell^{146b}, I.A. Connelly⁷⁹, V. Consorti⁵⁰, S. Constantinescu^{28b}, G. Conti³², F. Conventi^{105a,k}, M. Cooke¹⁶, B.D. Cooper⁸⁰, A.M. Cooper-Sarkar¹²¹, K.J.R. Cormier¹⁵⁹, T. Cornelissen¹⁷⁵, M. Corradi^{133a,133b}, F. Corriveau^{89,l}, A. Corso-Radu¹⁶³, A. Cortes-Gonzalez¹³, G. Cortiana¹⁰², G. Costa^{93a}, M.J. Costa¹⁶⁷, D. Costanzo¹⁴⁰, G. Cottin³⁰, G. Cowan⁷⁹, B.E. Cox⁸⁶, K. Cranmer¹¹¹, S.J. Crawley⁵⁵, G. Cree³¹, S. Crépe-Renaudin⁵⁷, F. Crescioli⁸², W.A. Cribbs^{147a,147b}, M. Crispin Ortuzar¹²¹, M. Cristinziani²³, V. Croft¹⁰⁷, G. Crosetti^{39a,39b},

T. Cuhadar Donszelmann¹⁴⁰, J. Cummings¹⁷⁶, M. Curatolo⁴⁹, J. Cúth⁸⁵, C. Cuthbert¹⁵¹, H. Czirr¹⁴², P. Czodrowski³, G. D'amen^{22a,22b}, S. D'Auria⁵⁵, M. D'Onofrio⁷⁶, M.J. Da Cunha Sargedas De Sousa^{127a,127b}, C. Da Via⁸⁶, W. Dabrowski^{40a}, T. Dado^{145a}, T. Dai⁹¹, O. Dale¹⁵, F. Dallaire⁹⁶, C. Dallapiccola⁸⁸, M. Dam³⁸, J.R. Dandoy³³, N.P. Dang⁵⁰, A.C. Daniells¹⁹, N.S. Dann⁸⁶, M. Danninger¹⁶⁸, M. Dano Hoffmann¹³⁷, V. Dao⁵⁰, G. Darbo^{52a}, S. Darmora⁸, J. Dassoulas³, A. Dattagupta⁶³, W. Davey²³, C. David¹⁶⁹, T. Davidek¹³⁰, M. Davies¹⁵⁴, P. Davison⁸⁰, E. Dawe⁹⁰, I. Dawson¹⁴⁰, R.K. Daya-Ishmukhametova⁸⁸, K. De⁸, R. de Asmundis^{105a}, A. De Benedetti¹¹⁴, S. De Castro^{22a,22b}, S. De Cecco⁸², N. De Groot¹⁰⁷, P. de Jong¹⁰⁸, H. De la Torre⁸⁴, F. De Lorenzi⁶⁶, A. De Maria⁵⁶, D. De Pedis^{133a}, A. De Salvo^{133a}, U. De Sanctis¹⁵⁰, A. De Santo¹⁵⁰, J.B. De Vivie De Regie¹¹⁸, W.J. Dearnaley⁷⁴, R. Debbe²⁷, C. Debenedetti¹³⁸, D.V. Dedovich⁶⁷, N. Dehghanian³, I. Deigaard¹⁰⁸, M. Del Gaudio^{39a,39b}, J. Del Peso⁸⁴, T. Del Prete^{125a,125b}, D. Delgove¹¹⁸, F. Deliot¹³⁷, C.M. Delitzsch⁵¹, M. Deliyergiyev⁷⁷, A. Dell'Acqua³², L. Dell'Asta²⁴, M. Dell'Orso^{125a,125b}, M. Della Pietra^{105a,k}, D. della Volpe⁵¹, M. Delmastro⁵, P.A. Delsart⁵⁷, C. Deluca¹⁰⁸, D.A. DeMarco¹⁵⁹, S. Demers¹⁷⁶, M. Demichev⁶⁷, A. Demilly⁸², S.P. Denisov¹³¹, D. Denysiuk¹³⁷, D. Derendarz⁴¹, J.E. Derkaoui^{136d}, F. Derue⁸², P. Dervan⁷⁶, K. Desch²³, C. Deterre⁴⁴, K. Dette⁴⁵, P.O. Deviveiros³², A. Dewhurst¹³², S. Dhaliwal²⁵, A. Di Ciaccio^{134a,134b}, L. Di Ciaccio⁵, W.K. Di Clemente¹²³, C. Di Donato^{133a,133b}, A. Di Girolamo³², B. Di Girolamo³², B. Di Micco^{135a,135b}, R. Di Nardo³², A. Di Simone⁵⁰, R. Di Sipio¹⁵⁹, D. Di Valentino³¹, C. Diaconu⁸⁷, M. Diamond¹⁵⁹, F.A. Dias⁴⁸, M.A. Diaz^{34a}, E.B. Diehl⁹¹, J. Dietrich¹⁷, S. Diglio⁸⁷, A. Dimitrievska¹⁴, J. Dingfelder²³, P. Dita^{28b}, S. Dita^{28b}, F. Dittus³², F. Djama⁸⁷, T. Djobava^{53b}, J.I. Djuvsland^{60a}, M.A.B. do Vale^{26c}, D. Dobos³², M. Dobre^{28b}, C. Doglioni⁸³, T. Dohmae¹⁵⁶, J. Dolejsi¹³⁰, Z. Dolezal¹³⁰, B.A. Dolgoshein^{99,*}, M. Donadelli^{26d}, S. Donati^{125a,125b}, P. Dondero^{122a,122b}, J. Donini³⁶, J. Dopke¹³², A. Doria^{105a}, M.T. Dova⁷³, A.T. Doyle⁵⁵, E. Drechsler⁵⁶, M. Dris¹⁰, Y. Du^{35d}, J. Duarte-Campderros¹⁵⁴, E. Duchovni¹⁷², G. Duckeck¹⁰¹, O.A. Ducu^{96,m}, D. Duda¹⁰⁸, A. Dudarev³², E.M. Duffield¹⁶, L. Duflot¹¹⁸, L. Duguid⁷⁹, M. Dührssen³², M. Dumancic¹⁷², M. Dunford^{60a}, H. Duran Yildiz^{4a}, M. Düren⁵⁴, A. Durglishvili^{53b}, D. Duschinger⁴⁶, B. Dutta⁴⁴, M. Dyndal⁴⁴, C. Eckardt⁴⁴, K.M. Ecker¹⁰², R.C. Edgar⁹¹, N.C. Edwards⁴⁸, T. Eifert³², G. Eigen¹⁵, K. Einsweiler¹⁶, T. Ekelof¹⁶⁵, M. El Kacimi^{136c}, V. Ellajosyula⁸⁷, M. Ellert¹⁶⁵, S. Elles⁵, F. Ellinghaus¹⁷⁵, A.A. Elliot¹⁶⁹, N. Ellis³², J. Elmsheuser²⁷, M. Elsing³², D. Emelianov¹³², Y. Enari¹⁵⁶, O.C. Endner⁸⁵, M. Endo¹¹⁹, J.S. Ennis¹⁷⁰, J. Erdmann⁴⁵, A. Ereditato¹⁸, G. Ernis¹⁷⁵, J. Ernst², M. Ernst²⁷, S. Errede¹⁶⁶, E. Ertel⁸⁵, M. Escalier¹¹⁸, H. Esch⁴⁵, C. Escobar¹²⁶, B. Esposito⁴⁹, A.I. Etienne¹³⁷, E. Etzion¹⁵⁴, H. Evans⁶³, A. Ezhilov¹²⁴, F. Fabbri^{22a,22b}, L. Fabbri^{22a,22b}, G. Facini³³, R.M. Fakhruddinov¹³¹, S. Falciano^{133a}, R.J. Falla⁸⁰, J. Faltova³², Y. Fang^{35a}, M. Fanti^{93a,93b}, A. Farbin⁸, A. Farilla^{135a}, C. Farina¹²⁶, T. Farooque¹³, S. Farrell¹⁶, S.M. Farrington¹⁷⁰, P. Farthouat³², F. Fassi^{136c}, P. Fassnacht³², D. Fassouliotis⁹, M. Fauci Giannelli⁷⁹, A. Favareto^{52a,52b}, W.J. Fawcett¹²¹, L. Fayard¹¹⁸, O.L. Fedin^{124,n}, W. Fedorko¹⁶⁸, S. Feigl¹²⁰, L. Feligioni⁸⁷, C. Feng^{35d}, E.J. Feng³², H. Feng⁹¹, A.B. Fenyuk¹³¹, L. Feremenga⁸, P. Fernandez Martinez¹⁶⁷, S. Fernandez Perez¹³, J. Ferrando⁵⁵, A. Ferrari¹⁶⁵, P. Ferrari¹⁰⁸, R. Ferrari^{122a}, D.E. Ferreira de Lima^{60b}, A. Ferrer¹⁶⁷, D. Ferrere⁵¹, C. Ferretti⁹¹, A. Ferretto Parodi^{52a,52b}, F. Fiedler⁸⁵, A. Filipčič⁷⁷, M. Filipuzzi⁴⁴, F. Filthaut¹⁰⁷, M. Fincke-Keeler¹⁶⁹, K.D. Finelli¹⁵¹, M.C.N. Fiolhais^{127a,127c}, L. Fiorini¹⁶⁷, A. Firan⁴², A. Fischer², C. Fischer¹³, J. Fischer¹⁷⁵, W.C. Fisher⁹², N. Flaschel⁴⁴, I. Fleck¹⁴², P. Fleischmann⁹¹, G.T. Fletcher¹⁴⁰, R.R.M. Fletcher¹²³, T. Flick¹⁷⁵, A. Floderus⁸³, L.R. Flores Castillo^{62a}, M.J. Flowerdew¹⁰², G.T. Forcolin⁸⁶, A. Formica¹³⁷, A. Forti⁸⁶, A.G. Foster¹⁹, D. Fournier¹¹⁸, H. Fox⁷⁴, S. Fracchia¹³, P. Francavilla⁸², M. Franchini^{22a,22b}, D. Francis³², L. Franconi¹²⁰, M. Franklin⁵⁹, M. Frate¹⁶³, M. Fraternali^{122a,122b}, D. Freeborn⁸⁰, S.M. Fressard-Batraneau³², F. Friedrich⁴⁶, D. Froidevaux³², J.A. Frost¹²¹, C. Fukunaga¹⁵⁷, E. Fullana Torregrosa⁸⁵, T. Fusayasu¹⁰³, J. Fuster¹⁶⁷, C. Gabaldon⁵⁷, O. Gabizon¹⁷⁵, A. Gabrielli^{22a,22b}, A. Gabrielli¹⁶, G.P. Gach^{40a}, S. Gadatsch³², S. Gadomski⁵¹, G. Gagliardi^{52a,52b}, L.G. Gagnon⁹⁶, P. Gagnon⁶³, C. Galea¹⁰⁷, B. Galhardo^{127a,127c},

E.J. Gallas¹²¹, B.J. Gallop¹³², P. Gallus¹²⁹, G. Galster³⁸, K.K. Gan¹¹², J. Gao^{35b,87}, Y. Gao⁴⁸,
 Y.S. Gao^{144,f}, F.M. Garay Walls⁴⁸, C. García¹⁶⁷, J.E. García Navarro¹⁶⁷, M. Garcia-Sciveres¹⁶,
 R.W. Gardner³³, N. Garelli¹⁴⁴, V. Garonne¹²⁰, A. Gascon Bravo⁴⁴, C. Gatti⁴⁹, A. Gaudiello^{52a,52b},
 G. Gaudio^{122a}, B. Gaur¹⁴², L. Gauthier⁹⁶, I.L. Gavrilenko⁹⁷, C. Gay¹⁶⁸, G. Gaycken²³, E.N. Gazis¹⁰,
 Z. Gecse¹⁶⁸, C.N.P. Gee¹³², Ch. Geich-Gimbel²³, M. Geisen⁸⁵, M.P. Geisler^{60a}, C. Gemme^{52a},
 M.H. Genest⁵⁷, C. Geng^{35b,o}, S. Gentile^{133a,133b}, S. George⁷⁹, D. Gerbaudo¹³, A. Gershon¹⁵⁴,
 S. Ghasemi¹⁴², H. Ghazlane^{136b}, M. Ghneimat²³, B. Giacobbe^{22a}, S. Giagu^{133a,133b}, P. Giannetti^{125a,125b},
 B. Gibbard²⁷, S.M. Gibson⁷⁹, M. Gignac¹⁶⁸, M. Gilchriese¹⁶, T.P.S. Gillam³⁰, D. Gillberg³¹,
 G. Gilles¹⁷⁵, D.M. Gingrich^{3,d}, N. Giokaris⁹, M.P. Giordani^{164a,164c}, F.M. Giorgi^{22a}, F.M. Giorgi¹⁷,
 P.F. Giraud¹³⁷, P. Giromini⁵⁹, D. Giugni^{93a}, F. Giuli¹²¹, C. Giuliani¹⁰², M. Giulini^{60b}, B.K. Gjelsten¹²⁰,
 S. Gkaitatzis¹⁵⁵, I. Gkialas¹⁵⁵, E.L. Gkougkousis¹¹⁸, L.K. Gladilin¹⁰⁰, C. Glasman⁸⁴, J. Glatzer⁵⁰,
 P.C.F. Glaysher⁴⁸, A. Glazov⁴⁴, M. Goblirsch-Kolb¹⁰², J. Godlewski⁴¹, S. Goldfarb⁹¹, T. Golling⁵¹,
 D. Golubkov¹³¹, A. Gomes^{127a,127b,127d}, R. Gonçalo^{127a}, J. Goncalves Pinto Firmino Da Costa¹³⁷,
 G. Gonella⁵⁰, L. Gonella¹⁹, A. Gongadze⁶⁷, S. González de la Hoz¹⁶⁷, G. Gonzalez Parra¹³,
 S. Gonzalez-Sevilla⁵¹, L. Goossens³², P.A. Gorbounov⁹⁸, H.A. Gordon²⁷, I. Gorelov¹⁰⁶, B. Gorini³²,
 E. Gorini^{75a,75b}, A. Gorišek⁷⁷, E. Gornicki⁴¹, A.T. Goshaw⁴⁷, C. Gössling⁴⁵, M.I. Gostkin⁶⁷,
 C.R. Goudet¹¹⁸, D. Goujdami^{136c}, A.G. Goussiou¹³⁹, N. Govender^{146b,p}, E. Gozani¹⁵³, L. Graber⁵⁶,
 I. Grabowska-Bold^{40a}, P.O.J. Gradin⁵⁷, P. Grafström^{22a,22b}, J. Gramling⁵¹, E. Gramstad¹²⁰,
 S. Grancagnolo¹⁷, V. Gratchev¹²⁴, P.M. Gravila^{28e}, H.M. Gray³², E. Graziani^{135a}, Z.D. Greenwood^{81,q},
 C. Grefe²³, K. Gregersen⁸⁰, I.M. Gregor⁴⁴, P. Grenier¹⁴⁴, K. Grevtsov⁵, J. Griffiths⁸, A.A. Grillo¹³⁸,
 K. Grimm⁷⁴, S. Grinstein^{13,r}, Ph. Gris³⁶, J.-F. Grivaz¹¹⁸, S. Groh⁸⁵, J.P. Grohs⁴⁶, E. Gross¹⁷²,
 J. Grosse-Knetter⁵⁶, G.C. Grossi⁸¹, Z.J. Grout¹⁵⁰, L. Guan⁹¹, W. Guan¹⁷³, J. Guenther¹²⁹, F. Guescini⁵¹,
 D. Guest¹⁶³, O. Gueta¹⁵⁴, E. Guido^{52a,52b}, T. Guillemin⁵, S. Guindon², U. Gul⁵⁵, C. Gumpert³²,
 J. Guo^{35e}, Y. Guo^{35b,o}, S. Gupta¹²¹, G. Gustavino^{133a,133b}, P. Gutierrez¹¹⁴, N.G. Gutierrez Ortiz⁸⁰,
 C. Gutsche⁴⁶, C. Guyot¹³⁷, C. Gwenlan¹²¹, C.B. Gwilliam⁷⁶, A. Haas¹¹¹, C. Haber¹⁶, H.K. Hadavand⁸,
 N. Haddad^{136e}, A. Hadeef⁸⁷, P. Haefner²³, S. Hageböck²³, Z. Hajduk⁴¹, H. Hakobyan^{177,*}, M. Haleem⁴⁴,
 J. Haley¹¹⁵, G. Halladjian⁹², G.D. Hallewell⁸⁷, K. Hamacher¹⁷⁵, P. Hamal¹¹⁶, K. Hamano¹⁶⁹,
 A. Hamilton^{146a}, G.N. Hamity¹⁴⁰, P.G. Hamnett⁴⁴, L. Han^{35b}, K. Hanagaki^{68,s}, K. Hanawa¹⁵⁶,
 M. Hance¹³⁸, B. Haney¹²³, P. Hanke^{60a}, R. Hanna¹³⁷, J.B. Hansen³⁸, J.D. Hansen³⁸, M.C. Hansen²³,
 P.H. Hansen³⁸, K. Hara¹⁶¹, A.S. Hard¹⁷³, T. Harenberg¹⁷⁵, F. Hariri¹¹⁸, S. Harkusha⁹⁴,
 R.D. Harrington⁴⁸, P.F. Harrison¹⁷⁰, F. Hartjes¹⁰⁸, N.M. Hartmann¹⁰¹, M. Hasegawa⁶⁹, Y. Hasegawa¹⁴¹,
 A. Hasib¹¹⁴, S. Hassani¹³⁷, S. Haug¹⁸, R. Hauser⁹², L. Hauswald⁴⁶, M. Havranek¹²⁸, C.M. Hawkes¹⁹,
 R.J. Hawkings³², D. Hayden⁹², C.P. Hays¹²¹, J.M. Hays⁷⁸, H.S. Hayward⁷⁶, S.J. Haywood¹³²,
 S.J. Head¹⁹, T. Heck⁸⁵, V. Hedberg⁸³, L. Heelan⁸, S. Heim¹²³, T. Heim¹⁶, B. Heinemann¹⁶,
 J.J. Heinrich¹⁰¹, L. Heinrich¹¹¹, C. Heinz⁵⁴, J. Hejbal¹²⁸, L. Helary²⁴, S. Hellman^{147a,147b}, C. Helsens³²,
 J. Henderson¹²¹, R.C.W. Henderson⁷⁴, Y. Heng¹⁷³, S. Henkelmann¹⁶⁸, A.M. Henriques Correia³²,
 S. Henrot-Versille¹¹⁸, G.H. Herbert¹⁷, Y. Hernández Jiménez¹⁶⁷, G. Herten⁵⁰, R. Hertenberger¹⁰¹,
 L. Hervas³², G.G. Hesketh⁸⁰, N.P. Hessey¹⁰⁸, J.W. Hetherly⁴², R. Hickling⁷⁸, E. Higón-Rodríguez¹⁶⁷,
 E. Hill¹⁶⁹, J.C. Hill³⁰, K.H. Hiller⁴⁴, S.J. Hillier¹⁹, I. Hinchliffe¹⁶, E. Hines¹²³, R.R. Hinman¹⁶,
 M. Hirose¹⁵⁸, D. Hirschbuehl¹⁷⁵, J. Hobbs¹⁴⁹, N. Hod^{160a}, M.C. Hodgkinson¹⁴⁰, P. Hodgson¹⁴⁰,
 A. Hoecker³², M.R. Hoferkamp¹⁰⁶, F. Hoenig¹⁰¹, D. Hohn²³, T.R. Holmes¹⁶, M. Homann⁴⁵,
 T.M. Hong¹²⁶, B.H. Hooberman¹⁶⁶, W.H. Hopkins¹¹⁷, Y. Horii¹⁰⁴, A.J. Horton¹⁴³, J.-Y. Hostachy⁵⁷,
 S. Hou¹⁵², A. Hoummada^{136a}, J. Howarth⁴⁴, M. Hrabovsky¹¹⁶, I. Hristova¹⁷, J. Hrivnac¹¹⁸,
 T. Hryn'ova⁵, A. Hrynevich⁹⁵, C. Hsu^{146c}, P.J. Hsu^{152,t}, S.-C. Hsu¹³⁹, D. Hu³⁷, Q. Hu^{35b}, Y. Huang⁴⁴,
 Z. Hubacek¹²⁹, F. Hubaut⁸⁷, F. Huegging²³, T.B. Huffman¹²¹, E.W. Hughes³⁷, G. Hughes⁷⁴,
 M. Huhtinen³², T.A. Hülsing⁸⁵, P. Huo¹⁴⁹, N. Huseynov^{67,b}, J. Huston⁹², J. Huth⁵⁹, G. Iacobucci⁵¹,
 G. Iakovidis²⁷, I. Ibragimov¹⁴², L. Iconomidou-Fayard¹¹⁸, E. Ideal¹⁷⁶, Z. Idrissi^{136e}, P. Iengo³²,

O. Igonkina^{108,u}, T. Iizawa¹⁷¹, Y. Ikegami⁶⁸, M. Ikeno⁶⁸, Y. Ilchenko^{11,v}, D. Iliadis¹⁵⁵, N. Ilic¹⁴⁴, T. Ince¹⁰², G. Introzzi^{122a,122b}, P. Ioannou^{9,*}, M. Iodice^{135a}, K. Iordanidou³⁷, V. Ippolito⁵⁹, M. Ishino⁷⁰, M. Ishitsuka¹⁵⁸, R. Ishmukhametov¹¹², C. Issever¹²¹, S. Istin^{20a}, F. Ito¹⁶¹, J.M. Iturbe Ponce⁸⁶, R. Iuppa^{134a,134b}, W. Iwanski⁴¹, H. Iwasaki⁶⁸, J.M. Izen⁴³, V. Izzo^{105a}, S. Jabbar³, B. Jackson¹²³, M. Jackson⁷⁶, P. Jackson¹, V. Jain², K.B. Jakobi⁸⁵, K. Jakobs⁵⁰, S. Jakobsen³², T. Jakoubek¹²⁸, D.O. Jamin¹¹⁵, D.K. Jana⁸¹, E. Jansen⁸⁰, R. Jansky⁶⁴, J. Janssen²³, M. Janus⁵⁶, G. Jarlskog⁸³, N. Javadov^{67,b}, T. Javůrek⁵⁰, F. Jeanneau¹³⁷, L. Jeanty¹⁶, J. Jejelava^{53a,w}, G.-Y. Jeng¹⁵¹, D. Jennens⁹⁰, P. Jenni^{50,x}, J. Jentzsch⁴⁵, C. Jeske¹⁷⁰, S. Jézéquel⁵, H. Ji¹⁷³, J. Jia¹⁴⁹, H. Jiang⁶⁶, Y. Jiang^{35b}, S. Jiggins⁸⁰, J. Jimenez Pena¹⁶⁷, S. Jin^{35a}, A. Jinaru^{28b}, O. Jinnouchi¹⁵⁸, P. Johansson¹⁴⁰, K.A. Johns⁷, W.J. Johnson¹³⁹, K. Jon-And^{147a,147b}, G. Jones¹⁷⁰, R.W.L. Jones⁷⁴, S. Jones⁷, T.J. Jones⁷⁶, J. Jongmanns^{60a}, P.M. Jorge^{127a,127b}, J. Jovicevic^{160a}, X. Ju¹⁷³, A. Juste Rozas^{13,r}, M.K. Köhler¹⁷², A. Kaczmarska⁴¹, M. Kado¹¹⁸, H. Kagan¹¹², M. Kagan¹⁴⁴, S.J. Kahn⁸⁷, E. Kajomovitz⁴⁷, C.W. Kalderon¹²¹, A. Kaluza⁸⁵, S. Kama⁴², A. Kamenshchikov¹³¹, N. Kanaya¹⁵⁶, S. Kaneti³⁰, L. Kanjir⁷⁷, V.A. Kantserov⁹⁹, J. Kanzaki⁶⁸, B. Kaplan¹¹¹, L.S. Kaplan¹⁷³, A. Kapliy³³, D. Kar^{146c}, K. Karakostas¹⁰, A. Karamaoun³, N. Karastathis¹⁰, M.J. Kareem⁵⁶, E. Karentzos¹⁰, M. Karnevskiy⁸⁵, S.N. Karpov⁶⁷, Z.M. Karpova⁶⁷, K. Karthik¹¹¹, V. Kartvelishvili⁷⁴, A.N. Karyukhin¹³¹, K. Kasahara¹⁶¹, L. Kashif¹⁷³, R.D. Kass¹¹², A. Kastanas¹⁵, Y. Kataoka¹⁵⁶, C. Kato¹⁵⁶, A. Katre⁵¹, J. Katzy⁴⁴, K. Kawagoe⁷², T. Kawamoto¹⁵⁶, G. Kawamura⁵⁶, S. Kazama¹⁵⁶, V.F. Kazanin^{110,c}, R. Keeler¹⁶⁹, R. Kehoe⁴², J.S. Keller⁴⁴, J.J. Kempster⁷⁹, K. Kentaro¹⁰⁴, H. Keoshkerian¹⁵⁹, O. Kepka¹²⁸, B.P. Kerševan⁷⁷, S. Kersten¹⁷⁵, R.A. Keyes⁸⁹, F. Khalil-zada¹², A. Khanov¹¹⁵, A.G. Kharlamov^{110,c}, T.J. Khoo⁵¹, V. Khovanskiy⁹⁸, E. Khramov⁶⁷, J. Khubua^{53b,y}, S. Kido⁶⁹, H.Y. Kim⁸, S.H. Kim¹⁶¹, Y.K. Kim³³, N. Kimura¹⁵⁵, O.M. Kind¹⁷, B.T. King⁷⁶, M. King¹⁶⁷, S.B. King¹⁶⁸, J. Kirk¹³², A.E. Kiryunin¹⁰², T. Kishimoto⁶⁹, D. Kisielewska^{40a}, F. Kiss⁵⁰, K. Kiuchi¹⁶¹, O. Kivernyk¹³⁷, E. Kladiva^{145b}, M.H. Klein³⁷, M. Klein⁷⁶, U. Klein⁷⁶, K. Kleinknecht⁸⁵, P. Klimek^{147a,147b}, A. Klimentov²⁷, R. Klingenberg⁴⁵, J.A. Klinger¹⁴⁰, T. Klioutchnikova³², E.-E. Kluge^{60a}, P. Kluit¹⁰⁸, S. Kluth¹⁰², J. Knapik⁴¹, E. Kneringer⁶⁴, E.B.F.G. Knoops⁸⁷, A. Knue⁵⁵, A. Kobayashi¹⁵⁶, D. Kobayashi¹⁵⁸, T. Kobayashi¹⁵⁶, M. Kobel⁴⁶, M. Kocian¹⁴⁴, P. Kodys¹³⁰, T. Koffas³¹, E. Koffeman¹⁰⁸, T. Koi¹⁴⁴, H. Kolanoski¹⁷, M. Kolb^{60b}, I. Koletsou⁵, A.A. Komar^{97,*}, Y. Komori¹⁵⁶, T. Kondo⁶⁸, N. Kondrashova⁴⁴, K. Köneke⁵⁰, A.C. König¹⁰⁷, T. Kono^{68,z}, R. Konoplich^{111,aa}, N. Konstantinidis⁸⁰, R. Kopeliansky⁶³, S. Koperny^{40a}, L. Köpke⁸⁵, A.K. Kopp⁵⁰, K. Korcyl⁴¹, K. Kordas¹⁵⁵, A. Korn⁸⁰, A.A. Korol^{110,c}, I. Korolkov¹³, E.V. Korolkova¹⁴⁰, O. Kortner¹⁰², S. Kortner¹⁰², T. Kosek¹³⁰, V.V. Kostyukhin²³, A. Kotwal⁴⁷, A. Kourkouveli-Charalampidi¹⁵⁵, C. Kourkouvelis⁹, V. Kouskoura²⁷, A.B. Kowalewska⁴¹, R. Kowalewski¹⁶⁹, T.Z. Kowalski^{40a}, C. Kozakai¹⁵⁶, W. Kozanecki¹³⁷, A.S. Kozhin¹³¹, V.A. Kramarenko¹⁰⁰, G. Kramberger⁷⁷, D. Krasnopevtsev⁹⁹, M.W. Krasny⁸², A. Krasznahorkay³², J.K. Kraus²³, A. Kravchenko²⁷, M. Kretz^{60c}, J. Kretzschmar⁷⁶, K. Kreutzfeldt⁵⁴, P. Krieger¹⁵⁹, K. Krizka³³, K. Kroeninger⁴⁵, H. Kroha¹⁰², J. Kroll¹²³, J. Kroseberg²³, J. Krstic¹⁴, U. Kruchonak⁶⁷, H. Krüger²³, N. Krumnack⁶⁶, A. Kruse¹⁷³, M.C. Kruse⁴⁷, M. Kruskal²⁴, T. Kubota⁹⁰, H. Kucuk⁸⁰, S. Kudah^{4b}, J.T. Kuechler¹⁷⁵, S. Kuehn⁵⁰, A. Kugel^{60c}, F. Kuger¹⁷⁴, A. Kuhl¹³⁸, T. Kuhl⁴⁴, V. Kukhtin⁶⁷, R. Kukla¹³⁷, Y. Kulchitsky⁹⁴, S. Kuleshov^{34b}, M. Kuna^{133a,133b}, T. Kunigo⁷⁰, A. Kupco¹²⁸, H. Kurashige⁶⁹, Y.A. Kurochkin⁹⁴, V. Kus¹²⁸, E.S. Kuwertz¹⁶⁹, M. Kuze¹⁵⁸, J. Kvita¹¹⁶, T. Kwan¹⁶⁹, D. Kyriazopoulos¹⁴⁰, A. La Rosa¹⁰², J.L. La Rosa Navarro^{26d}, L. La Rotonda^{39a,39b}, C. Lacasta¹⁶⁷, F. Lacava^{133a,133b}, J. Lacey³¹, H. Lacker¹⁷, D. Lacour⁸², V.R. Lacuesta¹⁶⁷, E. Ladygin⁶⁷, R. Lafaye⁵, B. Laforge⁸², T. Lagouri¹⁷⁶, S. Lai⁵⁶, S. Lammers⁶³, W. Lampl⁷, E. Lançon¹³⁷, U. Landgraf⁵⁰, M.P.J. Landon⁷⁸, V.S. Lang^{60a}, J.C. Lange¹³, A.J. Lankford¹⁶³, F. Lanni²⁷, K. Lantzsche²³, A. Lanza^{122a}, S. Laplace⁸², C. Lapoire³², J.F. Laporte¹³⁷, T. Lari^{93a}, F. Lasagni Manghi^{22a,22b}, M. Lassnig³², P. Laurelli⁴⁹, W. Lavrijsen¹⁶, A.T. Law¹³⁸, P. Laycock⁷⁶, T. Lazovich⁵⁹, M. Lazzaroni^{93a,93b}, B. Le⁹⁰, O. Le Dortz⁸², E. Le Guirriec⁸⁷, E.P. Le Quilleuc¹³⁷, M. LeBlanc¹⁶⁹, T. LeCompte⁶,

F. Ledroit-Guillon⁵⁷, C.A. Lee²⁷, S.C. Lee¹⁵², L. Lee¹, G. Lefebvre⁸², M. Lefebvre¹⁶⁹, F. Legger¹⁰¹,
 C. Leggett¹⁶, A. Lehan⁷⁶, G. Lehmann Miotto³², X. Lei⁷, W.A. Leight³¹, A. Leisos^{155,ab},
 A.G. Leister¹⁷⁶, M.A.L. Leite^{26d}, R. Leitner¹³⁰, D. Lellouch¹⁷², B. Lemmer⁵⁶, K.J.C. Leney⁸⁰, T. Lenz²³,
 B. Lenzi³², R. Leone⁷, S. Leone^{125a,125b}, C. Leonidopoulos⁴⁸, S. Leontsinis¹⁰, G. Lerner¹⁵⁰, C. Leroy⁹⁶,
 A.A.J. Lesage¹³⁷, C.G. Lester³⁰, M. Levchenko¹²⁴, J. Levêque⁵, D. Levin⁹¹, L.J. Levinson¹⁷²,
 M. Levy¹⁹, D. Lewis⁷⁸, A.M. Leyko²³, M. Leyton⁴³, B. Li^{35b,o}, H. Li¹⁴⁹, H.L. Li³³, L. Li⁴⁷, L. Li^{35e},
 Q. Li^{35a}, S. Li⁴⁷, X. Li⁸⁶, Y. Li¹⁴², Z. Liang^{35a}, B. Liberti^{134a}, A. Liblong¹⁵⁹, P. Lichard³², K. Lie¹⁶⁶,
 J. Liebal²³, W. Liebig¹⁵, A. Limosani¹⁵¹, S.C. Lin^{152,ac}, T.H. Lin⁸⁵, B.E. Lindquist¹⁴⁹, A.E. Lioni⁵¹,
 E. Lipeles¹²³, A. Lipniacka¹⁵, M. Lisovsky^{60b}, T.M. Liss¹⁶⁶, A. Lister¹⁶⁸, A.M. Litke¹³⁸, B. Liu^{152,ad},
 D. Liu¹⁵², H. Liu⁹¹, H. Liu²⁷, J. Liu⁸⁷, J.B. Liu^{35b}, K. Liu⁸⁷, L. Liu¹⁶⁶, M. Liu⁴⁷, M. Liu^{35b}, Y.L. Liu^{35b},
 Y. Liu^{35b}, M. Livan^{122a,122b}, A. Lleres⁵⁷, J. Llorente Merino^{35a}, S.L. Lloyd⁷⁸, F. Lo Sterzo¹⁵²,
 E. Lobodzinska⁴⁴, P. Loch⁷, W.S. Lockman¹³⁸, F.K. Loebinger⁸⁶, A.E. Loevschall-Jensen³⁸,
 K.M. Loew²⁵, A. Loginov^{176,*}, T. Lohse¹⁷, K. Lohwasser⁴⁴, M. Lokajicek¹²⁸, B.A. Long²⁴,
 J.D. Long¹⁶⁶, R.E. Long⁷⁴, L. Longo^{75a,75b}, K.A. Looper¹¹², L. Lopes^{127a}, D. Lopez Mateos⁵⁹,
 B. Lopez Paredes¹⁴⁰, I. Lopez Paz¹³, A. Lopez Solis⁸², J. Lorenz¹⁰¹, N. Lorenzo Martinez⁶³,
 M. Losada²¹, P.J. Lösel¹⁰¹, X. Lou^{35a}, A. Lounis¹¹⁸, J. Love⁶, P.A. Love⁷⁴, H. Lu^{62a}, N. Lu⁹¹,
 H.J. Lubatti¹³⁹, C. Luci^{133a,133b}, A. Lucotte⁵⁷, C. Luedtke⁵⁰, F. Luehring⁶³, W. Lukas⁶⁴, L. Luminari^{133a},
 O. Lundberg^{147a,147b}, B. Lund-Jensen¹⁴⁸, P.M. Luzi⁸², D. Lynn²⁷, R. Lysak¹²⁸, E. Lytken⁸³,
 V. Lyubushkin⁶⁷, H. Ma²⁷, L.L. Ma^{35d}, Y. Ma^{35d}, G. Maccarrone⁴⁹, A. Macchiolo¹⁰²,
 C.M. Macdonald¹⁴⁰, B. Maček⁷⁷, J. Machado Miguens^{123,127b}, D. Madaffari⁸⁷, R. Madar³⁶,
 H.J. Maddocks¹⁶⁵, W.F. Mader⁴⁶, A. Madsen⁴⁴, J. Maeda⁶⁹, S. Maeland¹⁵, T. Maeno²⁷, A. Maevskiy¹⁰⁰,
 E. Magradze⁵⁶, J. Mahlstedt¹⁰⁸, C. Maiani¹¹⁸, C. Maidantchik^{26a}, A.A. Maier¹⁰², T. Maier¹⁰¹,
 A. Maio^{127a,127b,127d}, S. Majewski¹¹⁷, Y. Makida⁶⁸, N. Makovec¹¹⁸, B. Malaescu⁸², Pa. Malecki⁴¹,
 V.P. Maleev¹²⁴, F. Malek⁵⁷, U. Mallik⁶⁵, D. Malon⁶, C. Malone¹⁴⁴, S. Maltezos¹⁰, S. Malyukov³²,
 J. Mamuzic¹⁶⁷, G. Mancini⁴⁹, B. Mandelli³², L. Mandelli^{93a}, I. Mandić⁷⁷, J. Maneira^{127a,127b},
 L. Manhaes de Andrade Filho^{26b}, J. Manjarres Ramos^{160b}, A. Mann¹⁰¹, A. Manousos³²,
 B. Mansoulié¹³⁷, J.D. Mansour^{35a}, R. Mantifel⁸⁹, M. Mantoani⁵⁶, S. Manzoni^{93a,93b}, L. Mapelli³²,
 G. Marceca²⁹, L. March⁵¹, G. Marchiori⁸², M. Marcisovsky¹²⁸, M. Marjanovic¹⁴, D.E. Marley⁹¹,
 F. Marroquim^{26a}, S.P. Marsden⁸⁶, Z. Marshall¹⁶, S. Marti-Garcia¹⁶⁷, B. Martin⁹², T.A. Martin¹⁷⁰,
 V.J. Martin⁴⁸, B. Martin dit Latour¹⁵, M. Martinez^{13,r}, S. Martin-Haugh¹³², V.S. Martoiu^{28b},
 A.C. Martyniuk⁸⁰, M. Marx¹³⁹, A. Marzin³², L. Masetti⁸⁵, T. Mashimo¹⁵⁶, R. Mashinistov⁹⁷, J. Masik⁸⁶,
 A.L. Maslennikov^{110,c}, I. Massa^{22a,22b}, L. Massa^{22a,22b}, P. Mastrandrea⁵, A. Mastroberardino^{39a,39b},
 T. Masubuchi¹⁵⁶, P. Mättig¹⁷⁵, J. Mattmann⁸⁵, J. Maurer^{28b}, S.J. Maxfield⁷⁶, D.A. Maximov^{110,c},
 R. Mazini¹⁵², S.M. Mazza^{93a,93b}, N.C. Mc Fadden¹⁰⁶, G. Mc Goldrick¹⁵⁹, S.P. Mc Kee⁹¹, A. McCarn⁹¹,
 R.L. McCarthy¹⁴⁹, T.G. McCarthy¹⁰², L.I. McClymont⁸⁰, E.F. McDonald⁹⁰, K.W. McFarlane^{58,*},
 J.A. MCFayden⁸⁰, G. Mchedlidze⁵⁶, S.J. McMahon¹³², R.A. McPherson^{169,l}, M. Medinnis⁴⁴,
 S. Meehan¹³⁹, S. Mehlhase¹⁰¹, A. Mehta⁷⁶, K. Meier^{60a}, C. Meineck¹⁰¹, B. Meirose⁴³, D. Melini¹⁶⁷,
 B.R. Mellado Garcia^{146c}, M. Melo^{145a}, F. Meloni¹⁸, A. Mengarelli^{22a,22b}, S. Menke¹⁰², E. Meoni¹⁶²,
 S. Mergelmeyer¹⁷, P. Mermod⁵¹, L. Merola^{105a,105b}, C. Meroni^{93a}, F.S. Merritt³³, A. Messina^{133a,133b},
 J. Metcalfe⁶, A.S. Mete¹⁶³, C. Meyer⁸⁵, C. Meyer¹²³, J-P. Meyer¹³⁷, J. Meyer¹⁰⁸,
 H. Meyer Zu Theenhausen^{60a}, F. Miano¹⁵⁰, R.P. Middleton¹³², S. Miglioranza^{52a,52b}, L. Mijović²³,
 G. Mikenberg¹⁷², M. Mikestikova¹²⁸, M. Mikuž⁷⁷, M. Milesi⁹⁰, A. Milic⁶⁴, D.W. Miller³³, C. Mills⁴⁸,
 A. Milov¹⁷², D.A. Milstead^{147a,147b}, A.A. Minaenko¹³¹, Y. Minami¹⁵⁶, I.A. Minashvili⁶⁷, A.I. Mincer¹¹¹,
 B. Mindur^{40a}, M. Mineev⁶⁷, Y. Ming¹⁷³, L.M. Mir¹³, K.P. Mistry¹²³, T. Mitani¹⁷¹, J. Mitrevski¹⁰¹,
 V.A. Mitsou¹⁶⁷, A. Miucci⁵¹, P.S. Miyagawa¹⁴⁰, J.U. Mjörnmark⁸³, T. Moe^{147a,147b}, K. Mochizuki⁹⁶,
 S. Mohapatra³⁷, S. Molander^{147a,147b}, R. Moles-Valls²³, R. Monden⁷⁰, M.C. Mondragon⁹², K. Mönig⁴⁴,
 J. Monk³⁸, E. Monnier⁸⁷, A. Montalbano¹⁴⁹, J. Montejo Berlingen³², F. Monticelli⁷³, S. Monzani^{93a,93b},

R.W. Moore³, N. Morange¹¹⁸, D. Moreno²¹, M. Moreno Llácer⁵⁶, P. Morettini^{52a}, D. Mori¹⁴³, T. Mori¹⁵⁶, M. Morii⁵⁹, M. Morinaga¹⁵⁶, V. Morisbak¹²⁰, S. Moritz⁸⁵, A.K. Morley¹⁵¹, G. Mornacchi³², J.D. Morris⁷⁸, S.S. Mortensen³⁸, L. Morvaj¹⁴⁹, M. Mosidze^{53b}, J. Moss¹⁴⁴, K. Motohashi¹⁵⁸, R. Mount¹⁴⁴, E. Mountricha²⁷, S.V. Mouraviev^{97,*}, E.J.W. Moyse⁸⁸, S. Muanza⁸⁷, R.D. Mudd¹⁹, F. Mueller¹⁰², J. Mueller¹²⁶, R.S.P. Mueller¹⁰¹, T. Mueller³⁰, D. Muenstermann⁷⁴, P. Mullen⁵⁵, G.A. Mullier¹⁸, F.J. Munoz Sanchez⁸⁶, J.A. Murillo Quijada¹⁹, W.J. Murray^{170,132}, H. Musheghyan⁵⁶, M. Muškinja⁷⁷, A.G. Myagkov^{131,ae}, M. Myska¹²⁹, B.P. Nachman¹⁴⁴, O. Nackenhorst⁵¹, K. Nagai¹²¹, R. Nagai^{68,z}, K. Nagano⁶⁸, Y. Nagasaka⁶¹, K. Nagata¹⁶¹, M. Nagel⁵⁰, E. Nagy⁸⁷, A.M. Nairz³², Y. Nakahama³², K. Nakamura⁶⁸, T. Nakamura¹⁵⁶, I. Nakano¹¹³, H. Namasivayam⁴³, R.F. Naranjo Garcia⁴⁴, R. Narayan¹¹, D.I. Narrias Villar^{60a}, I. Naryshkin¹²⁴, T. Naumann⁴⁴, G. Navarro²¹, R. Nayyar⁷, H.A. Neal⁹¹, P.Yu. Nechaeva⁹⁷, T.J. Neep⁸⁶, P.D. Nef¹⁴⁴, A. Negri^{122a,122b}, M. Negrini^{22a}, S. Nektarijevic¹⁰⁷, C. Nellist¹¹⁸, A. Nelson¹⁶³, S. Nemecek¹²⁸, P. Nemethy¹¹¹, A.A. Nepomuceno^{26a}, M. Nessi^{32,af}, M.S. Neubauer¹⁶⁶, M. Neumann¹⁷⁵, R.M. Neves¹¹¹, P. Nevski²⁷, P.R. Newman¹⁹, D.H. Nguyen⁶, T. Nguyen Manh⁹⁶, R.B. Nickerson¹²¹, R. Nicolaidou¹³⁷, J. Nielsen¹³⁸, A. Nikiforov¹⁷, V. Nikolaenko^{131,ae}, I. Nikolic-Audit⁸², K. Nikolopoulos¹⁹, J.K. Nilsen¹²⁰, P. Nilsson²⁷, Y. Ninomiya¹⁵⁶, A. Nisati^{133a}, R. Nisius¹⁰², T. Nobe¹⁵⁶, L. Nodulman⁶, M. Nomachi¹¹⁹, I. Nomidis³¹, T. Nooney⁷⁸, S. Norberg¹¹⁴, M. Nordberg³², N. Norjoharuddeen¹²¹, O. Novgorodova⁴⁶, S. Nowak¹⁰², M. Nozaki⁶⁸, L. Nozka¹¹⁶, K. Ntekas¹⁰, E. Nurse⁸⁰, F. Nuti⁹⁰, F. O'grady⁷, D.C. O'Neil¹⁴³, A.A. O'Rourke⁴⁴, V. O'Shea⁵⁵, F.G. Oakham^{31,d}, H. Oberlack¹⁰², T. Obermann²³, J. Ocariz⁸², A. Ochi⁶⁹, I. Ochoa³⁷, J.P. Ochoa-Ricoux^{34a}, S. Oda⁷², S. Odaka⁶⁸, H. Ogren⁶³, A. Oh⁸⁶, S.H. Oh⁴⁷, C.C. Ohm¹⁶, H. Ohman¹⁶⁵, H. Oide³², H. Okawa¹⁶¹, Y. Okumura³³, T. Okuyama⁶⁸, A. Olariu^{28b}, L.F. Oleiro Seabra^{127a}, S.A. Olivares Pino⁴⁸, D. Oliveira Damazio²⁷, A. Olszewski⁴¹, J. Olszowska⁴¹, A. Onofre^{127a,127e}, K. Onogi¹⁰⁴, P.U.E. Onyisi^{11,v}, M.J. Oreglia³³, Y. Oren¹⁵⁴, D. Orestano^{135a,135b}, N. Orlando^{62b}, R.S. Orr¹⁵⁹, B. Osculati^{52a,52b}, R. Ospanov⁸⁶, G. Otero y Garzon²⁹, H. Otono⁷², M. Ouchrif^{136d}, F. Ould-Saada¹²⁰, A. Ouraou¹³⁷, K.P. Oussoren¹⁰⁸, Q. Ouyang^{35a}, M. Owen⁵⁵, R.E. Owen¹⁹, V.E. Ozcan^{20a}, N. Ozturk⁸, K. Pachal¹⁴³, A. Pacheco Pages¹³, L. Pacheco Rodriguez¹³⁷, C. Padilla Aranda¹³, M. Pagáčová⁵⁰, S. Pagan Griso¹⁶, F. Paige²⁷, P. Pais⁸⁸, K. Pajchel¹²⁰, G. Palacino^{160b}, S. Palestini³², M. Palka^{40b}, D. Pallin³⁶, A. Palma^{127a,127b}, E.St. Panagiotopoulou¹⁰, C.E. Pandini⁸², J.G. Panduro Vazquez⁷⁹, P. Pani^{147a,147b}, S. Panitkin²⁷, D. Pantea^{28b}, L. Paolozzi⁵¹, Th.D. Papadopoulou¹⁰, K. Papageorgiou¹⁵⁵, A. Paramonov⁶, D. Paredes Hernandez¹⁷⁶, A.J. Parker⁷⁴, M.A. Parker³⁰, K.A. Parker¹⁴⁰, F. Parodi^{52a,52b}, J.A. Parsons³⁷, U. Parzefall⁵⁰, V.R. Pascuzzi¹⁵⁹, E. Pasqualucci^{133a}, S. Passaggio^{52a}, Fr. Pastore⁷⁹, G. Pásztor^{31,ag}, S. Patarai¹⁷⁵, J.R. Pater⁸⁶, T. Pauly³², J. Pearce¹⁶⁹, B. Pearson¹¹⁴, L.E. Pedersen³⁸, M. Pedersen¹²⁰, S. Pedraza Lopez¹⁶⁷, R. Pedro^{127a,127b}, S.V. Peleganchuk^{110,c}, D. Pelikan¹⁶⁵, O. Penc¹²⁸, C. Peng^{35a}, H. Peng^{35b}, J. Penwell⁶³, B.S. Peralva^{26b}, M.M. Perego¹³⁷, D.V. Perepelitsa²⁷, E. Perez Codina^{160a}, L. Perini^{93a,93b}, H. Pernegger³², S. Perrella^{105a,105b}, R. Peschke⁴⁴, V.D. Peshekhonov⁶⁷, K. Peters⁴⁴, R.F.Y. Peters⁸⁶, B.A. Petersen³², T.C. Petersen³⁸, E. Petit⁵⁷, A. Petridis¹, C. Petridou¹⁵⁵, P. Petroff¹¹⁸, E. Petrolo^{133a}, M. Petrov¹²¹, F. Petrucci^{135a,135b}, N.E. Pettersson⁸⁸, A. Peyaud¹³⁷, R. Pezoa^{34b}, P.W. Phillips¹³², G. Piacquadio^{144,ah}, E. Pianori¹⁷⁰, A. Picazio⁸⁸, E. Piccaro⁷⁸, M. Piccinini^{22a,22b}, M.A. Pickering¹²¹, R. Piegai²⁹, J.E. Pilcher³³, A.D. Pilkington⁸⁶, A.W.J. Pin⁸⁶, M. Pinamonti^{164a,164c,ai}, J.L. Pinfold³, A. Pingel³⁸, S. Pires⁸², H. Pirumov⁴⁴, M. Pitt¹⁷², L. Plazak^{145a}, M.-A. Pleier²⁷, V. Pleskot⁸⁵, E. Plotnikova⁶⁷, P. Plucinski⁹², D. Pluth⁶⁶, R. Poettgen^{147a,147b}, L. Poggioli¹¹⁸, D. Pohl²³, G. Polesello^{122a}, A. Poley⁴⁴, A. Policicchio^{39a,39b}, R. Polifka¹⁵⁹, A. Polini^{22a}, C.S. Pollard⁵⁵, V. Polychronakos²⁷, K. Pommès³², L. Pontecorvo^{133a}, B.G. Pope⁹², G.A. Popeneciu^{28c}, D.S. Popovic¹⁴, A. Poppleton³², S. Pospisil¹²⁹, K. Potamianos¹⁶, I.N. Potrap⁶⁷, C.J. Potter³⁰, C.T. Potter¹¹⁷, G. Poulard³², J. Poveda³², V. Pozdnyakov⁶⁷, M.E. Pozo Astigarraga³², P. Pralavorio⁸⁷, A. Pranko¹⁶, S. Prell⁶⁶, D. Price⁸⁶, L.E. Price⁶, M. Primavera^{75a}, S. Prince⁸⁹, M. Proissl⁴⁸, K. Prokofiev^{62c}, F. Prokoshin^{34b},

S. Protopopescu²⁷, J. Proudfoot⁶, M. Przybycien^{40a}, D. Puddu^{135a,135b}, M. Purohit^{27,aj}, P. Puzo¹¹⁸,
 J. Qian⁹¹, G. Qin⁵⁵, Y. Qin⁸⁶, A. Quadt⁵⁶, W.B. Quayle^{164a,164b}, M. Queitsch-Maitland⁸⁶, D. Quilty⁵⁵,
 S. Raddum¹²⁰, V. Radeka²⁷, V. Radescu^{60b}, S.K. Radhakrishnan¹⁴⁹, P. Radloff¹¹⁷, P. Rados⁹⁰,
 F. Ragusa^{93a,93b}, G. Rahal¹⁷⁸, J.A. Raine⁸⁶, S. Rajagopalan²⁷, M. Rammensee³², C. Rangel-Smith¹⁶⁵,
 M.G. Ratti^{93a,93b}, F. Rauscher¹⁰¹, S. Rave⁸⁵, T. Ravenscroft⁵⁵, I. Ravinovich¹⁷², M. Raymond³²,
 A.L. Read¹²⁰, N.P. Readioff⁷⁶, M. Reale^{75a,75b}, D.M. Rebuzzi^{122a,122b}, A. Redelbach¹⁷⁴, G. Redlinger²⁷,
 R. Reece¹³⁸, K. Reeves⁴³, L. Rehnisch¹⁷, J. Reichert¹²³, H. Reisin²⁹, C. Rembser³², H. Ren^{35a},
 M. Rescigno^{133a}, S. Resconi^{93a}, O.L. Rezanova^{110,c}, P. Reznicek¹³⁰, R. Rezvani⁹⁶, R. Richter¹⁰²,
 S. Richter⁸⁰, E. Richter-Was^{40b}, O. Ricken²³, M. Ridel⁸², P. Rieck¹⁷, C.J. Riegel¹⁷⁵, J. Rieger⁵⁶,
 O. Rifki¹¹⁴, M. Rijssenbeek¹⁴⁹, A. Rimoldi^{122a,122b}, M. Rimoldi¹⁸, L. Rinaldi^{22a}, B. Ristic⁵¹, E. Ritsch³²,
 I. Riu¹³, F. Rizatdinova¹¹⁵, E. Rizvi⁷⁸, C. Rizzi¹³, S.H. Robertson^{89,l}, A. Robichaud-Veronneau⁸⁹,
 D. Robinson³⁰, J.E.M. Robinson⁴⁴, A. Robson⁵⁵, C. Roda^{125a,125b}, Y. Rodina⁸⁷, A. Rodriguez Perez¹³,
 D. Rodriguez Rodriguez¹⁶⁷, S. Roe³², C.S. Rogan⁵⁹, O. Røhne¹²⁰, A. Romaniouk⁹⁹, M. Romano^{22a,22b},
 S.M. Romano Saez³⁶, E. Romero Adam¹⁶⁷, N. Rompotis¹³⁹, M. Ronzani⁵⁰, L. Roos⁸², E. Ros¹⁶⁷,
 S. Rosati^{133a}, K. Rosbach⁵⁰, P. Rose¹³⁸, O. Rosenthal¹⁴², N.-A. Rosien⁵⁶, V. Rossetti^{147a,147b},
 E. Rossi^{105a,105b}, L.P. Rossi^{52a}, J.H.N. Rosten³⁰, R. Rosten¹³⁹, M. Rotaru^{28b}, I. Roth¹⁷², J. Rothberg¹³⁹,
 D. Rousseau¹¹⁸, C.R. Royon¹³⁷, A. Rozanov⁸⁷, Y. Rozen¹⁵³, X. Ruan^{146c}, F. Rubbo¹⁴⁴,
 M.S. Rudolph¹⁵⁹, F. Rühr⁵⁰, A. Ruiz-Martinez³¹, Z. Rurikova⁵⁰, N.A. Rusakovich⁶⁷, A. Ruschke¹⁰¹,
 H.L. Russell¹³⁹, J.P. Rutherford⁷, N. Ruthmann³², Y.F. Ryabov¹²⁴, M. Rybar¹⁶⁶, G. Rybkin¹¹⁸, S. Ryu⁶,
 A. Ryzhov¹³¹, G.F. Rzehorz⁵⁶, A.F. Saavedra¹⁵¹, G. Sabato¹⁰⁸, S. Sacerdoti²⁹, H.F.W. Sadrozinski¹³⁸,
 R. Sadykov⁶⁷, F. Safai Tehrani^{133a}, P. Saha¹⁰⁹, M. Sahinsoy^{60a}, M. Saimpert¹³⁷, T. Saito¹⁵⁶,
 H. Sakamoto¹⁵⁶, Y. Sakurai¹⁷¹, G. Salamanna^{135a,135b}, A. Salamon^{134a,134b}, J.E. Salazar Loyola^{34b},
 D. Salek¹⁰⁸, P.H. Sales De Bruin¹³⁹, D. Salihagic¹⁰², A. Salnikov¹⁴⁴, J. Salt¹⁶⁷, D. Salvatore^{39a,39b},
 F. Salvatore¹⁵⁰, A. Salvucci^{62a}, A. Salzburger³², D. Sammel⁵⁰, D. Sampsonidis¹⁵⁵, A. Sanchez^{105a,105b},
 J. Sánchez¹⁶⁷, V. Sanchez Martinez¹⁶⁷, H. Sandaker¹²⁰, R.L. Sandbach⁷⁸, H.G. Sander⁸⁵,
 M. Sandhoff¹⁷⁵, C. Sandoval²¹, R. Sandstroem¹⁰², D.P.C. Sankey¹³², M. Sannino^{52a,52b}, A. Sansoni⁴⁹,
 C. Santoni³⁶, R. Santonico^{134a,134b}, H. Santos^{127a}, I. Santoyo Castillo¹⁵⁰, K. Sapp¹²⁶, A. Saponov⁶⁷,
 J.G. Saraiva^{127a,127d}, B. Sarrazin²³, O. Sasaki⁶⁸, Y. Sasaki¹⁵⁶, K. Sato¹⁶¹, G. Sauvage^{5,*}, E. Sauvan⁵,
 G. Savage⁷⁹, P. Savard^{159,d}, C. Sawyer¹³², L. Sawyer^{81,q}, J. Saxon³³, C. Sbarra^{22a}, A. Sbrizzi^{22a,22b},
 T. Scanlon⁸⁰, D.A. Scannicchio¹⁶³, M. Scarcella¹⁵¹, V. Scarfone^{39a,39b}, J. Schaarschmidt¹⁷²,
 P. Schacht¹⁰², B.M. Schachtner¹⁰¹, D. Schaefer³², R. Schaefer⁴⁴, J. Schaeffer⁸⁵, S. Schaepe²³,
 S. Schaetzel^{60b}, U. Schäfer⁸⁵, A.C. Schaffer¹¹⁸, D. Schaile¹⁰¹, R.D. Schamberger¹⁴⁹, V. Scharf^{60a},
 V.A. Schegelsky¹²⁴, D. Scheirich¹³⁰, M. Schernau¹⁶³, C. Schiavi^{52a,52b}, S. Schier¹³⁸, C. Schillo⁵⁰,
 M. Schioppa^{39a,39b}, S. Schlenker³², K.R. Schmidt-Sommerfeld¹⁰², K. Schmieden³², C. Schmitt⁸⁵,
 S. Schmitt⁴⁴, S. Schmitz⁸⁵, B. Schneider^{160a}, U. Schnoor⁵⁰, L. Schoeffel¹³⁷, A. Schoening^{60b},
 B.D. Schoenrock⁹², E. Schopf²³, M. Schott⁸⁵, J. Schovancova⁸, S. Schramm⁵¹, M. Schreyer¹⁷⁴,
 N. Schuh⁸⁵, M.J. Schultens²³, H.-C. Schultz-Coulon^{60a}, H. Schulz¹⁷, M. Schumacher⁵⁰,
 B.A. Schumm¹³⁸, Ph. Schune¹³⁷, A. Schwartzman¹⁴⁴, T.A. Schwarz⁹¹, Ph. Schwegler¹⁰²,
 H. Schweiger⁸⁶, Ph. Schwemling¹³⁷, R. Schwienhorst⁹², J. Schwindling¹³⁷, T. Schwindt²³, G. Sciolla²⁵,
 F. Scuri^{125a,125b}, F. Scutti⁹⁰, J. Searcy⁹¹, P. Seema²³, S.C. Seidel¹⁰⁶, A. Seiden¹³⁸, F. Seifert¹²⁹,
 J.M. Seixas^{26a}, G. Sekhniaidze^{105a}, K. Sekhon⁹¹, S.J. Sekula⁴², D.M. Seliverstov^{124,*},
 N. Semprini-Cesari^{22a,22b}, C. Serfon¹²⁰, L. Serin¹¹⁸, L. Serkin^{164a,164b}, M. Sessa^{135a,135b}, R. Seuster¹⁶⁹,
 H. Severini¹¹⁴, T. Sfiligoj⁷⁷, F. Sforza³², A. Sfyrila⁵¹, E. Shabalina⁵⁶, N.W. Shaikh^{147a,147b}, L.Y. Shan^{35a},
 R. Shang¹⁶⁶, J.T. Shank²⁴, M. Shapiro¹⁶, P.B. Shatalov⁹⁸, K. Shaw^{164a,164b}, S.M. Shaw⁸⁶,
 A. Shcherbakova^{147a,147b}, C.Y. Shehu¹⁵⁰, P. Sherwood⁸⁰, L. Shi^{152,ak}, S. Shimizu⁶⁹, C.O. Shimmin¹⁶³,
 M. Shimojima¹⁰³, M. Shiyakova^{67,al}, A. Shmeleva⁹⁷, D. Shoaleh Saadi⁹⁶, M.J. Shochet³³,
 S. Shojaii^{93a,93b}, S. Shrestha¹¹², E. Shulga⁹⁹, M.A. Shupe⁷, P. Sicho¹²⁸, A.M. Sickles¹⁶⁶, P.E. Sidebo¹⁴⁸,

O. Sidiropoulou¹⁷⁴, D. Sidorov¹¹⁵, A. Sidoti^{22a,22b}, F. Siegert⁴⁶, Dj. Sijacki¹⁴, J. Silva^{127a,127d}, S.B. Silverstein^{147a}, V. Simak¹²⁹, O. Simard⁵, Lj. Simic¹⁴, S. Simion¹¹⁸, E. Simioni⁸⁵, B. Simmons⁸⁰, D. Simon³⁶, M. Simon⁸⁵, P. Sinervo¹⁵⁹, N.B. Sinev¹¹⁷, M. Sioli^{22a,22b}, G. Siragusa¹⁷⁴, S.Yu. Sivoklov¹⁰⁰, J. Sjölin^{147a,147b}, T.B. Sjursen¹⁵, M.B. Skinner⁷⁴, H.P. Skottowe⁵⁹, P. Skubic¹¹⁴, M. Slater¹⁹, T. Slavicek¹²⁹, M. Slawinska¹⁰⁸, K. Sliwa¹⁶², R. Slovak¹³⁰, V. Smakhtin¹⁷², B.H. Smart⁵, L. Smestad¹⁵, J. Smiesko^{145a}, S.Yu. Smirnov⁹⁹, Y. Smirnov⁹⁹, L.N. Smirnova^{100,am}, O. Smirnova⁸³, M.N.K. Smith³⁷, R.W. Smith³⁷, M. Smizanska⁷⁴, K. Smolek¹²⁹, A.A. Snasarev⁹⁷, S. Snyder²⁷, R. Sobie^{169,l}, F. Socher⁴⁶, A. Soffer¹⁵⁴, D.A. Soh¹⁵², G. Sokhrannyi⁷⁷, C.A. Solans Sanchez³², M. Solar¹²⁹, E.Yu. Soldatov⁹⁹, U. Soldevila¹⁶⁷, A.A. Solodkov¹³¹, A. Soloshenko⁶⁷, O.V. Solovyanov¹³¹, V. Solovyevev¹²⁴, P. Sommer⁵⁰, H. Son¹⁶², H.Y. Song^{35b,an}, A. Sood¹⁶, A. Sopczak¹²⁹, V. Sopko¹²⁹, V. Sorin¹³, D. Sosa^{60b}, C.L. Sotiropoulou^{125a,125b}, R. Soualah^{164a,164c}, A.M. Soukharev^{110,c}, D. South⁴⁴, B.C. Sowden⁷⁹, S. Spagnolo^{75a,75b}, M. Spalla^{125a,125b}, M. Spangenberg¹⁷⁰, F. Spanò⁷⁹, D. Sperlich¹⁷, F. Spettel¹⁰², R. Spighi^{22a}, G. Spigo³², L.A. Spiller⁹⁰, M. Spousta¹³⁰, R.D. St. Denis^{55,*}, A. Stabile^{93a}, R. Stamen^{60a}, S. Stamm¹⁷, E. Stanecka⁴¹, R.W. Stanek⁶, C. Stanescu^{135a}, M. Stanescu-Bellu⁴⁴, M.M. Stanitzki⁴⁴, S. Stapnes¹²⁰, E.A. Starchenko¹³¹, G.H. Stark³³, J. Stark⁵⁷, P. Staroba¹²⁸, P. Starovoitov^{60a}, S. Stärz³², R. Staszewski⁴¹, P. Steinberg²⁷, B. Stelzer¹⁴³, H.J. Stelzer³², O. Stelzer-Chilton^{160a}, H. Stenzel⁵⁴, G.A. Stewart⁵⁵, J.A. Stillings²³, M.C. Stockton⁸⁹, M. Stoebe⁸⁹, G. Stoica^{28b}, P. Stolte⁵⁶, S. Stonjek¹⁰², A.R. Stradling⁸, A. Straessner⁴⁶, M.E. Stramaglia¹⁸, J. Strandberg¹⁴⁸, S. Strandberg^{147a,147b}, A. Strandlie¹²⁰, M. Strauss¹¹⁴, P. Strizenc^{145b}, R. Ströhmer¹⁷⁴, D.M. Strom¹¹⁷, R. Stroynowski⁴², A. Strubig¹⁰⁷, S.A. Stucci¹⁸, B. Stugu¹⁵, N.A. Styles⁴⁴, D. Su¹⁴⁴, J. Su¹²⁶, R. Subramaniam⁸¹, S. Suchek^{60a}, Y. Sugaya¹¹⁹, M. Suk¹²⁹, V.V. Sulin⁹⁷, S. Sultansoy^{4c}, T. Sumida⁷⁰, S. Sun⁵⁹, X. Sun^{35a}, J.E. Sundermann⁵⁰, K. Suruliz¹⁵⁰, G. Susinno^{39a,39b}, M.R. Sutton¹⁵⁰, S. Suzuki⁶⁸, M. Svatos¹²⁸, M. Swiatlowski³³, I. Sykora^{145a}, T. Sykora¹³⁰, D. Ta⁵⁰, C. Taccini^{135a,135b}, K. Tackmann⁴⁴, J. Taenzer¹⁵⁹, A. Taffard¹⁶³, R. Tafirout^{160a}, N. Taiblum¹⁵⁴, H. Takai²⁷, R. Takashima⁷¹, T. Takeshita¹⁴¹, Y. Takubo⁶⁸, M. Talby⁸⁷, A.A. Talyshev^{110,c}, K.G. Tan⁹⁰, J. Tanaka¹⁵⁶, R. Tanaka¹¹⁸, S. Tanaka⁶⁸, B.B. Tannenwald¹¹², S. Tapia Araya^{34b}, S. Tapprogge⁸⁵, S. Tarem¹⁵³, G.F. Tartarelli^{93a}, P. Tas¹³⁰, M. Tasevsky¹²⁸, T. Tashiro⁷⁰, E. Tassi^{39a,39b}, A. Tavares Delgado^{127a,127b}, Y. Tayalati^{136d}, A.C. Taylor¹⁰⁶, G.N. Taylor⁹⁰, P.T.E. Taylor⁹⁰, W. Taylor^{160b}, F.A. Teischinger³², P. Teixeira-Dias⁷⁹, K.K. Temming⁵⁰, D. Temple¹⁴³, H. Ten Kate³², P.K. Teng¹⁵², J.J. Teoh¹¹⁹, F. Tepe¹⁷⁵, S. Terada⁶⁸, K. Terashi¹⁵⁶, J. Terron⁸⁴, S. Terzo¹⁰², M. Testa⁴⁹, R.J. Teuscher^{159,l}, T. Thevenaux-Pelzer⁸⁷, J.P. Thomas¹⁹, J. Thomas-Wilsker⁷⁹, E.N. Thompson³⁷, P.D. Thompson¹⁹, A.S. Thompson⁵⁵, L.A. Thomsen¹⁷⁶, E. Thomson¹²³, M. Thomson³⁰, M.J. Tibbetts¹⁶, R.E. Ticse Torres⁸⁷, V.O. Tikhomirov^{97,ao}, Yu.A. Tikhonov^{110,c}, S. Timoshenko⁹⁹, P. Tipton¹⁷⁶, S. Tisserant⁸⁷, K. Todome¹⁵⁸, T. Todorov^{5,*}, S. Todorova-Nova¹³⁰, J. Tojo⁷², S. Tokár^{145a}, K. Tokushuku⁶⁸, E. Tolley⁵⁹, L. Tomlinson⁸⁶, M. Tomoto¹⁰⁴, L. Tompkins^{144,ap}, K. Toms¹⁰⁶, B. Tong⁵⁹, E. Torrence¹¹⁷, H. Torres¹⁴³, E. Torró Pastor¹³⁹, J. Toth^{87,aq}, F. Touchard⁸⁷, D.R. Tovey¹⁴⁰, T. Trefzger¹⁷⁴, A. Tricoli²⁷, I.M. Trigger^{160a}, S. Trincas-Duvoid⁸², M.F. Tripiana¹³, W. Trischuk¹⁵⁹, B. Trocme⁵⁷, A. Trofymov⁴⁴, C. Troncon^{93a}, M. Trottier-McDonald¹⁶, M. Trovatelli¹⁶⁹, L. Truong^{164a,164c}, M. Trzebinski⁴¹, A. Trzupek⁴¹, J.C-L. Tseng¹²¹, P.V. Tsiarshka⁹⁴, G. Tsipolitis¹⁰, N. Tsirintanis⁹, S. Tsiskaridze¹³, V. Tsiskaridze⁵⁰, E.G. Tskhadadze^{53a}, K.M. Tsui^{62a}, I.I. Tsukerman⁹⁸, V. Tsulaia¹⁶, S. Tsuno⁶⁸, D. Tsybychev¹⁴⁹, A. Tudorache^{28b}, V. Tudorache^{28b}, A.N. Tuna⁵⁹, S.A. Tupputi^{22a,22b}, S. Turchikhin^{100,am}, D. Turecek¹²⁹, D. Turgeman¹⁷², R. Turra^{93a,93b}, A.J. Turvey⁴², P.M. Tuts³⁷, M. Tyndel¹³², G. Ucchielli^{22a,22b}, I. Ueda¹⁵⁶, R. Ueno³¹, M. Ughetto^{147a,147b}, F. Ukegawa¹⁶¹, G. Unal³², A. Undrus²⁷, G. Unel¹⁶³, F.C. Ungaro⁹⁰, Y. Unno⁶⁸, C. Unverdorben¹⁰¹, J. Urban^{145b}, P. Urquijo⁹⁰, P. Urrejola⁸⁵, G. Usai⁸, A. Usanova⁶⁴, L. Vacavant⁸⁷, V. Vacek¹²⁹, B. Vachon⁸⁹, C. Valderanis¹⁰¹, E. Valdes Santurio^{147a,147b}, N. Valencic¹⁰⁸, S. Valentineti^{22a,22b}, A. Valero¹⁶⁷, L. Valery¹³, S. Valkar¹³⁰, S. Vallecorsa⁵¹, J.A. Valls Ferrer¹⁶⁷, W. Van Den Wollenberg¹⁰⁸,

P.C. Van Der Deijl¹⁰⁸, R. van der Geer¹⁰⁸, H. van der Graaf¹⁰⁸, N. van Eldik¹⁵³, P. van Gemmeren⁶, J. Van Nieuwkoop¹⁴³, I. van Vulpen¹⁰⁸, M.C. van Woerden³², M. Vanadia^{133a,133b}, W. Vandelli³², R. Vanguri¹²³, A. Vaniachine¹³¹, P. Vankov¹⁰⁸, G. Vardanyan¹⁷⁷, R. Vari^{133a}, E.W. Varnes⁷, T. Varol⁴², D. Varouchas⁸², A. Vartapetian⁸, K.E. Varvell¹⁵¹, J.G. Vasquez¹⁷⁶, F. Vazeille³⁶, T. Vazquez Schroeder⁸⁹, J. Veatch⁵⁶, L.M. Veloce¹⁵⁹, F. Veloso^{127a,127c}, S. Veneziano^{133a}, A. Ventura^{75a,75b}, M. Venturi¹⁶⁹, N. Venturi¹⁵⁹, A. Venturini²⁵, V. Vercesi^{122a}, M. Verducci^{133a,133b}, W. Verkerke¹⁰⁸, J.C. Vermeulen¹⁰⁸, A. Vest^{46,ar}, M.C. Vetterli^{143,d}, O. Viazlo⁸³, I. Vichou^{166,*}, T. Vickey¹⁴⁰, O.E. Vickey Boeriu¹⁴⁰, G.H.A. Viehhauser¹²¹, S. Viel¹⁶, L. Vigani¹²¹, R. Vigne⁶⁴, M. Villa^{22a,22b}, M. Villaplana Perez^{93a,93b}, E. Vilucchi⁴⁹, M.G. Vinciter³¹, V.B. Vinogradov⁶⁷, C. Vittori^{22a,22b}, I. Vivarelli¹⁵⁰, S. Vlachos¹⁰, M. Vlasak¹²⁹, M. Vogel¹⁷⁵, P. Vokac¹²⁹, G. Volpi^{125a,125b}, M. Volpi⁹⁰, H. von der Schmitt¹⁰², E. von Toerne²³, V. Vorobel¹³⁰, K. Vorobev⁹⁹, M. Vos¹⁶⁷, R. Voss³², J.H. Vossebeld⁷⁶, N. Vranjes¹⁴, M. Vranjes Milosavljevic¹⁴, V. Vrba¹²⁸, M. Vreeswijk¹⁰⁸, R. Vuillermet³², I. Vukotic³³, Z. Vykydal¹²⁹, P. Wagner²³, W. Wagner¹⁷⁵, H. Wahlberg⁷³, S. Wahrmond⁴⁶, J. Wakabayashi¹⁰⁴, J. Walder⁷⁴, R. Walker¹⁰¹, W. Walkowiak¹⁴², V. Wallangen^{147a,147b}, C. Wang^{35c}, C. Wang^{35d,87}, F. Wang¹⁷³, H. Wang¹⁶, H. Wang⁴², J. Wang⁴⁴, J. Wang¹⁵¹, K. Wang⁸⁹, R. Wang⁶, S.M. Wang¹⁵², T. Wang²³, T. Wang³⁷, W. Wang^{35b}, X. Wang¹⁷⁶, C. Wanotayaroj¹¹⁷, A. Warburton⁸⁹, C.P. Ward³⁰, D.R. Wardrope⁸⁰, A. Washbrook⁴⁸, P.M. Watkins¹⁹, A.T. Watson¹⁹, M.F. Watson¹⁹, G. Watts¹³⁹, S. Watts⁸⁶, B.M. Waugh⁸⁰, S. Webb⁸⁵, M.S. Weber¹⁸, S.W. Weber¹⁷⁴, J.S. Webster⁶, A.R. Weidberg¹²¹, B. Weinert⁶³, J. Weingarten⁵⁶, C. Weiser⁵⁰, H. Weits¹⁰⁸, P.S. Wells³², T. Wenaus²⁷, T. Wengler³², S. Wenig³², N. Wermes²³, M. Werner⁵⁰, M.D. Werner⁶⁶, P. Werner³², M. Wessels^{60a}, J. Wetter¹⁶², K. Whalen¹¹⁷, N.L. Whallon¹³⁹, A.M. Wharton⁷⁴, A. White⁸, M.J. White¹, R. White^{34b}, D. Whiteson¹⁶³, F.J. Wickens¹³², W. Wiedenmann¹⁷³, M. Wielers¹³², P. Wienemann²³, C. Wiglesworth³⁸, L.A.M. Wiik-Fuchs²³, A. Wildauer¹⁰², F. Wilk⁸⁶, H.G. Wilkens³², H.H. Williams¹²³, S. Williams¹⁰⁸, C. Willis⁹², S. Willocq⁸⁸, J.A. Wilson¹⁹, I. Wingerter-Seez⁵, F. Winklmeier¹¹⁷, O.J. Winston¹⁵⁰, B.T. Winter²³, M. Wittgen¹⁴⁴, J. Wittkowski¹⁰¹, S.J. Wollstadt⁸⁵, M.W. Wolter⁴¹, H. Wolters^{127a,127c}, B.K. Wosiek⁴¹, J. Wotschack³², M.J. Woudstra⁸⁶, K.W. Wozniak⁴¹, M. Wu⁵⁷, M. Wu³³, S.L. Wu¹⁷³, X. Wu⁵¹, Y. Wu⁹¹, T.R. Wyatt⁸⁶, B.M. Wynne⁴⁸, S. Xella³⁸, D. Xu^{35a}, L. Xu²⁷, B. Yabsley¹⁵¹, S. Yacoob^{146a}, R. Yakabe⁶⁹, D. Yamaguchi¹⁵⁸, Y. Yamaguchi¹¹⁹, A. Yamamoto⁶⁸, S. Yamamoto¹⁵⁶, T. Yamanaka¹⁵⁶, K. Yamauchi¹⁰⁴, Y. Yamazaki⁶⁹, Z. Yan²⁴, H. Yang^{35e}, H. Yang¹⁷³, Y. Yang¹⁵², Z. Yang¹⁵, W-M. Yao¹⁶, Y.C. Yap⁸², Y. Yasu⁶⁸, E. Yatsenko⁵, K.H. Yau Wong²³, J. Ye⁴², S. Ye²⁷, I. Yeletskikh⁶⁷, A.L. Yen⁵⁹, E. Yildirim⁸⁵, K. Yorita¹⁷¹, R. Yoshida⁶, K. Yoshihara¹²³, C. Young¹⁴⁴, C.J.S. Young³², S. Youssef²⁴, D.R. Yu¹⁶, J. Yu⁸, J.M. Yu⁹¹, J. Yu⁶⁶, L. Yuan⁶⁹, S.P.Y. Yuen²³, I. Yusuff^{30,as}, B. Zabinski⁴¹, R. Zaidan^{35d}, A.M. Zaitsev^{131,ae}, N. Zakharчук⁴⁴, J. Zalieckas¹⁵, A. Zaman¹⁴⁹, S. Zambito⁵⁹, L. Zanello^{133a,133b}, D. Zanzi⁹⁰, C. Zeitnitz¹⁷⁵, M. Zeman¹²⁹, A. Zemla^{40a}, J.C. Zeng¹⁶⁶, Q. Zeng¹⁴⁴, K. Zengel²⁵, O. Zenin¹³¹, T. Ženiš^{145a}, D. Zerwas¹¹⁸, D. Zhang⁹¹, F. Zhang¹⁷³, G. Zhang^{35b,an}, H. Zhang^{35c}, J. Zhang⁶, L. Zhang⁵⁰, R. Zhang²³, R. Zhang^{35b,at}, X. Zhang^{35d}, Z. Zhang¹¹⁸, X. Zhao⁴², Y. Zhao^{35d}, Z. Zhao^{35b}, A. Zhemchugov⁶⁷, J. Zhong¹²¹, B. Zhou⁹¹, C. Zhou⁴⁷, L. Zhou³⁷, L. Zhou⁴², M. Zhou¹⁴⁹, N. Zhou^{35f}, C.G. Zhu^{35d}, H. Zhu^{35a}, J. Zhu⁹¹, Y. Zhu^{35b}, X. Zhuang^{35a}, K. Zhukov⁹⁷, A. Zibell¹⁷⁴, D. Zieminska⁶³, N.I. Zimine⁶⁷, C. Zimmermann⁸⁵, S. Zimmermann⁵⁰, Z. Zinonos⁵⁶, M. Zinser⁸⁵, M. Ziolkowski¹⁴², L. Živković¹⁴, G. Zobernig¹⁷³, A. Zoccoli^{22a,22b}, M. zur Nedden¹⁷, G. Zurzolo^{105a,105b}, L. Zwalinski³².

¹ Department of Physics, University of Adelaide, Adelaide, Australia

² Physics Department, SUNY Albany, Albany NY, United States of America

³ Department of Physics, University of Alberta, Edmonton AB, Canada

⁴ (a) Department of Physics, Ankara University, Ankara; (b) Istanbul Aydin University, Istanbul; (c)

Division of Physics, TOBB University of Economics and Technology, Ankara, Turkey

- ⁵ LAPP, CNRS/IN2P3 and Université Savoie Mont Blanc, Annecy-le-Vieux, France
- ⁶ High Energy Physics Division, Argonne National Laboratory, Argonne IL, United States of America
- ⁷ Department of Physics, University of Arizona, Tucson AZ, United States of America
- ⁸ Department of Physics, The University of Texas at Arlington, Arlington TX, United States of America
- ⁹ Physics Department, University of Athens, Athens, Greece
- ¹⁰ Physics Department, National Technical University of Athens, Zografou, Greece
- ¹¹ Department of Physics, The University of Texas at Austin, Austin TX, United States of America
- ¹² Institute of Physics, Azerbaijan Academy of Sciences, Baku, Azerbaijan
- ¹³ Institut de Física d'Altes Energies (IFAE), The Barcelona Institute of Science and Technology, Barcelona, Spain, Spain
- ¹⁴ Institute of Physics, University of Belgrade, Belgrade, Serbia
- ¹⁵ Department for Physics and Technology, University of Bergen, Bergen, Norway
- ¹⁶ Physics Division, Lawrence Berkeley National Laboratory and University of California, Berkeley CA, United States of America
- ¹⁷ Department of Physics, Humboldt University, Berlin, Germany
- ¹⁸ Albert Einstein Center for Fundamental Physics and Laboratory for High Energy Physics, University of Bern, Bern, Switzerland
- ¹⁹ School of Physics and Astronomy, University of Birmingham, Birmingham, United Kingdom
- ²⁰ ^(a) Department of Physics, Bogazici University, Istanbul; ^(b) Department of Physics Engineering, Gaziantep University, Gaziantep; ^(d) Istanbul Bilgi University, Faculty of Engineering and Natural Sciences, Istanbul, Turkey; ^(e) Bahcesehir University, Faculty of Engineering and Natural Sciences, Istanbul, Turkey, Turkey
- ²¹ Centro de Investigaciones, Universidad Antonio Narino, Bogota, Colombia
- ²² ^(a) INFN Sezione di Bologna; ^(b) Dipartimento di Fisica e Astronomia, Università di Bologna, Bologna, Italy
- ²³ Physikalisches Institut, University of Bonn, Bonn, Germany
- ²⁴ Department of Physics, Boston University, Boston MA, United States of America
- ²⁵ Department of Physics, Brandeis University, Waltham MA, United States of America
- ²⁶ ^(a) Universidade Federal do Rio De Janeiro COPPE/EE/IF, Rio de Janeiro; ^(b) Electrical Circuits Department, Federal University of Juiz de Fora (UFJF), Juiz de Fora; ^(c) Federal University of Sao Joao del Rei (UFSJ), Sao Joao del Rei; ^(d) Instituto de Fisica, Universidade de Sao Paulo, Sao Paulo, Brazil
- ²⁷ Physics Department, Brookhaven National Laboratory, Upton NY, United States of America
- ²⁸ ^(a) Transilvania University of Brasov, Brasov, Romania; ^(b) National Institute of Physics and Nuclear Engineering, Bucharest; ^(c) National Institute for Research and Development of Isotopic and Molecular Technologies, Physics Department, Cluj Napoca; ^(d) University Politehnica Bucharest, Bucharest; ^(e) West University in Timisoara, Timisoara, Romania
- ²⁹ Departamento de Física, Universidad de Buenos Aires, Buenos Aires, Argentina
- ³⁰ Cavendish Laboratory, University of Cambridge, Cambridge, United Kingdom
- ³¹ Department of Physics, Carleton University, Ottawa ON, Canada
- ³² CERN, Geneva, Switzerland
- ³³ Enrico Fermi Institute, University of Chicago, Chicago IL, United States of America
- ³⁴ ^(a) Departamento de Física, Pontificia Universidad Católica de Chile, Santiago; ^(b) Departamento de Física, Universidad Técnica Federico Santa María, Valparaíso, Chile
- ³⁵ ^(a) Institute of High Energy Physics, Chinese Academy of Sciences, Beijing; ^(b) Department of Modern Physics, University of Science and Technology of China, Anhui; ^(c) Department of Physics, Nanjing University, Jiangsu; ^(d) School of Physics, Shandong University, Shandong; ^(e) Department of Physics and Astronomy, Shanghai Key Laboratory for Particle Physics and Cosmology, Shanghai Jiao

Tong University, Shanghai; (also affiliated with PKU-CHEP); ^(f) Physics Department, Tsinghua University, Beijing 100084, China

³⁶ Laboratoire de Physique Corpusculaire, Clermont Université and Université Blaise Pascal and CNRS/IN2P3, Clermont-Ferrand, France

³⁷ Nevis Laboratory, Columbia University, Irvington NY, United States of America

³⁸ Niels Bohr Institute, University of Copenhagen, Kobenhavn, Denmark

³⁹ ^(a) INFN Gruppo Collegato di Cosenza, Laboratori Nazionali di Frascati; ^(b) Dipartimento di Fisica, Università della Calabria, Rende, Italy

⁴⁰ ^(a) AGH University of Science and Technology, Faculty of Physics and Applied Computer Science, Krakow; ^(b) Marian Smoluchowski Institute of Physics, Jagiellonian University, Krakow, Poland

⁴¹ Institute of Nuclear Physics Polish Academy of Sciences, Krakow, Poland

⁴² Physics Department, Southern Methodist University, Dallas TX, United States of America

⁴³ Physics Department, University of Texas at Dallas, Richardson TX, United States of America

⁴⁴ DESY, Hamburg and Zeuthen, Germany

⁴⁵ Lehrstuhl für Experimentelle Physik IV, Technische Universität Dortmund, Dortmund, Germany

⁴⁶ Institut für Kern- und Teilchenphysik, Technische Universität Dresden, Dresden, Germany

⁴⁷ Department of Physics, Duke University, Durham NC, United States of America

⁴⁸ SUPA - School of Physics and Astronomy, University of Edinburgh, Edinburgh, United Kingdom

⁴⁹ INFN Laboratori Nazionali di Frascati, Frascati, Italy

⁵⁰ Fakultät für Mathematik und Physik, Albert-Ludwigs-Universität, Freiburg, Germany

⁵¹ Section de Physique, Université de Genève, Geneva, Switzerland

⁵² ^(a) INFN Sezione di Genova; ^(b) Dipartimento di Fisica, Università di Genova, Genova, Italy

⁵³ ^(a) E. Andronikashvili Institute of Physics, Iv. Javakhishvili Tbilisi State University, Tbilisi; ^(b) High Energy Physics Institute, Tbilisi State University, Tbilisi, Georgia

⁵⁴ II Physikalisches Institut, Justus-Liebig-Universität Giessen, Giessen, Germany

⁵⁵ SUPA - School of Physics and Astronomy, University of Glasgow, Glasgow, United Kingdom

⁵⁶ II Physikalisches Institut, Georg-August-Universität, Göttingen, Germany

⁵⁷ Laboratoire de Physique Subatomique et de Cosmologie, Université Grenoble-Alpes, CNRS/IN2P3, Grenoble, France

⁵⁸ Department of Physics, Hampton University, Hampton VA, United States of America

⁵⁹ Laboratory for Particle Physics and Cosmology, Harvard University, Cambridge MA, United States of America

⁶⁰ ^(a) Kirchoff-Institut für Physik, Ruprecht-Karls-Universität Heidelberg, Heidelberg; ^(b)

Physikalisches Institut, Ruprecht-Karls-Universität Heidelberg, Heidelberg; ^(c) ZITI Institut für technische Informatik, Ruprecht-Karls-Universität Heidelberg, Mannheim, Germany

⁶¹ Faculty of Applied Information Science, Hiroshima Institute of Technology, Hiroshima, Japan

⁶² ^(a) Department of Physics, The Chinese University of Hong Kong, Shatin, N.T., Hong Kong; ^(b)

Department of Physics, The University of Hong Kong, Hong Kong; ^(c) Department of Physics, The Hong Kong University of Science and Technology, Clear Water Bay, Kowloon, Hong Kong, China

⁶³ Department of Physics, Indiana University, Bloomington IN, United States of America

⁶⁴ Institut für Astro- und Teilchenphysik, Leopold-Franzens-Universität, Innsbruck, Austria

⁶⁵ University of Iowa, Iowa City IA, United States of America

⁶⁶ Department of Physics and Astronomy, Iowa State University, Ames IA, United States of America

⁶⁷ Joint Institute for Nuclear Research, JINR Dubna, Dubna, Russia

⁶⁸ KEK, High Energy Accelerator Research Organization, Tsukuba, Japan

⁶⁹ Graduate School of Science, Kobe University, Kobe, Japan

⁷⁰ Faculty of Science, Kyoto University, Kyoto, Japan

- 71 Kyoto University of Education, Kyoto, Japan
- 72 Department of Physics, Kyushu University, Fukuoka, Japan
- 73 Instituto de Física La Plata, Universidad Nacional de La Plata and CONICET, La Plata, Argentina
- 74 Physics Department, Lancaster University, Lancaster, United Kingdom
- 75 ^(a) INFN Sezione di Lecce; ^(b) Dipartimento di Matematica e Fisica, Università del Salento, Lecce, Italy
- 76 Oliver Lodge Laboratory, University of Liverpool, Liverpool, United Kingdom
- 77 Department of Physics, Jožef Stefan Institute and University of Ljubljana, Ljubljana, Slovenia
- 78 School of Physics and Astronomy, Queen Mary University of London, London, United Kingdom
- 79 Department of Physics, Royal Holloway University of London, Surrey, United Kingdom
- 80 Department of Physics and Astronomy, University College London, London, United Kingdom
- 81 Louisiana Tech University, Ruston LA, United States of America
- 82 Laboratoire de Physique Nucléaire et de Hautes Energies, UPMC and Université Paris-Diderot and CNRS/IN2P3, Paris, France
- 83 Fysiska institutionen, Lunds universitet, Lund, Sweden
- 84 Departamento de Física Teórica C-15, Universidad Autónoma de Madrid, Madrid, Spain
- 85 Institut für Physik, Universität Mainz, Mainz, Germany
- 86 School of Physics and Astronomy, University of Manchester, Manchester, United Kingdom
- 87 CPPM, Aix-Marseille Université and CNRS/IN2P3, Marseille, France
- 88 Department of Physics, University of Massachusetts, Amherst MA, United States of America
- 89 Department of Physics, McGill University, Montreal QC, Canada
- 90 School of Physics, University of Melbourne, Victoria, Australia
- 91 Department of Physics, The University of Michigan, Ann Arbor MI, United States of America
- 92 Department of Physics and Astronomy, Michigan State University, East Lansing MI, United States of America
- 93 ^(a) INFN Sezione di Milano; ^(b) Dipartimento di Fisica, Università di Milano, Milano, Italy
- 94 B.I. Stepanov Institute of Physics, National Academy of Sciences of Belarus, Minsk, Republic of Belarus
- 95 National Scientific and Educational Centre for Particle and High Energy Physics, Minsk, Republic of Belarus
- 96 Group of Particle Physics, University of Montreal, Montreal QC, Canada
- 97 P.N. Lebedev Physical Institute of the Russian Academy of Sciences, Moscow, Russia
- 98 Institute for Theoretical and Experimental Physics (ITEP), Moscow, Russia
- 99 National Research Nuclear University MEPhI, Moscow, Russia
- 100 D.V. Skobeltsyn Institute of Nuclear Physics, M.V. Lomonosov Moscow State University, Moscow, Russia
- 101 Fakultät für Physik, Ludwig-Maximilians-Universität München, München, Germany
- 102 Max-Planck-Institut für Physik (Werner-Heisenberg-Institut), München, Germany
- 103 Nagasaki Institute of Applied Science, Nagasaki, Japan
- 104 Graduate School of Science and Kobayashi-Maskawa Institute, Nagoya University, Nagoya, Japan
- 105 ^(a) INFN Sezione di Napoli; ^(b) Dipartimento di Fisica, Università di Napoli, Napoli, Italy
- 106 Department of Physics and Astronomy, University of New Mexico, Albuquerque NM, United States of America
- 107 Institute for Mathematics, Astrophysics and Particle Physics, Radboud University Nijmegen/Nikhef, Nijmegen, Netherlands
- 108 Nikhef National Institute for Subatomic Physics and University of Amsterdam, Amsterdam, Netherlands

- ¹⁰⁹ Department of Physics, Northern Illinois University, DeKalb IL, United States of America
- ¹¹⁰ Budker Institute of Nuclear Physics, SB RAS, Novosibirsk, Russia
- ¹¹¹ Department of Physics, New York University, New York NY, United States of America
- ¹¹² Ohio State University, Columbus OH, United States of America
- ¹¹³ Faculty of Science, Okayama University, Okayama, Japan
- ¹¹⁴ Homer L. Dodge Department of Physics and Astronomy, University of Oklahoma, Norman OK, United States of America
- ¹¹⁵ Department of Physics, Oklahoma State University, Stillwater OK, United States of America
- ¹¹⁶ Palacký University, RCPTM, Olomouc, Czech Republic
- ¹¹⁷ Center for High Energy Physics, University of Oregon, Eugene OR, United States of America
- ¹¹⁸ LAL, Univ. Paris-Sud, CNRS/IN2P3, Université Paris-Saclay, Orsay, France
- ¹¹⁹ Graduate School of Science, Osaka University, Osaka, Japan
- ¹²⁰ Department of Physics, University of Oslo, Oslo, Norway
- ¹²¹ Department of Physics, Oxford University, Oxford, United Kingdom
- ¹²² ^(a) INFN Sezione di Pavia; ^(b) Dipartimento di Fisica, Università di Pavia, Pavia, Italy
- ¹²³ Department of Physics, University of Pennsylvania, Philadelphia PA, United States of America
- ¹²⁴ National Research Centre "Kurchatov Institute" B.P.Konstantinov Petersburg Nuclear Physics Institute, St. Petersburg, Russia
- ¹²⁵ ^(a) INFN Sezione di Pisa; ^(b) Dipartimento di Fisica E. Fermi, Università di Pisa, Pisa, Italy
- ¹²⁶ Department of Physics and Astronomy, University of Pittsburgh, Pittsburgh PA, United States of America
- ¹²⁷ ^(a) Laboratório de Instrumentação e Física Experimental de Partículas - LIP, Lisboa; ^(b) Faculdade de Ciências, Universidade de Lisboa, Lisboa; ^(c) Department of Physics, University of Coimbra, Coimbra; ^(d) Centro de Física Nuclear da Universidade de Lisboa, Lisboa; ^(e) Departamento de Física, Universidade do Minho, Braga; ^(f) Departamento de Física Teórica y del Cosmos and CAFPE, Universidad de Granada, Granada (Spain); ^(g) Dep Física and CEFITEC of Faculdade de Ciências e Tecnologia, Universidade Nova de Lisboa, Caparica, Portugal
- ¹²⁸ Institute of Physics, Academy of Sciences of the Czech Republic, Praha, Czech Republic
- ¹²⁹ Czech Technical University in Prague, Praha, Czech Republic
- ¹³⁰ Faculty of Mathematics and Physics, Charles University in Prague, Praha, Czech Republic
- ¹³¹ State Research Center Institute for High Energy Physics (Protvino), NRC KI, Russia
- ¹³² Particle Physics Department, Rutherford Appleton Laboratory, Didcot, United Kingdom
- ¹³³ ^(a) INFN Sezione di Roma; ^(b) Dipartimento di Fisica, Sapienza Università di Roma, Roma, Italy
- ¹³⁴ ^(a) INFN Sezione di Roma Tor Vergata; ^(b) Dipartimento di Fisica, Università di Roma Tor Vergata, Roma, Italy
- ¹³⁵ ^(a) INFN Sezione di Roma Tre; ^(b) Dipartimento di Matematica e Fisica, Università Roma Tre, Roma, Italy
- ¹³⁶ ^(a) Faculté des Sciences Ain Chock, Réseau Universitaire de Physique des Hautes Energies - Université Hassan II, Casablanca; ^(b) Centre National de l'Énergie des Sciences Techniques Nucleaires, Rabat; ^(c) Faculté des Sciences Semlalia, Université Cadi Ayyad, LPHEA-Marrakech; ^(d) Faculté des Sciences, Université Mohamed Premier and LTPM, Oujda; ^(e) Faculté des sciences, Université Mohammed V, Rabat, Morocco
- ¹³⁷ DSM/IRFU (Institut de Recherches sur les Lois Fondamentales de l'Univers), CEA Saclay (Commissariat à l'Énergie Atomique et aux Énergies Alternatives), Gif-sur-Yvette, France
- ¹³⁸ Santa Cruz Institute for Particle Physics, University of California Santa Cruz, Santa Cruz CA, United States of America
- ¹³⁹ Department of Physics, University of Washington, Seattle WA, United States of America

- ¹⁴⁰ Department of Physics and Astronomy, University of Sheffield, Sheffield, United Kingdom
- ¹⁴¹ Department of Physics, Shinshu University, Nagano, Japan
- ¹⁴² Fachbereich Physik, Universität Siegen, Siegen, Germany
- ¹⁴³ Department of Physics, Simon Fraser University, Burnaby BC, Canada
- ¹⁴⁴ SLAC National Accelerator Laboratory, Stanford CA, United States of America
- ¹⁴⁵ ^(a) Faculty of Mathematics, Physics & Informatics, Comenius University, Bratislava; ^(b) Department of Subnuclear Physics, Institute of Experimental Physics of the Slovak Academy of Sciences, Kosice, Slovak Republic
- ¹⁴⁶ ^(a) Department of Physics, University of Cape Town, Cape Town; ^(b) Department of Physics, University of Johannesburg, Johannesburg; ^(c) School of Physics, University of the Witwatersrand, Johannesburg, South Africa
- ¹⁴⁷ ^(a) Department of Physics, Stockholm University; ^(b) The Oskar Klein Centre, Stockholm, Sweden
- ¹⁴⁸ Physics Department, Royal Institute of Technology, Stockholm, Sweden
- ¹⁴⁹ Departments of Physics & Astronomy and Chemistry, Stony Brook University, Stony Brook NY, United States of America
- ¹⁵⁰ Department of Physics and Astronomy, University of Sussex, Brighton, United Kingdom
- ¹⁵¹ School of Physics, University of Sydney, Sydney, Australia
- ¹⁵² Institute of Physics, Academia Sinica, Taipei, Taiwan
- ¹⁵³ Department of Physics, Technion: Israel Institute of Technology, Haifa, Israel
- ¹⁵⁴ Raymond and Beverly Sackler School of Physics and Astronomy, Tel Aviv University, Tel Aviv, Israel
- ¹⁵⁵ Department of Physics, Aristotle University of Thessaloniki, Thessaloniki, Greece
- ¹⁵⁶ International Center for Elementary Particle Physics and Department of Physics, The University of Tokyo, Tokyo, Japan
- ¹⁵⁷ Graduate School of Science and Technology, Tokyo Metropolitan University, Tokyo, Japan
- ¹⁵⁸ Department of Physics, Tokyo Institute of Technology, Tokyo, Japan
- ¹⁵⁹ Department of Physics, University of Toronto, Toronto ON, Canada
- ¹⁶⁰ ^(a) TRIUMF, Vancouver BC; ^(b) Department of Physics and Astronomy, York University, Toronto ON, Canada
- ¹⁶¹ Faculty of Pure and Applied Sciences, and Center for Integrated Research in Fundamental Science and Engineering, University of Tsukuba, Tsukuba, Japan
- ¹⁶² Department of Physics and Astronomy, Tufts University, Medford MA, United States of America
- ¹⁶³ Department of Physics and Astronomy, University of California Irvine, Irvine CA, United States of America
- ¹⁶⁴ ^(a) INFN Gruppo Collegato di Udine, Sezione di Trieste, Udine; ^(b) ICTP, Trieste; ^(c) Dipartimento di Chimica, Fisica e Ambiente, Università di Udine, Udine, Italy
- ¹⁶⁵ Department of Physics and Astronomy, University of Uppsala, Uppsala, Sweden
- ¹⁶⁶ Department of Physics, University of Illinois, Urbana IL, United States of America
- ¹⁶⁷ Instituto de Física Corpuscular (IFIC) and Departamento de Física Atómica, Molecular y Nuclear and Departamento de Ingeniería Electrónica and Instituto de Microelectrónica de Barcelona (IMB-CNM), University of Valencia and CSIC, Valencia, Spain
- ¹⁶⁸ Department of Physics, University of British Columbia, Vancouver BC, Canada
- ¹⁶⁹ Department of Physics and Astronomy, University of Victoria, Victoria BC, Canada
- ¹⁷⁰ Department of Physics, University of Warwick, Coventry, United Kingdom
- ¹⁷¹ Waseda University, Tokyo, Japan
- ¹⁷² Department of Particle Physics, The Weizmann Institute of Science, Rehovot, Israel
- ¹⁷³ Department of Physics, University of Wisconsin, Madison WI, United States of America

- ¹⁷⁴ Fakultät für Physik und Astronomie, Julius-Maximilians-Universität, Würzburg, Germany
- ¹⁷⁵ Fakultät für Mathematik und Naturwissenschaften, Fachgruppe Physik, Bergische Universität Wuppertal, Wuppertal, Germany
- ¹⁷⁶ Department of Physics, Yale University, New Haven CT, United States of America
- ¹⁷⁷ Yerevan Physics Institute, Yerevan, Armenia
- ¹⁷⁸ Centre de Calcul de l'Institut National de Physique Nucléaire et de Physique des Particules (IN2P3), Villeurbanne, France
- ^a Also at Department of Physics, King's College London, London, United Kingdom
- ^b Also at Institute of Physics, Azerbaijan Academy of Sciences, Baku, Azerbaijan
- ^c Also at Novosibirsk State University, Novosibirsk, Russia
- ^d Also at TRIUMF, Vancouver BC, Canada
- ^e Also at Department of Physics & Astronomy, University of Louisville, Louisville, KY, United States of America
- ^f Also at Department of Physics, California State University, Fresno CA, United States of America
- ^g Also at Department of Physics, University of Fribourg, Fribourg, Switzerland
- ^h Also at Departament de Física de la Universitat Autònoma de Barcelona, Barcelona, Spain
- ⁱ Also at Departamento de Física e Astronomia, Faculdade de Ciências, Universidade do Porto, Portugal
- ^j Also at Tomsk State University, Tomsk, Russia
- ^k Also at Università di Napoli Parthenope, Napoli, Italy
- ^l Also at Institute of Particle Physics (IPP), Canada
- ^m Also at National Institute of Physics and Nuclear Engineering, Bucharest, Romania
- ⁿ Also at Department of Physics, St. Petersburg State Polytechnical University, St. Petersburg, Russia
- ^o Also at Department of Physics, The University of Michigan, Ann Arbor MI, United States of America
- ^p Also at Centre for High Performance Computing, CSIR Campus, Rosebank, Cape Town, South Africa
- ^q Also at Louisiana Tech University, Ruston LA, United States of America
- ^r Also at Institutio Catalana de Recerca i Estudis Avancats, ICREA, Barcelona, Spain
- ^s Also at Graduate School of Science, Osaka University, Osaka, Japan
- ^t Also at Department of Physics, National Tsing Hua University, Taiwan
- ^u Also at Institute for Mathematics, Astrophysics and Particle Physics, Radboud University Nijmegen/Nikhef, Nijmegen, Netherlands
- ^v Also at Department of Physics, The University of Texas at Austin, Austin TX, United States of America
- ^w Also at Institute of Theoretical Physics, Ilia State University, Tbilisi, Georgia
- ^x Also at CERN, Geneva, Switzerland
- ^y Also at Georgian Technical University (GTU), Tbilisi, Georgia
- ^z Also at O Chadai Academic Production, Ochanomizu University, Tokyo, Japan
- ^{aa} Also at Manhattan College, New York NY, United States of America
- ^{ab} Also at Hellenic Open University, Patras, Greece
- ^{ac} Also at Academia Sinica Grid Computing, Institute of Physics, Academia Sinica, Taipei, Taiwan
- ^{ad} Also at School of Physics, Shandong University, Shandong, China
- ^{ae} Also at Moscow Institute of Physics and Technology State University, Dolgoprudny, Russia
- ^{af} Also at Section de Physique, Université de Genève, Geneva, Switzerland
- ^{ag} Also at Eotvos Lorand University, Budapest, Hungary
- ^{ah} Also at Departments of Physics & Astronomy and Chemistry, Stony Brook University, Stony Brook NY, United States of America
- ^{ai} Also at International School for Advanced Studies (SISSA), Trieste, Italy
- ^{aj} Also at Department of Physics and Astronomy, University of South Carolina, Columbia SC, United States of America

- ak* Also at School of Physics and Engineering, Sun Yat-sen University, Guangzhou, China
- al* Also at Institute for Nuclear Research and Nuclear Energy (INRNE) of the Bulgarian Academy of Sciences, Sofia, Bulgaria
- am* Also at Faculty of Physics, M.V.Lomonosov Moscow State University, Moscow, Russia
- an* Also at Institute of Physics, Academia Sinica, Taipei, Taiwan
- ao* Also at National Research Nuclear University MEPhI, Moscow, Russia
- ap* Also at Department of Physics, Stanford University, Stanford CA, United States of America
- aq* Also at Institute for Particle and Nuclear Physics, Wigner Research Centre for Physics, Budapest, Hungary
- ar* Also at Flensburg University of Applied Sciences, Flensburg, Germany
- as* Also at University of Malaya, Department of Physics, Kuala Lumpur, Malaysia
- at* Also at CPPM, Aix-Marseille Université and CNRS/IN2P3, Marseille, France
- * Deceased